

# CASE FILE COPY

NACA TN 3153

## NATIONAL ADVISORY COMMITTEE FOR AERONAUTICS

TECHNICAL NOTE 3153

JUL 12 1954

VARIATION OF LOCAL LIQUID-WATER CONCENTRATION ABOUT AN  
ELLIPSOID OF FINENESS RATIO 5 MOVING IN A  
DROPLET FIELD

By Robert G. Dorsch and Rinaldo J. Brun

Lewis Flight Propulsion Laboratory  
Cleveland, Ohio

PROPERTY OF  
ENGINEERING LIBRARY



Washington  
July 1954

2

VARIATION OF LOCAL LIQUID-WATER CONCENTRATION ABOUT AN ELLIPSOID OF  
FINENESS RATIO 5 MOVING IN A DROPLET FIELD

By Robert G. Dorsch and Rinaldo J. Brun

## SUMMARY

Trajectories of water droplets about an ellipsoid of revolution with a fineness ratio of 5 (which often approximates the shape of an aircraft fuselage or missile) were computed with the aid of a differential analyzer. Analyses of these trajectories indicate that the local concentration of liquid water at various points about an ellipsoid in flight through a droplet field varies considerably and under some conditions may be several times the free-stream concentration. Curves of the local concentration factor as a function of spatial position were obtained and are presented in terms of dimensionless parameters  $Re_0$  (free-stream Reynolds number) and  $K$  (inertia), which contain flight and atmospheric conditions. These curves show that the local concentration factor at any point is very sensitive to change in the dimensionless parameters  $Re_0$  and  $K$ . These data indicate that the expected local concentration factors should be considered when choosing the location of, or when determining anti-icing heat requirements for, water- or ice-sensitive devices that protrude into the stream from an aircraft fuselage or missile. Similarly, the concentration factor should be considered when choosing the location on an aircraft of instruments that measure liquid-water content or droplet-size distribution in the atmosphere.

## INTRODUCTION

It is generally recognized that an aircraft moving through a cloud alters the concentration of cloud droplets in the immediate vicinity of the aircraft. For example, the peculiar distributions of ice often found on aircraft antenna support arms or on pitot static tubes after flight through supercooled clouds are indications that the concentration of liquid water in the vicinity of the fuselage is considerably altered by the air flow about the fuselage. This effect is illustrated by the photographs of figure 1, which show ice formed on instrument support rods mounted on the side and bottom of the fuselage of a B-25 aircraft during

flight through a supercooled cloud. As indicated by the ice formations of figure 1, there is frequently a region of reduced (or zero) droplet concentration next to the aircraft surface, followed by a narrow region of greatly increased droplet concentration farther out. Beyond the narrow region of high concentration, the droplet concentration gradually decreases toward the free-stream value with increase in distance from the surface of the aircraft.

A knowledge of this spatial variation of local droplet concentration about an aircraft or missile during flight through clouds, drizzle, or rain is often important when choosing the location of devices which protrude into the stream or when determining the heat required to protect the devices from ice. Examples of such devices are: (1) water- or ice-sensitive external accessories and aircraft instrument sensing elements, (2) intake ducts and vents, (3) antenna masts, (4) ice detectors, and (5) instruments for measuring liquid-water content and droplet-size distribution. In addition, at places where a body of revolution joins an airfoil (e.g., where a rocket pod is attached to a wing), the local impingement of cloud droplets on the airfoil, and therefore the heat required for ice protection, will be altered by the effect of the body of revolution on the local droplet concentration. Similarly, droplet impingement on objects mounted on a wing will be affected by the variation in droplet concentration caused by the air flow about the wing.

As part of an evaluation of the effect of the air-flow field on the droplet concentration about an aircraft or missile in flight through a droplet field, a study of the droplet concentration about a prolate ellipsoid of revolution of fineness ratio 5 was undertaken. An ellipsoid of revolution was chosen because it is a good approximation of the shape of the fuselage of many aircraft and missiles. Droplet trajectories about the ellipsoid of fineness ratio 5 in axisymmetric, incompressible flow were calculated with the aid of a differential analyzer at the NACA Lewis laboratory. Droplet trajectories were calculated as far back as the midpoint of the ellipsoid and as far out in the radial direction as 1.6 times the semiminor axis. These trajectories were analyzed to determine the relation between the droplet concentration at various points in space and the following variables: ellipsoid length and velocity, droplet size, and flight altitude and air temperature. The results of the analyses are summarized in this report in terms of the dimensionless parameters  $Re_0$  and  $K$ , which contain these variables. Although the calculations were made for incompressible flow, they should be applicable throughout the subsonic region because of the small effect of compressibility on droplet trajectories (ref. 1) and the high flight critical Mach number of the ellipsoid.

## SYMBOLS

The following symbols are used in this report:

A	annular area perpendicular to major axis through which droplet flux is flowing, sq ft
C	local concentration factor, $d(r_0^2)/d(r^2)$ , dimensionless
d	droplet diameter, microns
$d_{med}$	volume-median droplet diameter, microns
F	flux density of liquid water, lb/(hr)(sq ft)
K	inertia parameter, $1.704 \times 10^{-12} d^2 U / \mu L$ , dimensionless [the density of water, 1.94 slugs/cu ft, is included in the constant]
$K_{med}$	inertia parameter based on volume-median droplet diameter, dimensionless
L	major axis of ellipsoid, ft
N	local droplet flux, number/(cm <sup>2</sup> )(sec)
n	local droplet-number density, number/cc
$n_0$	free-stream droplet-number density, number/cc
$Re_0$	free-stream Reynolds number with respect to droplet, $4.813 \times 10^{-6} \rho_a U / \mu$ , dimensionless
$Re_{0,med}$	free-stream Reynolds number based on volume-median droplet diameter, dimensionless
r, z	cylindrical coordinates, ratio to major axis, dimensionless
$r_s$	ordinate of ellipsoid surface, ratio to major axis, dimensionless
$r_0$	starting ordinate at $z = -\infty$ of droplet trajectory, ratio to major axis, dimensionless
U	free-stream velocity or flight speed, mph
u	local air velocity, ratio to free-stream velocity, dimensionless

3106

NACA TN 3153



$u'$	local air velocity, mph
$v$	local droplet velocity, ratio to free-stream velocity, dimensionless
$v'$	local droplet velocity, mph
$w$	local liquid-water content, g/cu m
$w_i$	indicated liquid-water content, g/cu m
$w_0$	free-stream liquid-water content, g/cu m
$\mu$	viscosity of air, slugs/(ft)(sec)
$\rho_a$	density of air, slugs/cu ft
$\sigma$	difference between local air- and droplet-velocity components, dimensionless

Subscripts:

$av$	average of quantity over area A
$r$	radial component
$z$	axial component
$0$	free-stream conditions

#### METHOD OF COMPUTING DROPLET TRAJECTORIES

The droplet trajectories about the ellipsoid of revolution of fineness ratio 5 (20 percent thick) were calculated with the aid of a differential analyzer in the same manner as those of reference 2, except that emphasis was placed on the behavior of the droplet trajectories in the space around the ellipsoid rather than on the impingement of droplets upon the ellipsoid surface. The trajectories were computed out to  $r = 0.16$  at  $z = 0$  (fig. 2), and all nonimpinging trajectories were computed back as far as the midpoint of the ellipsoid ( $z = 0$ ). Trajectories were calculated in the  $z, r$  plane for various values of the parameter  $1/K$  from 0.1 to 90 and values of free-stream Reynolds number  $Re_0$  from 0 to 8192.

In order that these dimensionless parameters have more physical significance in the following discussions, some typical combinations of  $K$  and  $Re_0$  are presented in table I in terms of the length and the velocity

of the ellipsoid, the droplet size, and the flight pressure altitude and temperature. A typical set of trajectories for  $1/K = 15$  and  $Re_0 = 128$  is shown in figure 3.

The incompressible, nonviscous air-flow field used in calculating the droplet trajectories about the prolate ellipsoid of revolution was obtained from the exact solution of the Laplace equation in prolate elliptic coordinates given by Lamb (ref. 3). The details of obtaining the velocity components in the  $z, r$  plane from Lamb's potential function are given in reference 2.

### RESULTS OF TRAJECTORY COMPUTATIONS

A series of droplet trajectories about an ellipsoid of revolution with a fineness ratio of 5 (20 percent thick) in subsonic axisymmetric air flow was computed for various combinations of the dimensionless parameters  $1/K$  and  $Re_0$ . (A procedure for rapid calculation of  $1/K$  and  $Re_0$  from practical flight conditions is given in ref. 4.) From these trajectories, the variation of droplet concentration (or flux density) with radial distance from the ellipsoid was determined at three positions along the axis of the ellipsoid.

#### Average Mass Flux Density of Water in Droplet Form

The average mass flux of water in droplet form per unit area through an annular area of space (of width  $r_2 - r_1$ , (fig. 2)) perpendicular to the major axis of the ellipsoid is obtained from the law of conservation of matter. Consider the liquid water in droplet form moving between two surfaces formed by rotating two neighboring trajectories in the  $r, z$  plane about the axis of the ellipsoid as shown in figure 2. Then,

$$w_0 U A_0 = w_{av} v'_{z,av} A \quad (1)$$

and

$$\frac{F_{av}}{F_0} = \frac{w_{av} v'_{z,av}}{w_0 U} = \frac{A_0}{A} = \frac{r_{0,2}^2 - r_{0,1}^2}{r_2^2 - r_1^2} = \frac{\Delta(r_0^2)}{\Delta(r^2)} \quad (2)$$

The subscript 0 refers to conditions at large distances ahead of the ellipsoid (free-stream conditions), and the subscript av refers to the average of a quantity over the annular area A. The annular area A is measured in a plane perpendicular to the major axis of the ellipsoid

(fig. 2). From equation (2), the average flux density through an annular area  $A$  or a sector of the annular area  $A$  can be written as follows:

$$F_{av} = 0.33w_0U \frac{\Delta(r_0^2)}{\Delta(r^2)} \text{ lb/(hr)(sq ft)} \quad (3)$$

The constant 0.33 is a conversion factor for the units used.

Curves of  $r_0^2$  as a function of  $r^2$  for various values of  $Re_0$  and  $1/K$  at constant  $z$  positions corresponding to the midpoint region ( $z = 0$ ), a position  $1/4$  major axis length from the nose ( $z = -0.25$ ), and the nose region ( $z = -0.5$ ), which were obtained from the calculated droplet trajectories, are presented in figure 4.

Equation (3) and figure 4 can be used, for example, to determine the average mass flux density of water in droplet form passing through a sector of an annular area  $A$  such as the entrance area of a small thin-lipped inlet (with inlet velocity ratio equal to 1) attached to the ellipsoid moving at velocity  $U$  through a droplet field with a liquid-water content of  $w_0$ .

#### Local Liquid-Water Flux Density

The local mass flux of water in droplet form per unit area perpendicular to the major axis at a point in the vicinity of the moving ellipsoid can be obtained from equation (3) by letting  $\Delta(r^2)$  approach zero. Then

$$F = 0.33w_0UC, \text{ lb/(hr)(sq ft)} \quad (4)$$

where

$$C = d(r_0^2)/d(r^2)$$

The local concentration factor  $C$  at a point in space is obtained from the slope of the curves of  $r_0^2$  as a function of  $r^2$  (fig. 4) at the point of interest for the  $Re_0$  and  $K$  combination being considered.

The concentration factor as a function of  $r$  for selected values of  $Re_0$  and  $K$  at  $z = 0$ ,  $z = -0.25$ , and  $z = -0.5$  is given in

3106 figure 5. Examination of figure 5 shows that the concentration factor approaches 1 (free-stream value) at large values of  $r$  for all  $z$  positions. At  $z = -0.50$ , the concentration factor decreases to values less than 1 for small values of  $r$ . At the  $z = -0.25$  and  $z = 0$  positions, the concentration factor increases from values near 1 at large values of  $r$  to peak values at small values of  $r$ . In addition, for most values of  $Re_0$  and  $K$  at the  $z = -0.25$  and  $z = 0$  positions, there is a region of zero concentration between the surface of the ellipsoid and the peak value of the concentration factor. Because of relatively low accuracy in obtaining values of local concentration factor greater than 4, the average value of  $C$  over an  $r$  interval of 0.001 or 0.002 units (as indicated by a bracket in the figure) is given instead of the peak value whenever the peak value is greater than 4.

In order to determine  $C$  for various values of  $Re_0$  and  $1/K$  not given in figure 5, it is necessary to interpolate or extrapolate the data. The peculiar variation of  $C$  with  $Re_0$  and  $1/K$  makes this interpolation or extrapolation difficult. Therefore, as an aid in interpolation and extrapolation, the peak value of  $C$  of figure 5 for the  $z = 0$  and  $z = -0.25$  positions is plotted as a function of  $1/K$  for constant  $Re_0$  in figure 6. Although peak values of  $C$  greater than 4 were not presented in figure 5 because of their relative inaccuracy, they are used in figure 6 in order to facilitate interpolation and extrapolation. In addition, the  $r$  position of the peak value of  $C$  at  $z = 0$  and  $z = -0.25$  is plotted as a function of  $1/K$  for constant  $Re_0$  in figure 7. With the use of figures 6 and 7, the peak value of  $C$  and its  $r$  position can be determined for the value of  $Re_0$  and  $1/K$  of interest. With the position and value of the peak obtained by this method, the remaining portion of the curve of  $C$  as a function of  $r$  can be obtained by using the shape of the curve corresponding to the nearest values of  $Re_0$  and  $1/K$  as a guide.

The local liquid-water content in grams per cubic meter can be obtained at any point in space by dividing the droplet flux by the  $z$ -component of the local droplet velocity at that point:

$$w = \frac{w_0 U}{v_z'} C, \text{ g/cu m} \quad (5)$$

Inasmuch as the  $z$ -component of the local droplet velocity at a given point in the vicinity of a body of revolution is not readily determinable, it is usually necessary to estimate it from the local air velocity. The difference between the dimensionless local air- and droplet-velocity components as a function of radial distance  $r$  at the  $z = 0$  position of

the ellipsoid is shown in figure 8. Examination of this figure shows that the dimensionless local air- and droplet-velocity components about an ellipsoid of fineness ratio 5 are often very nearly equal at the  $z = 0$  position. Examination of the air-flow field about the ellipsoid (ref. 2) and figure 8 shows that at  $z = 0$  the ratio  $U/v'_z$  is usually nearly equal to 1 (within 6 percent).

#### Local Droplet-Number Flux Density

By reasoning similar to that of the preceding section, the local droplet-number flux density at a point in the vicinity of the ellipsoid moving through a droplet field can be written in the form

$$N = 44.7n_0UC, \text{ number}/(\text{cm}^2)(\text{sec}) \quad (6)$$

The constant 44.7 is a conversion factor for the units used. The concentration factor  $C$  is obtained from figure 5.

If, instead of the droplet-number flux density, the instantaneous number of droplets per cubic centimeter at a point in space in the vicinity of the ellipsoid is desired, then the local flux density at the point must be divided by the  $z$ -component of the local droplet velocity at the point. That is,

$$n = \frac{n_0U}{v'_z} C, \text{ number/cc} \quad (7)$$

Again, since the  $z$ -component of the local droplet velocity is usually unknown, it must be estimated from the local air velocity at that point, as discussed in the preceding section.

#### Shadow Zone

The region of zero concentration adjacent to the surface of the ellipsoid, which is evident in figure 5, will be called the shadow zone. This region is protected from droplet penetration by the air-flow characteristics ahead of and in the vicinity of the forward positions of the ellipsoid. The thickness  $(r - r_g)$  of the shadow zone at each  $z$  position of the body for various  $Re_0$  and  $K$  values is given in figure 9. Generally, the thickness of the shadow zone increases as  $z$  approaches 0. The shadow-zone thickness is 0 at the nose for all values of  $Re_0$  and  $K$  shown in figure 9 and becomes of finite thickness at a  $z$  position that depends on  $Re_0$  and  $K$ .

## Local Concentration in Clouds with Nonuniform Droplet Size

The data presented in figures 4 to 9 apply directly only to flights in clouds, rain, or drizzle composed of droplets that are all uniform in size. The droplets encountered in the atmosphere at any instant may, however, be of mixed sizes. Therefore, if the free-stream droplet-size distribution is known or can be estimated, the data must be accordingly modified (or weighted) before the local flux density of liquid water at a point in the vicinity of the ellipsoid can be found.

For nonuniform droplets, the local flux density can be determined from equations (4) or (6) by using the weighted value of the concentration factor  $C$  that corresponds to the droplet-size distribution present in the cloud. The weighted value of  $C$  can be obtained by plotting  $C$  for each droplet size in the distribution (based on values of  $l/K$  and  $Re_0$  corresponding to each droplet diam.) as a function of the cumulative volume (in percent) of water corresponding to each droplet size and integrating the resultant curve. The details of this method of weighting are given in reference 2.

The effect of droplet-size distribution on the concentration factor is illustrated in figure 10. In this figure, the variation with  $r$  of the concentration factor about the ellipsoid, at the  $z = 0$  position for flight through clouds with a Langmuir "C" droplet-size distribution (ref. 5, reproduced in table II herein), is compared with that for flight through clouds with uniform droplets having a diameter equal to the volume-median diameter of the "C" distribution in each of four cases.

As the droplet-size distribution becomes broader, the peak value of the concentration factor considerably decreases and the former shadow zone becomes an area with a small (but increasing with  $r$ ) concentration factor, rather than one with zero concentration factor.

## DISCUSSION OF RESULTS

The variation of local concentration factor with spatial position and  $Re_0$  and  $l/K$  presented in figure 5 indicates that the droplet concentration in the vicinity of the ellipsoid differs considerably from the free-stream concentration. Under some circumstances, the local droplet flux per unit area may vary from 0 to many times the free-stream value within a short distance. As shown in figure 10, this effect is greater for droplets of uniform size than for clouds with a distribution of droplet sizes, because of the partial "averaging out" of maximum and minimum regions for droplets of varying sizes. In addition, the concentration factor is very sensitive to small changes in  $l/K$  and  $Re_0$ , as can be

5106

2-12

seen from figure 5. This sensitivity to  $l/K$  and  $Re_0$  is brought out more clearly in the variation of peak value of concentration factor with  $l/K$  and  $Re_0$  presented in figure 6. Figure 6 shows that at  $z = -0.25$  and  $z = 0$ , there is a narrow region of  $l/K$  for each  $Re_0$  in which the peak value of concentration factor is large. For values of  $l/K$  larger or smaller than those in the narrow-peak region, the peak value of the concentration factor decreases rapidly.

The variation of concentration of liquid-water content with  $z$  and  $r$  position, droplet-size distribution, and  $l/K_{med}$  and  $Re_{0,med}$  indicates that care should be exercised in locating instrument sensing elements and small inlets or vents that protrude from the surface and are sensitive to impinging water or ice formation. If possible, they should be located where a minimum concentration factor exists. When it is necessary to provide ice protection for these protuberances, consideration should be given to the concentration factors expected. In some cases, part of the device may accumulate ice at a rate which would be several times that expected from the free-stream liquid-water content.

When estimating the effect of a body of revolution on droplet flux in its vicinity from the data calculated from the ellipsoid, the degree of aerodynamic and physical similarity must be considered. The slope of the surface at the  $z$  position of interest, the bluntness of the nose, and sudden changes in slope, such as those due to windshields, are particularly important.

#### Comparison with Observed Icing Deposits

Qualitative observations of ice formations on aircraft pitot tubes, antenna support arms, and other shaft-like protuberances into the air stream bear out the shape of the curves shown in figure 10. Inasmuch as the concentration factor determines the shape of the ice formation on a rod of small diameter (greater than 90-percent collection efficiency), these curves give directly the shape of the expected ice formation on such a rod located at the indicated positions. The thickness of the ice formation would depend, of course, on the velocity, liquid-water content, and time of exposure. The curve of figure 10(c) was calculated for values of  $Re_{0,med}$ ,  $l/K_{med}$ , and  $z$  position comparable to those existing when the support rods shown in figure 1 were iced. A comparison of the curve of figure 10(c) with the shape of the ice on the support rods shows that there is good qualitative agreement between the calculated concentration of liquid water and that indicated by an actual ice formation.

Effect of Local Concentration Factor on Liquid-Water-Content and  
Droplet-Size-Distribution Measurements

Most atmospheric liquid-water-content and droplet-size-distribution measurements have been made from aircraft in flight. For mechanical reasons, the measurements have frequently been made rather close to the fuselage. For this reason, measurements of liquid-water content and droplet-size distribution are affected by the local concentration factor at the point of measurement and may not indicate the desired free-stream values.

Liquid-water-content measuring instruments with high collection efficiency. - For liquid-water measuring devices with high collection or sampling efficiency (over 95 percent for most conditions), which essentially measure local flux density directly, the indicated liquid-water content obtained by using the free-stream velocity will be high or low in proportion to the weighted concentration factor, as can be seen from the following relation:

$$w_i = F/0.33U = w_0 C, \text{ g/cu m} \quad (8)$$

If the z-component of the local air velocity  $u'_z$  is used instead of the free-stream velocity in the calculation of liquid-water content, then,

$$w_i = F/0.33u'_z = w_0 (U/u'_z) C, \text{ g/cu m} \quad (9)$$

Equations similar in form to equation (8) are often used for liquid-water-content calculations, because frequently the only velocity known is the airspeed of the aircraft.

Examples of instruments of this type are the orifice-type icing-rate meters (refs. 6 and 7), the heated-wire liquid-water-content meter (ref. 8), and cloud-droplet cameras (refs. 9 and 10). The physical arrangement of these instruments is often such that the problem of instrument location on an aircraft is particularly important. The point of measurement of these instruments may be as close as 6 to 12 inches from the fuselage. Fortunately, many of the measurements of liquid-water content that have been taken with instruments of this type have been made from aircraft of the order of 100 feet long at velocities of the order of 300 mph. These conditions, along with cloud droplets of the order of 20 microns in diameter, give  $Re_0$  of 128.7 and  $1/K$  of 165.6 at a pressure altitude of 15,000 feet and an air temperature of  $1^\circ$  F. Examination of figure 5 at the  $z = 0$  position (which is comparable to the position on an aircraft fuselage at which the slope of the surface becomes 0) indicates that, if all the droplets are 20 microns, the concentration factor

3105

CF-2 back



is 1.26 at 6 inches from the surface of the ellipsoid ( $r = 0.105$ ) and 1.17 at 12 inches from the surface ( $r = 0.11$ ). If a "C" distribution of droplet sizes is present with a volume-median droplet size of 20 microns, then the variation of local concentration with  $r$  for the ellipsoid would be as given in figure 10(d), which shows that the weighted concentration factor at 6 inches from the surface is 1.26 and at 12 inches is 1.14. Thus, if an icing-rate meter were mounted at the  $z = 0$  position on a 100-foot-long ellipsoid of fineness ratio 5, it would measure a liquid-water content of the order of 26 percent high at 6 inches and 14 to 17 percent high at 12 inches. In addition, inasmuch as these calculations are based on axisymmetric flow, any yawing motion of the ellipsoid in flight will introduce a time-dependent variation of the local concentration factor that would be difficult to calculate. While the effect on the concentration factor in the preceding example was modest (of the order of 15 to 30 percent), the picture is altered considerably if, for the preceding example, the droplet size is 60 instead of 20 microns and the droplet-size distribution is uniform. Then,  $Re_0 = 386.1$  and  $1/K = 18.4$ , and the concentration factor at the  $z = 0$  position and 6 inches from the surface is 0, and at 12 inches from the surface it is about 2.8. Thus, at the 6-inch position the indicated water content for these conditions is 0, and at the 12-inch position it is 280 percent too high. If, instead of uniform droplets, a "C" distribution (table II) of droplets with a volume-median size of 60 microns is present, then the concentration factor at the  $z = 0$  position at distances of 6 and 12 inches from the surface is 0.24 and 1.3, respectively. These examples illustrate the sensitivity of the concentration factor near the ellipsoid surface to changes in the physical environment and the importance of avoiding taking measurements of liquid-water content in a comparable region in the vicinity of an aircraft, as the correction of the indicated water content to free-stream content would be very involved.

Rotating multicylinders. - If the liquid-water-content measuring device has a low collection efficiency (which varies with drop size and flight condition), or depends on a difference in collection efficiency among its component parts, or both, as do rotating multicylinders (refs. 11 and 12), the situation is more complicated, because the indicated water content will not necessarily vary directly with the weighted concentration factor at the point of measurement. This is true because the amount of droplet flux intercepted by each cylinder depends on its collection efficiency. The collection efficiency in turn depends on the droplet velocity, which is one of the two quantities making up flux density (eq. (2)). In addition, reference 13 shows that a variation in droplet concentration over a set of rotating cylinders introduces a false relation between cylinder diameter and relative collection efficiency and thereby affects the droplet-size-distribution and the liquid-water-content measurement. In addition, there is the effect of the change in local droplet-size distribution (which is discussed in the following section) on the measurements

of liquid-water content by the cylinders. Because rotating-multicylinder measurements of liquid-water content and droplet-size distribution are interrelated, a change in local droplet-size distribution will also alter the indicated liquid-water content at the point of interest. These complicating factors make the evaluation of liquid-water-content data taken with rotating cylinders very difficult if the cylinders are located close to the aircraft fuselage.

Fortunately, most liquid-water-content data taken with rotating multicylinders are not too much in error from these factors, because the cylinders are, in practice, generally located far enough from the fuselage so that approximately free-stream conditions prevail. Therefore, the average concentration factor at the position of measurement gives a fair indication of the degree of error in measuring liquid-water content. In typical installations (ref. 11), the lowest cylinder is about 16 inches from the aircraft surface and the top cylinder is about 34 inches from the surface. With the assumed 100-foot ellipsoid moving at 300 mph at 15,000 feet with an air temperature of 1° F and a "C" distribution with a 20-micron volume-median droplet diameter, the variation of concentration factor is given in figure 10(d). At 16 inches from the surface  $C = 1.095$  (about 10 percent high), and at 34 inches  $C = 1.04$  (about 4 percent high). Thus the liquid-water-content measurements would be less than 10 percent too high. Actually, the values of liquid-water content summarized in references 14 and 15 may have a somewhat smaller error due to this effect than indicated by this example, because many of the measurements were obtained by using the local airspeed rather than the free-stream velocity for calculating the total catch of each cylinder. However, in spite of the relatively good location of rotating multicylinders, observers have reported occasional cases where the lower cylinder caught excessively large or small amounts of ice. This was particularly true if the aircraft had a tendency to yaw during the measurements and thus alter the position of the shadow and peak-concentration zones.

Droplet-size-distribution measurements. - Because the local concentration factor is dependent on droplet size, the local droplet-size distribution varies in the vicinity of a body of revolution. Suppose, for example, that the droplet-size distribution of a cloud is given by

$$n_0 = n_1 + n_2 + n_3 + \dots + n_j = \text{droplets/cc}$$

where  $n_j$  = number of droplets in the  $j^{\text{th}}$  size group. Then, since each droplet-size group will have a different concentration factor at a point in the vicinity of the body of revolution, there results from equation (7) (assuming  $U/v_z^2$  nearly equal to 1, as it usually is at the  $z = 0$  and  $z = -0.25$  positions)

$$n = n_1 C_1 + n_2 C_2 + n_3 C_3 + \dots + n_j C_j$$

or

$$n = \sum_j n_j C_j, \text{ droplets/cc} \quad (10)$$

Thus, both the local number of droplets per cubic centimeter and the droplet-size distribution will be different from the free-stream values. When  $U/v'_z$  is not nearly equal to 1 (e.g., near the nose region), then equation (10) has the form

$$n = U \sum_j n_j C_j / v'_{z,j} \quad (11)$$

Equations (10) and (11) clearly indicate that care should be exercised in the choice of location of droplet-size-distribution measuring instruments, such as a cloud-droplet camera, in order to avoid regions in which either the concentration factor or the ratio  $U/v'_z$  differs greatly from 1.

#### CONCLUDING REMARKS

The data of this report are applicable in a quantitative manner only to ellipsoids of revolution with a fineness ratio of 5. They also apply approximately in the vicinity of the nose section of a body of revolution that can be physically matched with the nose section of a fineness-ratio-5 ellipsoid of a given length. Because many bodies of revolution of interest are different in shape from an ellipsoid, the data of this report are primarily useful in pointing out in a qualitative manner the type of variation in liquid-water concentration that might be expected in the vicinity of a body of revolution in flight through a droplet field. The analysis indicates that, for some combinations of the dimensionless parameters  $Re_0$  and  $K$ , the value of the local concentration of liquid water may vary from 0 to several times the free-stream value, depending on the location of the point being considered. Further, the calculations show that the magnitude of the concentration factor at any point is very sensitive to change in the parameters  $Re_0$  and  $K$ .

Lewis Flight Propulsion Laboratory  
National Advisory Committee for Aeronautics  
Cleveland, Ohio, April 26, 1954

## REFERENCES

1. Brun, Rinaldo J., Serafini, John S., and Gallagher, Helen M.: Impingement of Cloud Droplets on Aerodynamic Bodies as Affected by Compressibility of Air Flow Around the Body. NACA TN 2903, 1953.
2. Dorsch, Robert G., Brun, Rinaldo, J., and Gregg, John L.: Impingement of Water Droplets on an Ellipsoid with Fineness Ratio 5 in Axisymmetric Flow. NACA TN 3099, 1954.
3. Lamb, Horace: Hydrodynamics. First Am. ed., Dover Pub., 1945.
4. Brun, Rinaldo J., Gallagher, Helen M., and Vogt, Dortha E.: Impingement of Water Droplets on NACA 65<sub>1</sub>-208 and 65<sub>1</sub>-212 Airfoils at 4° Angle of Attack. NACA TN 2952, 1953.
5. Langmuir, Irving, and Blodgett, Katherine B.: A Mathematical Investigation of Water Droplet Trajectories. Tech. Rep. No. 5418, Air Materiel Command, AAF, Feb. 19, 1946. (Contract No. W-33-038-ac-9151 with General Electric Co.)
6. Fraser, D.: Orifice-Type Ice Detector: Preliminary Icing Tunnel Tests of Functioning as Ice Detector, Rate-of-Icing Meter, and Icing-Severity Meter. Lab. Rep. LR-3, Nat. Aero. Establishment, Ottawa (Canada), July 1951.
7. Perkins, Porter J., McCullough, Stuart, and Lewis, Ralph D.: A Simplified Instrument for Recording and Indicating Frequency and Intensity of Icing Conditions Encountered in Flight. NACA RM E51E16, 1951.
8. Neel, Carr B., Jr., and Steinmetz, Charles P.: The Calculated and Measured Performance Characteristics of a Heated-Wire Liquid-Water-Content Meter for Measuring Icing Severity. NACA TN 2615, 1952.
9. McCullough, Stuart, and Perkins, Porter J.: Flight Camera for Photographing Cloud Droplets in Natural Suspension in the Atmosphere. NACA RM E50K01a, 1951.
10. Pettit, K. G.: Nephelometric Instrumentation for Aircraft Icing Research. Rep. No. MD-33, National Res. Council of Canada (Ottawa), Aug. 1950.
11. Lewis, William, Perkins, Porter J., and Brun, Rinaldo J.: Procedure for Measuring Liquid-Water Content and Droplet Sizes in Supercooled Clouds by Rotating Multicylinder Method. NACA RM E53D23, 1953.

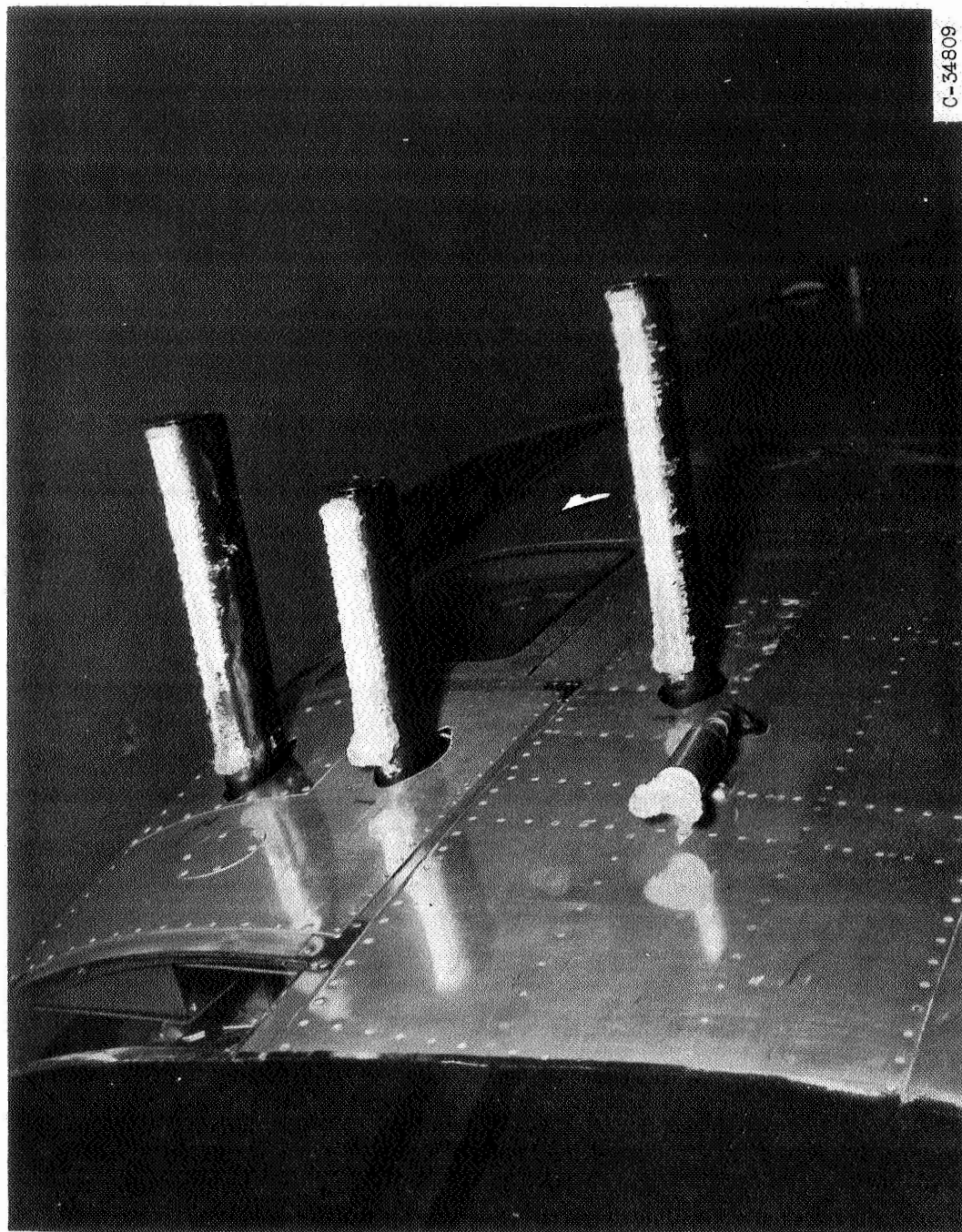
12. Brun, Rinaldo J., and Mergler, Harry W.: Impingement of Water Droplets on a Cylinder in an Incompressible Flow Field and Evaluation of Rotating Multicylinder Method for Measurement of Droplet-Size Distribution, Volume-Median Droplet Size, and Liquid-Water Content in Clouds. NACA TN 2904, 1953.
13. Lewis, William, Kline, Dwight B., and Steinmetz, Charles P.: A Further Investigation of the Meteorological Conditions Conducive to Aircraft Icing. NACA TN 1424, 1947.
14. Lewis, William, and Bergrun, Norman R.: A Probability Analysis of the Meteorological Factors Conducive to Aircraft Icing in the United States. NACA TN 2738, 1952.
15. Hacker, Paul T., and Dorsch, Robert G.: A Summary of Meteorological Conditions Associated with Aircraft Icing and a Proposed Method of Selecting Design Criteria for Ice-Protection Equipment. NACA TN 2569, 1951.

TABLE I. - RELATION OF DIMENSIONLESS PARAMETERS TO BODY SIZE AND ATMOSPHERIC AND FLIGHT CONDITIONS

Atmospheric condition	Ellipsoid velocity, U, mph	Drop-let diameter, d, microns	Major axis, L, ft	Pressure altitude, ft													
				5000						15,000						25,000	
				Temperature, °F													
				20				1				-25					
Re <sub>0</sub>	K	1/K	Re <sub>0</sub>	K	1/K	Re <sub>0</sub>	K	1/K	Re <sub>0</sub>	K	1/K						
Cloud droplets	50	10	3	14.7	0.008123	123.1	10.72	0.008383	119.3	7.836	0.008793	113.7					
			30	14.7	.0008123	1231	10.72	.0008383	1193	7.836	.0008793	1137					
			100	14.7	.0002437	4103	10.72	.0002515	3976	7.836	.0002638	3791					
		50	73.54	0.2031	4.924	53.62	0.2096	4.771	39.17	0.2198	4.550						
			73.54	.02031	49.24	53.62	.02096	47.71	39.17	.02198	45.50						
			73.54	.006092	164.1	53.62	.006289	159.0	39.17	.006594	151.7						
	100	20	58.81	0.01949	51.31	42.89	0.02012	49.70	31.34	0.02110	47.39						
		50	58.81	.003898	256.5	42.89	.004024	248.5	31.34	.00422	237.0						
		300	58.81	.0006497	1539	42.89	.0006707	1491	31.34	.0007033	1422						
	300	20	176.4	0.05846	17.11	128.7	0.06037	16.56	94.00	0.06330	15.8						
		50	176.4	.01169	85.54	128.7	.01267	82.85	94.00	.01266	78.99						
		100	88.2	0.001462	684.0	64.4	0.010509	662.7	47.01	0.001583	631.7						
		20	176.4	0.005846	171.1	128.7	0.006037	165.6	94.00	0.006330	158.0						
		300	176.4	.001949	513.1	128.7	.002012	497.0	94.00	.002110	473.9						
	500	20	294.1	0.09745	10.26	214.5	0.1006	9.940	156.7	0.1055	9.479						
		50	294.1	.01949	51.31	214.5	.02012	49.70	156.7	.02110	47.39						
		100	294.1	.009745	102.6	214.5	.01006	99.40	156.7	.01055	94.79						
		50	735.4	2.031	0.4924	536.2	2.096	0.4771	391.7	2.198	0.4550						
		30	735.4	.2031	4.924	536.2	.2096	4.771	391.7	.2198	4.550						
		100	735.4	.06092	16.41	536.2	.06289	15.90	391.7	.06594	15.17						
Drizzle	100	400	1176	7.796	0.1283	857.7	8.050	0.1242	626.7	8.442	0.1185						
	300	400	3529	2.339	0.4275	2574	2.415	0.4141	1880	2.532	0.3949						
		300	3529	.7797	1.283	2574	.8050	1.242	1880	.8440	1.185						
	500	400	5882	1.299	0.7698	4289	1.342	0.7452	3134	1.407	0.7107						
Rain	300	1000	8823	29.24	0.03420	6434	30.18	0.03313	4701	31.66	0.03159						
		100	8823	14.62	.06840	6434	15.09	.06827	4701	15.83	.06317						
		300	8823	4.873	.20520	6434	5.030	.1968	4701	5.277	.1895						

TABLE II. - "C" DROPLET-SIZE DISTRIBUTION  
(ref. 5)

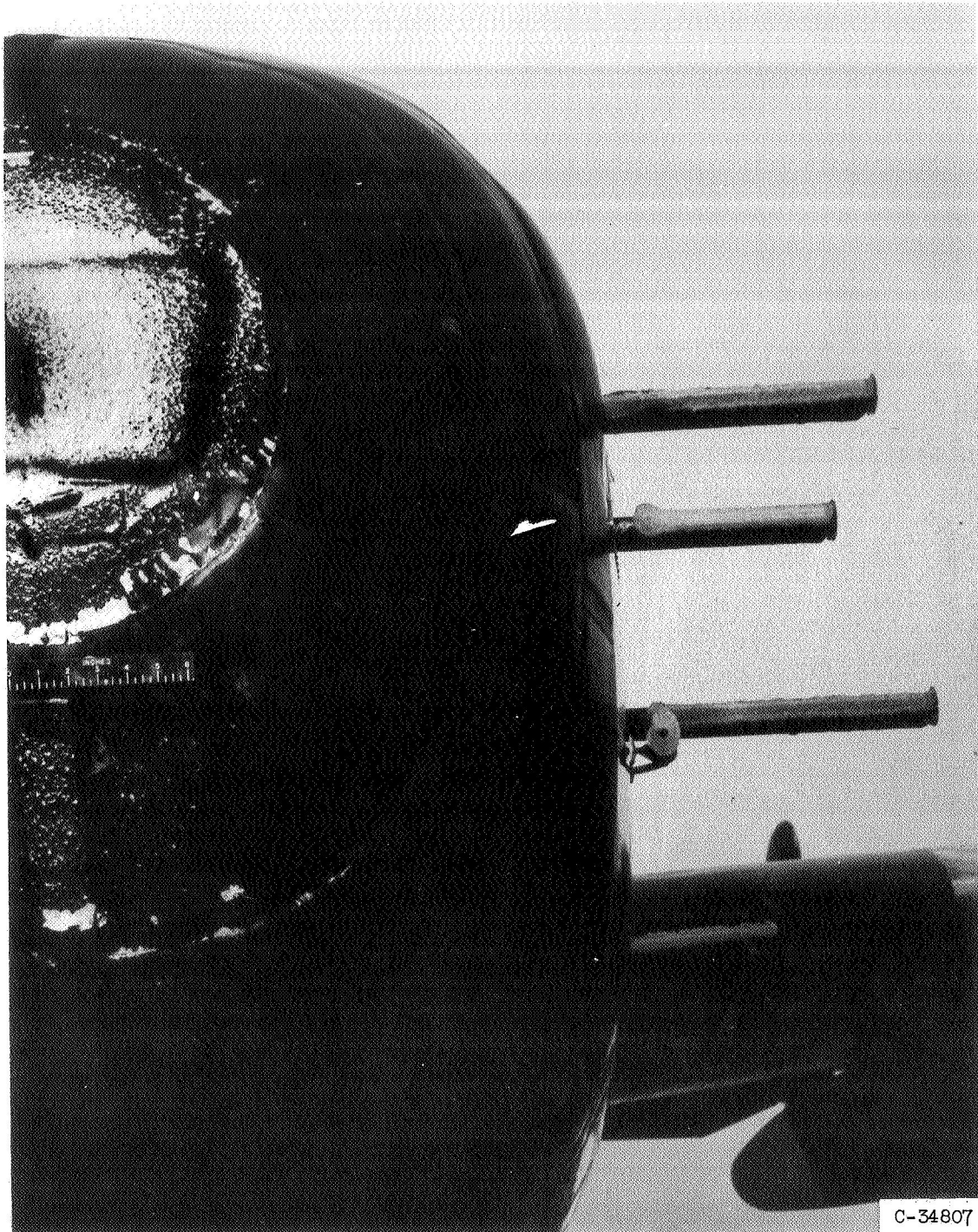
Total liquid water in each group, percent	Ratio of av. drop diam. of each group to volume-median droplet diam., $d/d_{med}$
5	0.42
10	.61
20	.77
30	1.00
20	1.26
10	1.51
5	1.81



(a) Side view of ice on 1-inch-thick icing-rate-meter support rods.

Figure 1. - Ice formations on B-25 aircraft after flight at 200 mph through supercooled clouds.

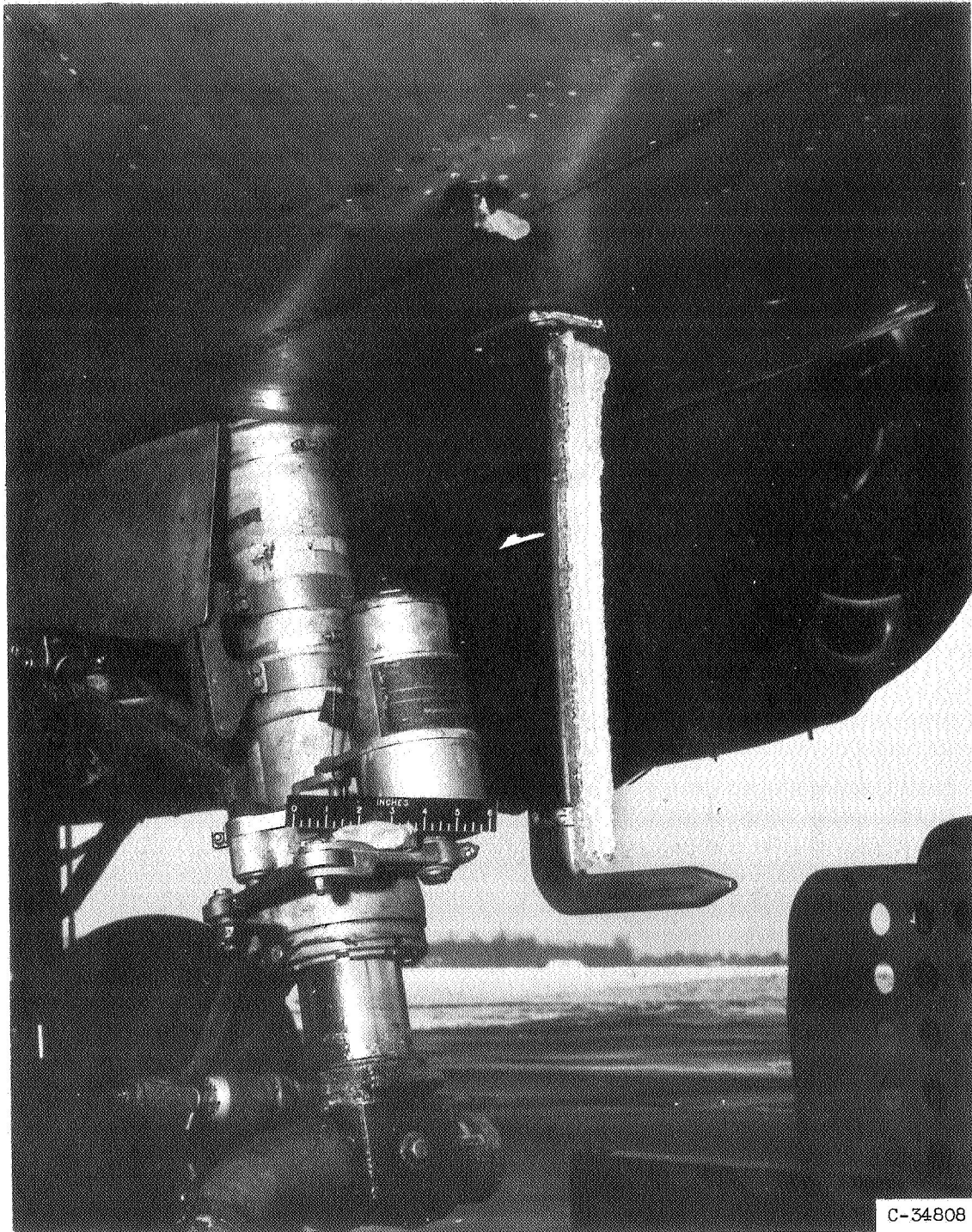




(b) Front view of ice on 1-inch-thick icing-rate-meter support rods.

Figure 1. - Continued. Ice formations on B-25 aircraft after flight at 200 mph through supercooled clouds.

3106



(c) Ice accumulation on pressure probe.

Figure 1. - Concluded. Ice formations on B-25 aircraft after flight at 200 mph through supercooled clouds.

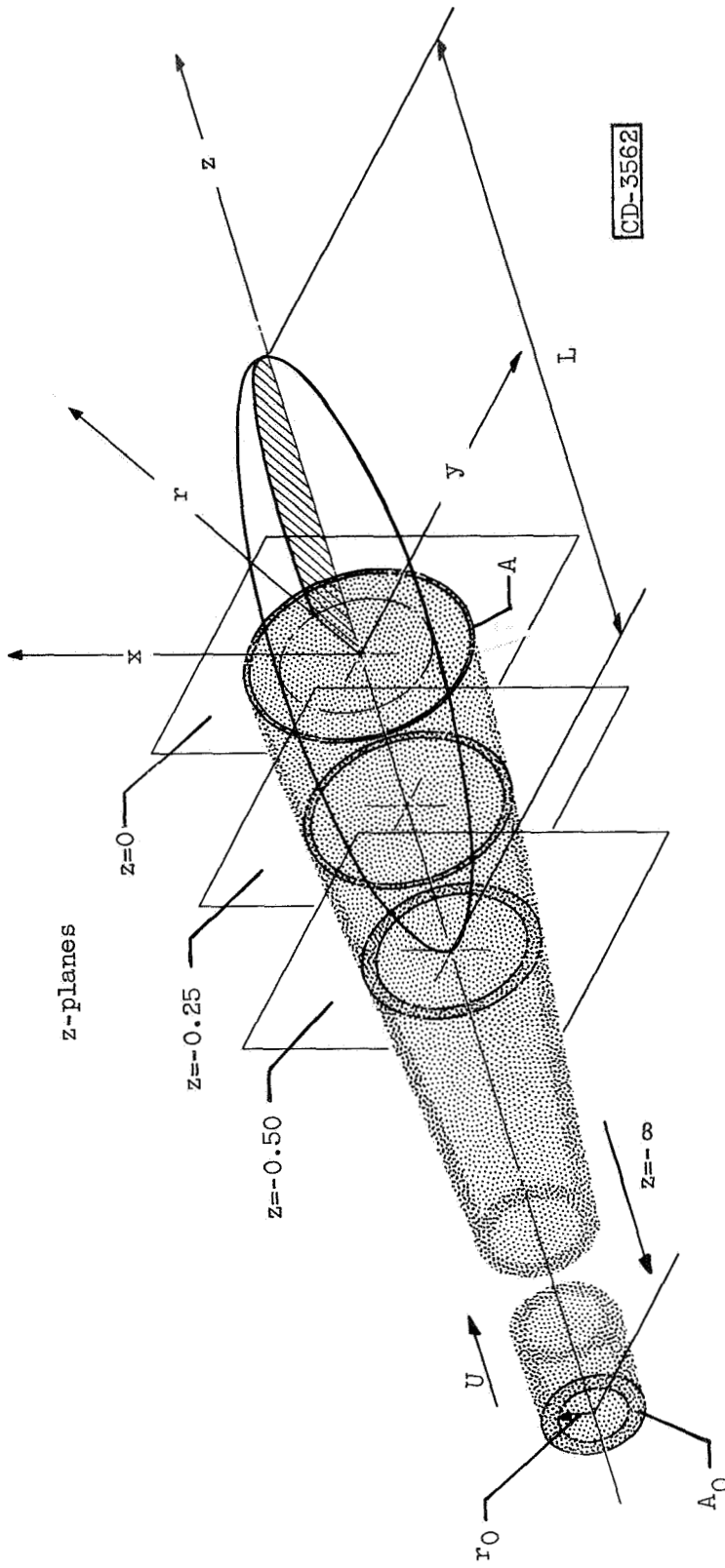


Figure 2. - Coordinate system for droplet trajectory calculations.

3106

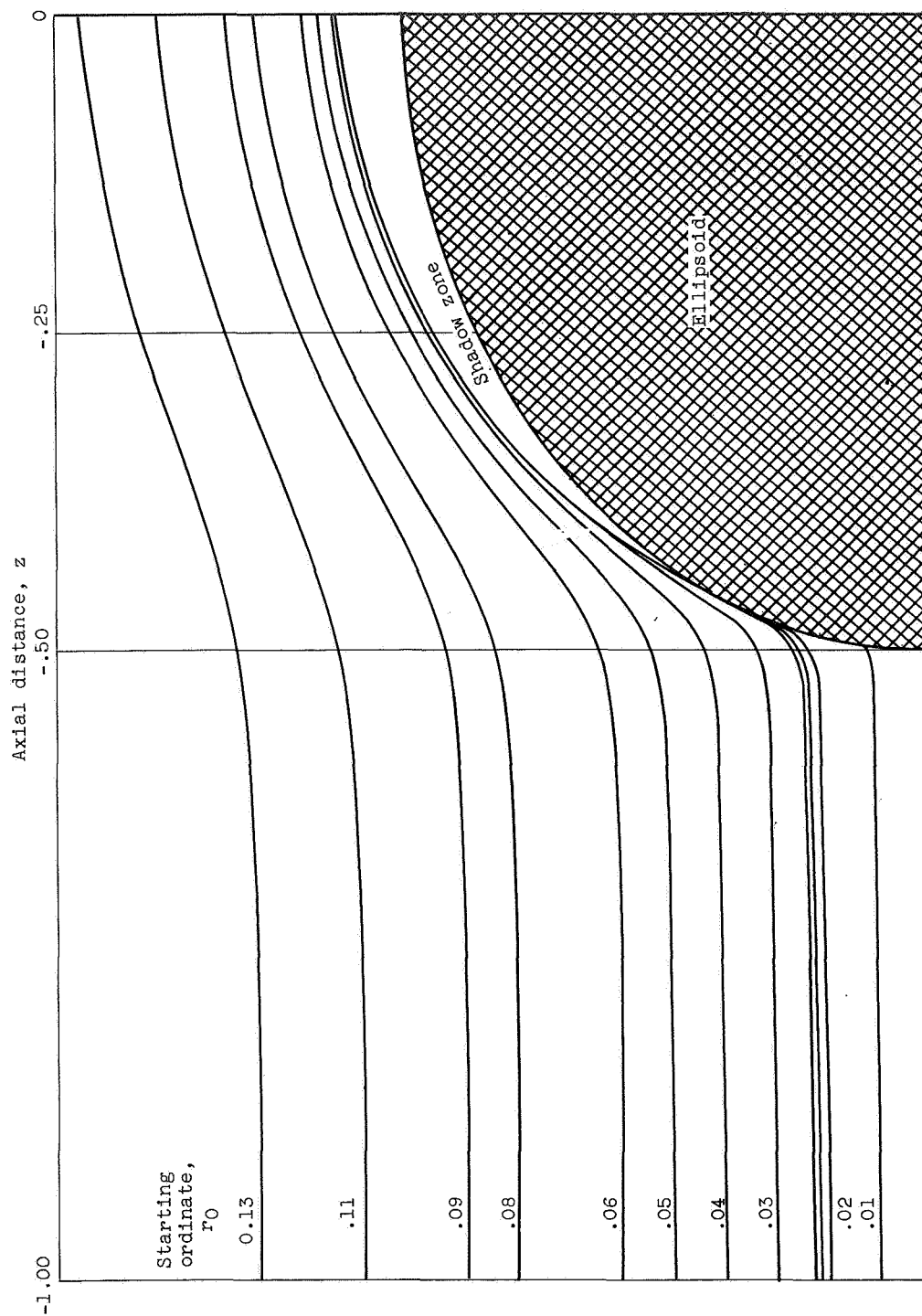
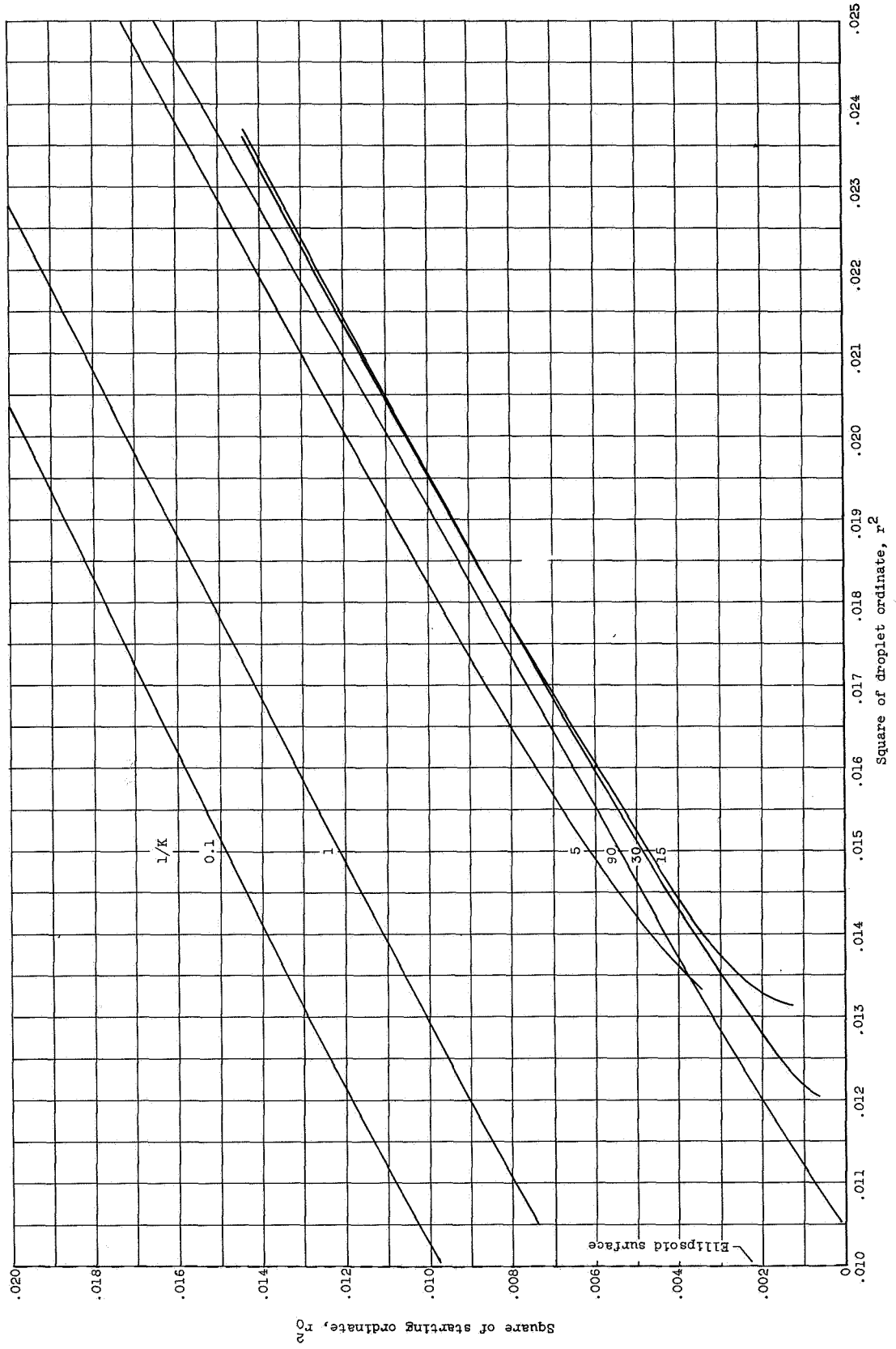


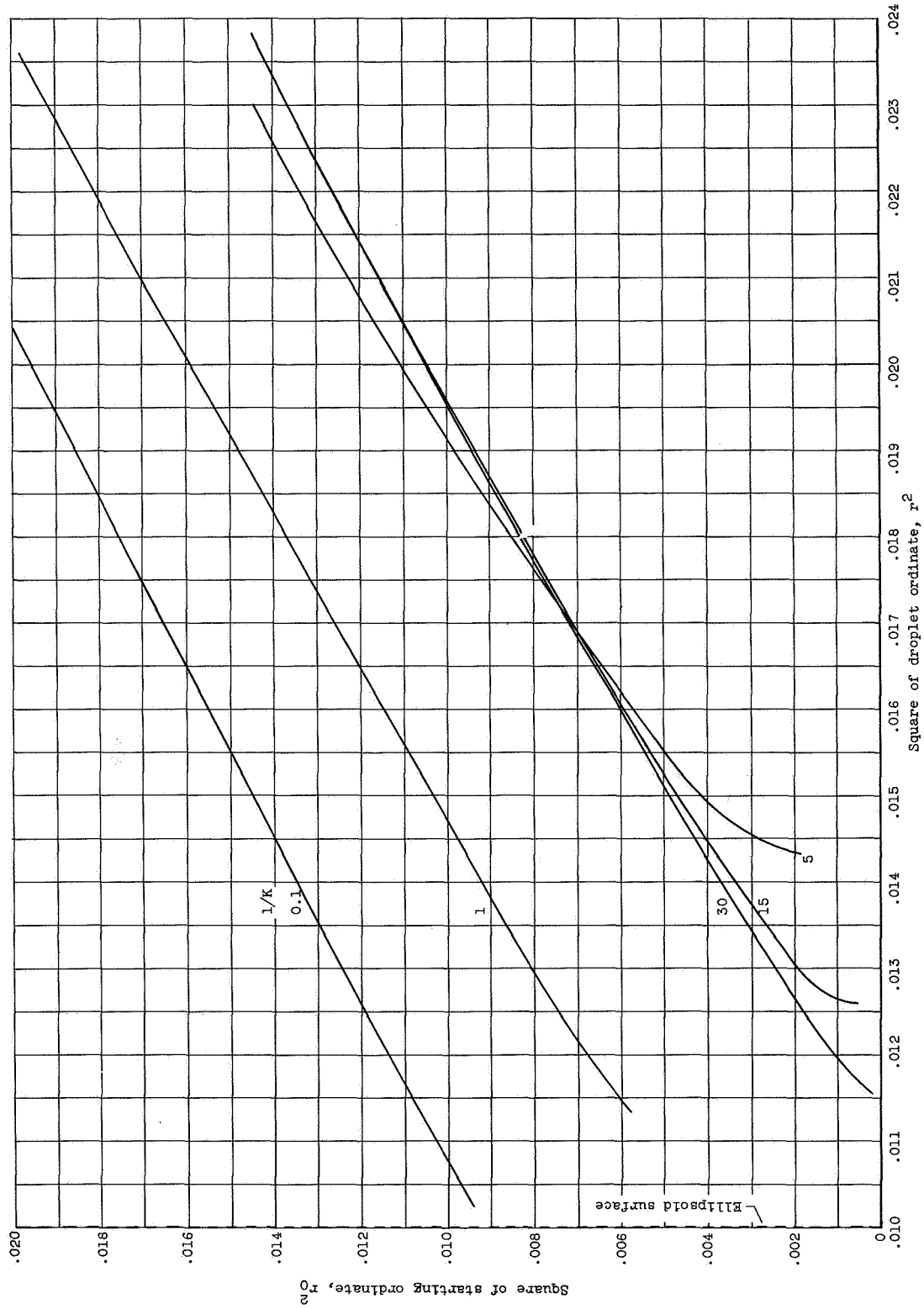
Figure 3. - Droplet trajectories about ellipsoid of fineness ratio 5 for free-stream Reynolds number  $Re_0$  of 128 and  $1/K$  of 15. (Ordinate scale expanded 4 times that of abscissa.)



(a)  $z = 0$ ;  $Re_0 = 0$ .  
Figure 4. - Square of starting ordinate as function of square of droplet ordinate at constant z-position.

3106

CE-4



(b)  $z = 0$ ;  $Re_0 = 128$ .  
Figure 4. - Continued. Square of starting ordinate as function of square of droplet ordinate at constant z-position.

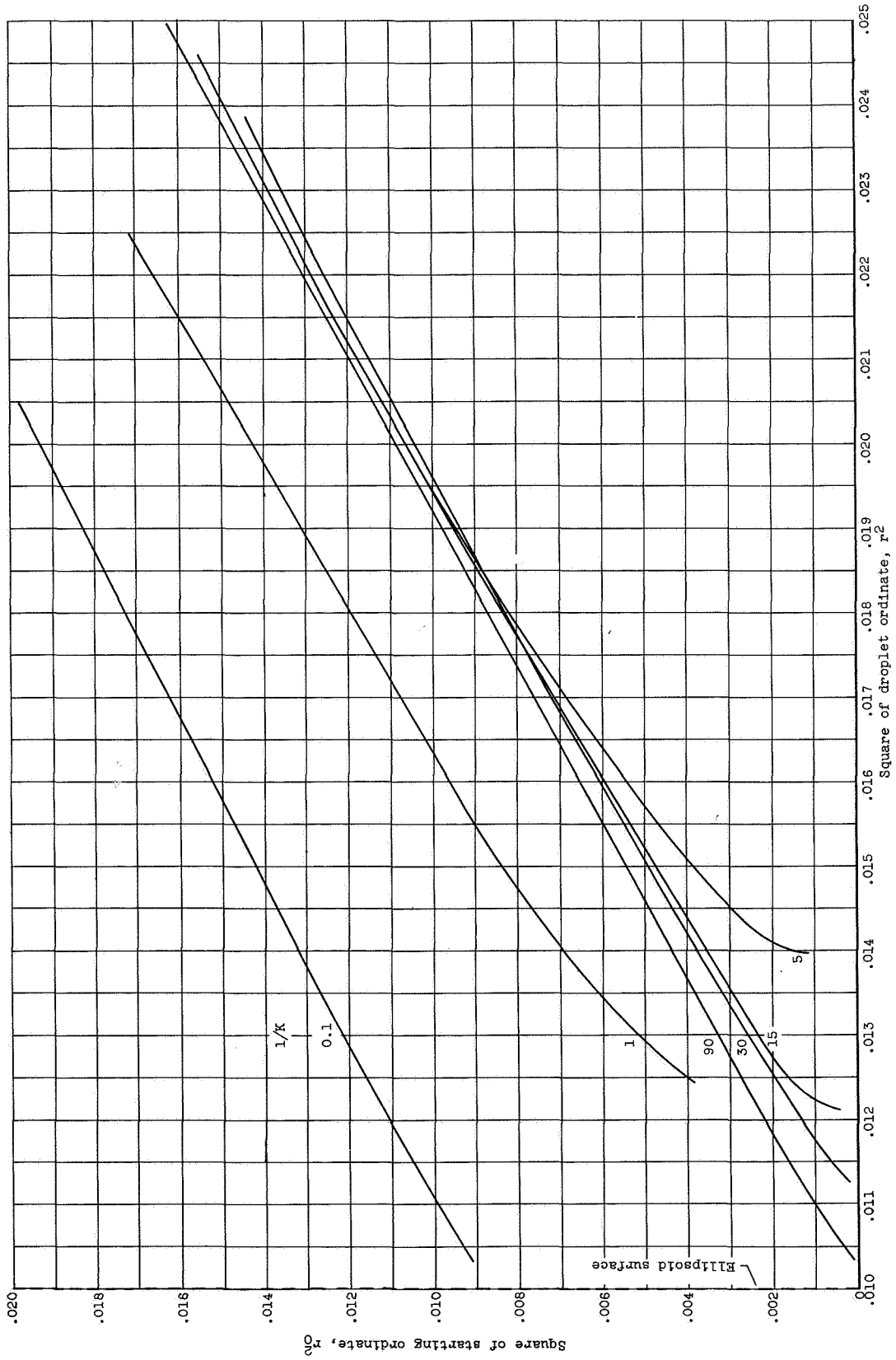


Figure 4. - Continued. Square of starting ordinate as function of square of droplet ordinate at constant z-position.  
(c)  $z = 0$ ;  $Re_0 = 512$ .



3106

U. S. DEPARTMENT OF COMMERCE

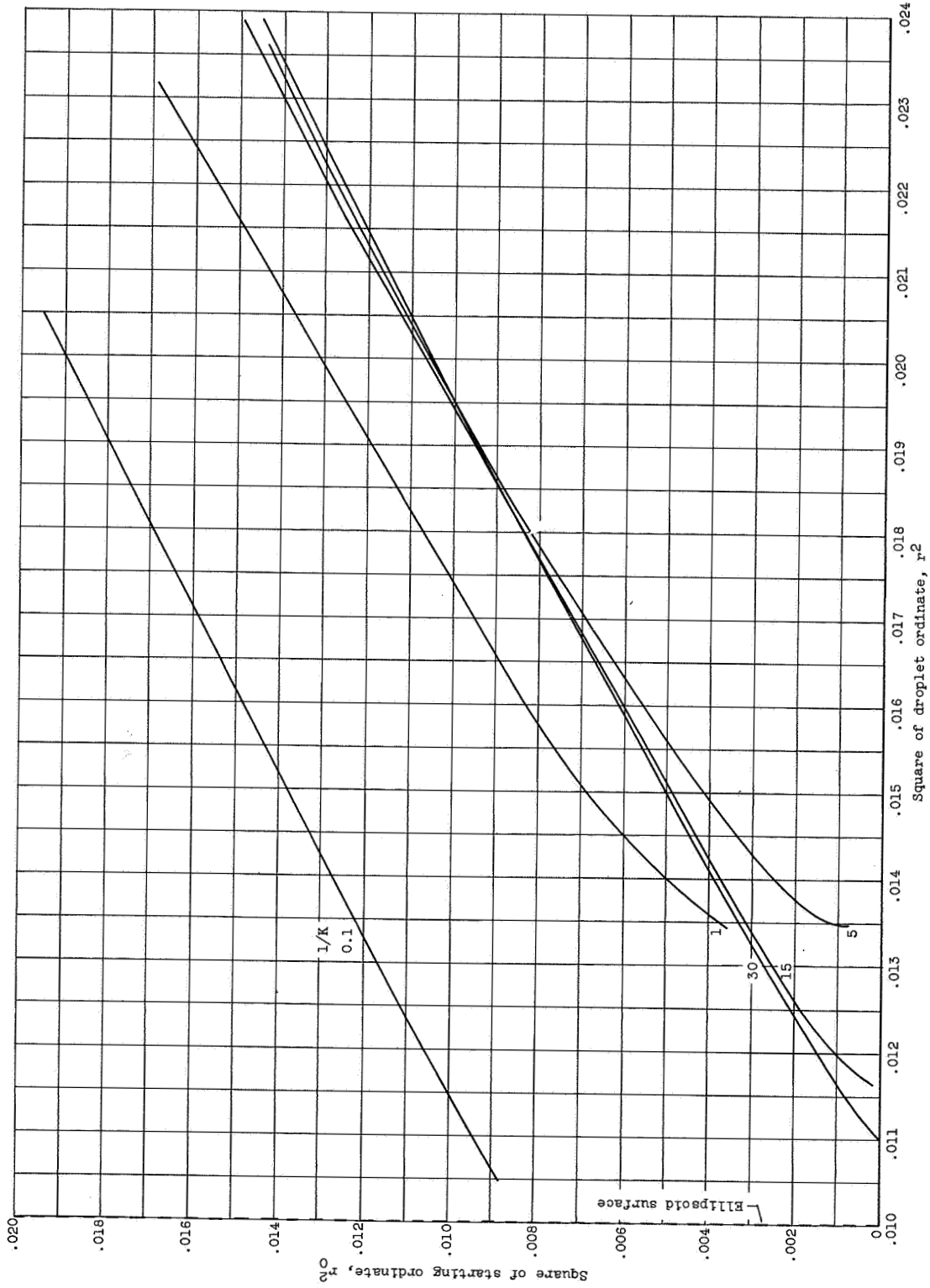


Figure 4. - Continued. Square of starting ordinate as function of square of droplet ordinate at constant z-position. (d)  $z = 0$ ;  $Re_0 = 1024$ .



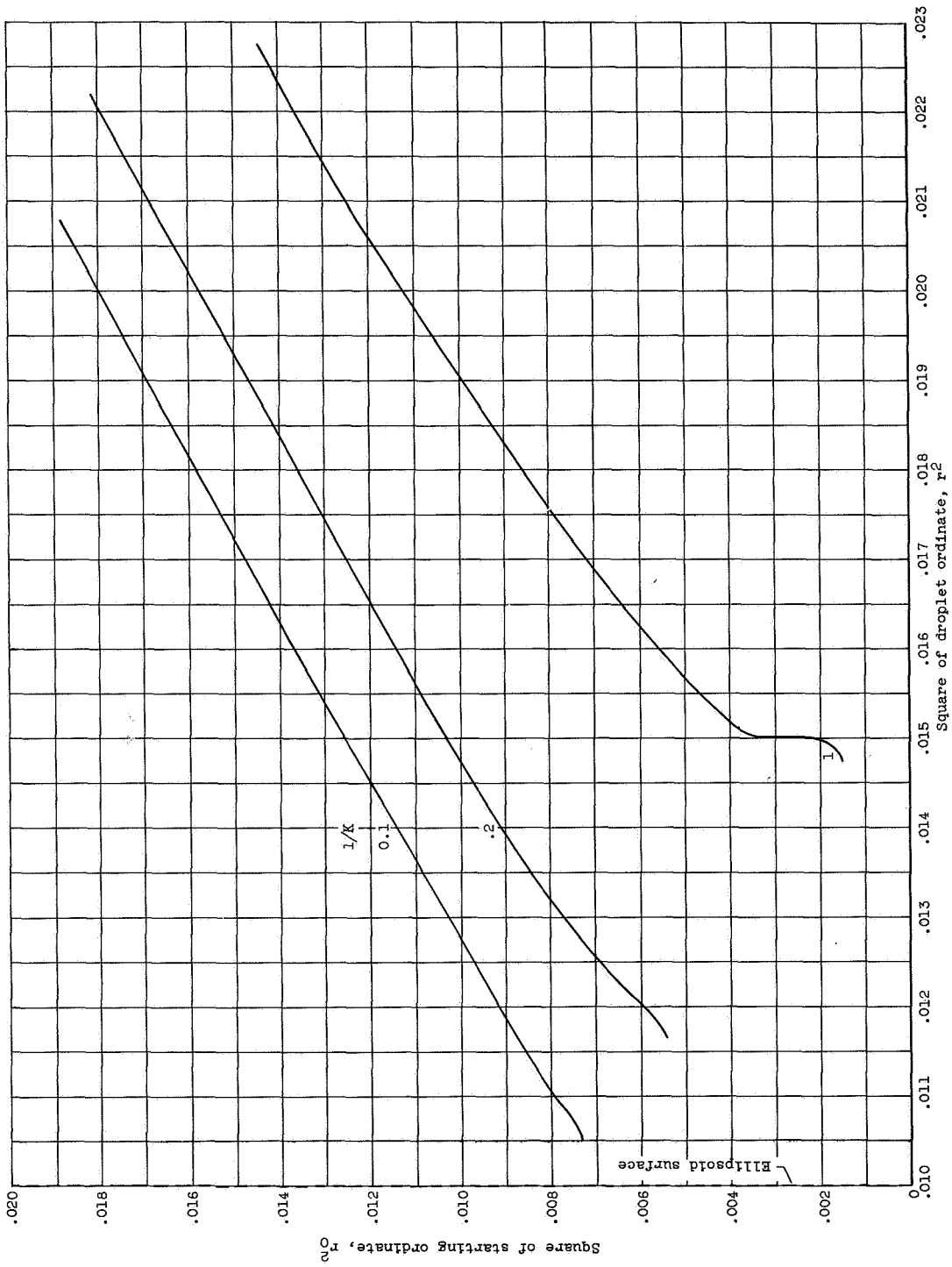
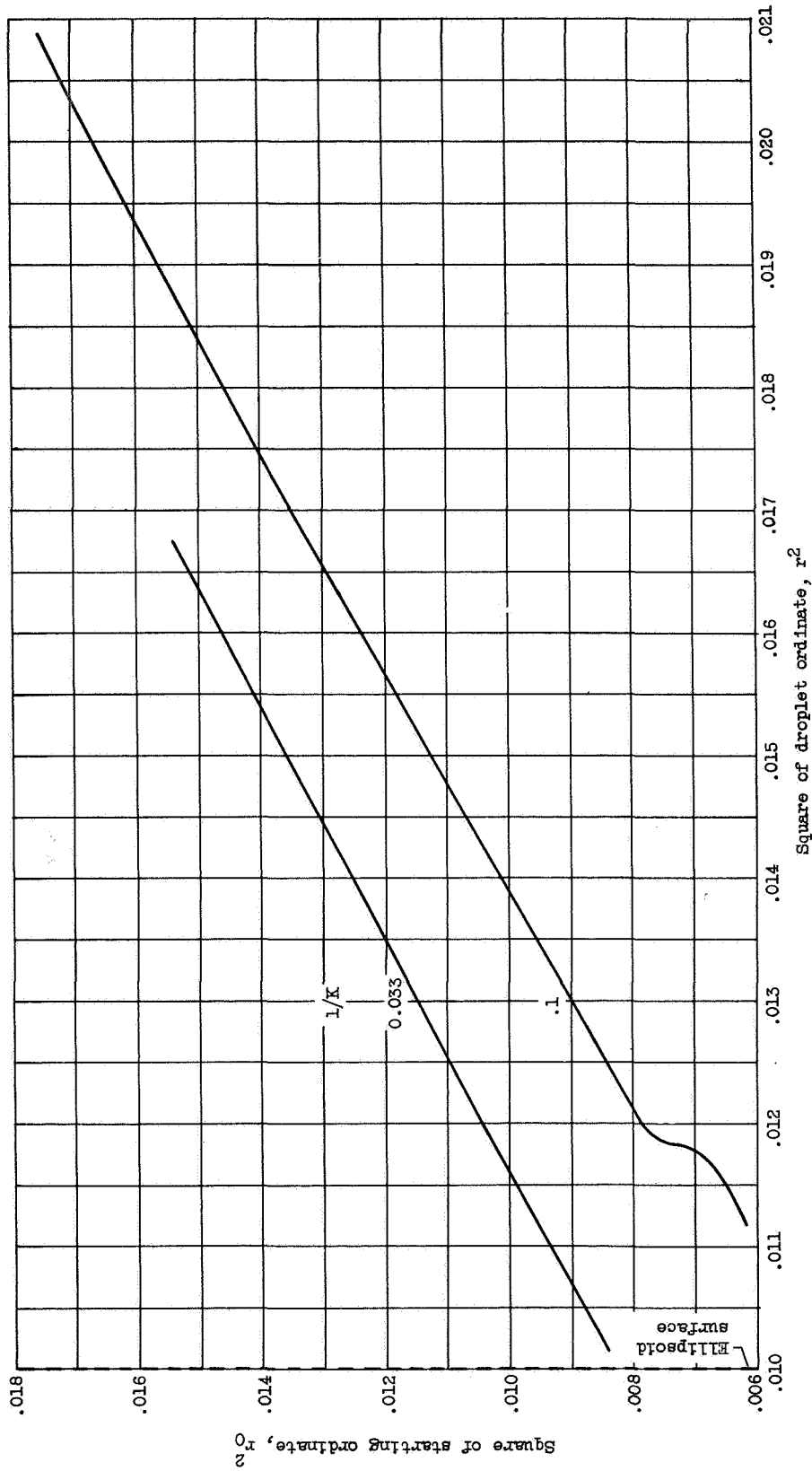


Figure 4. - Continued. Square of starting ordinate as function of square of droplet ordinate at constant z-position.  
(e)  $z = 0$ ;  $Re_0 = 4096$ .



(f)  $z = 0$ ;  $Re_0 = 8192$ .

Figure 4. - Continued. Square of starting ordinate as function of square of droplet ordinate at constant z-position.

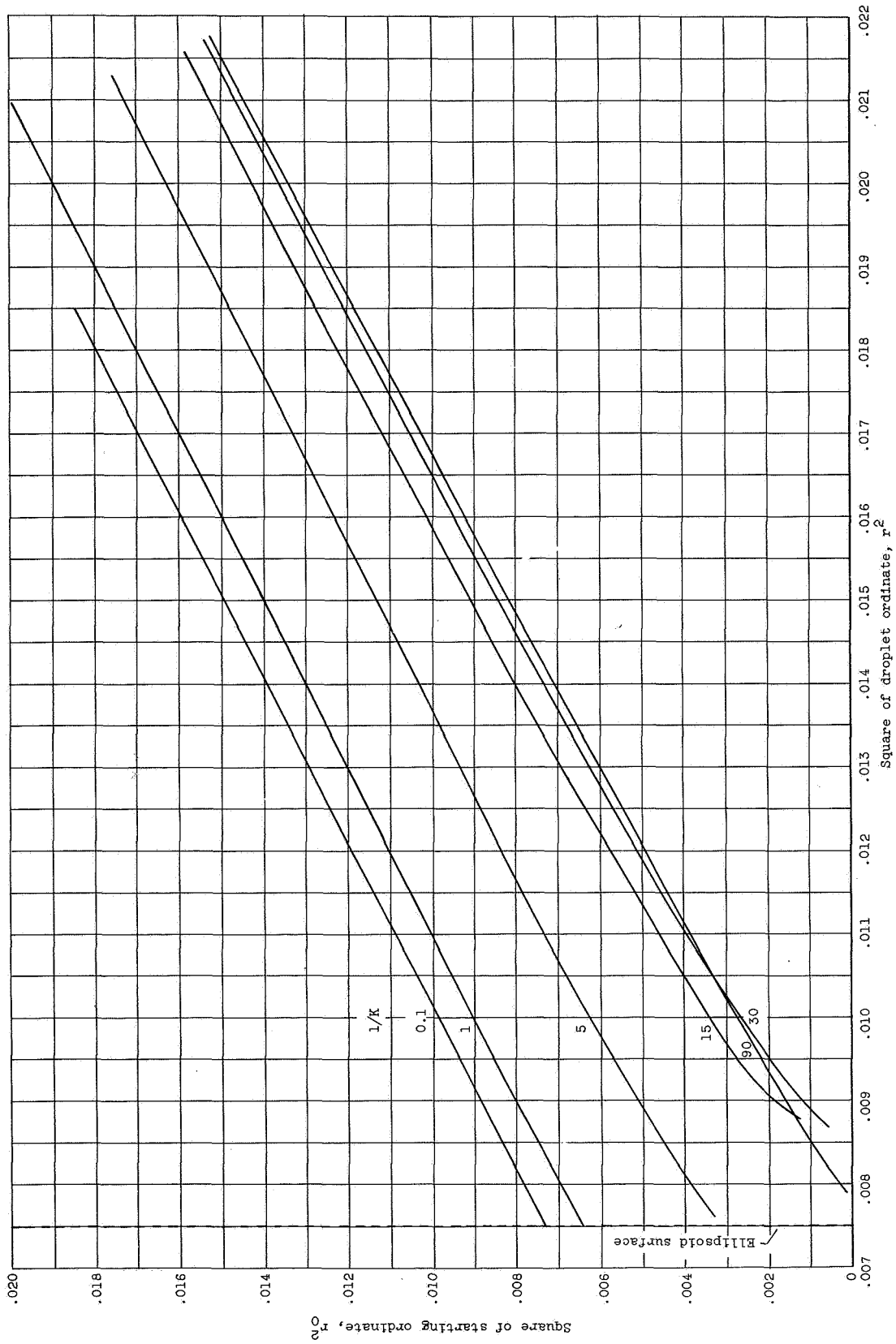


Figure 4. - Continued. Square of starting ordinate as function of square of droplet ordinate at constant z-position.  
(g)  $z = -0.25$ ;  $Re_0 = 0$ .

3106

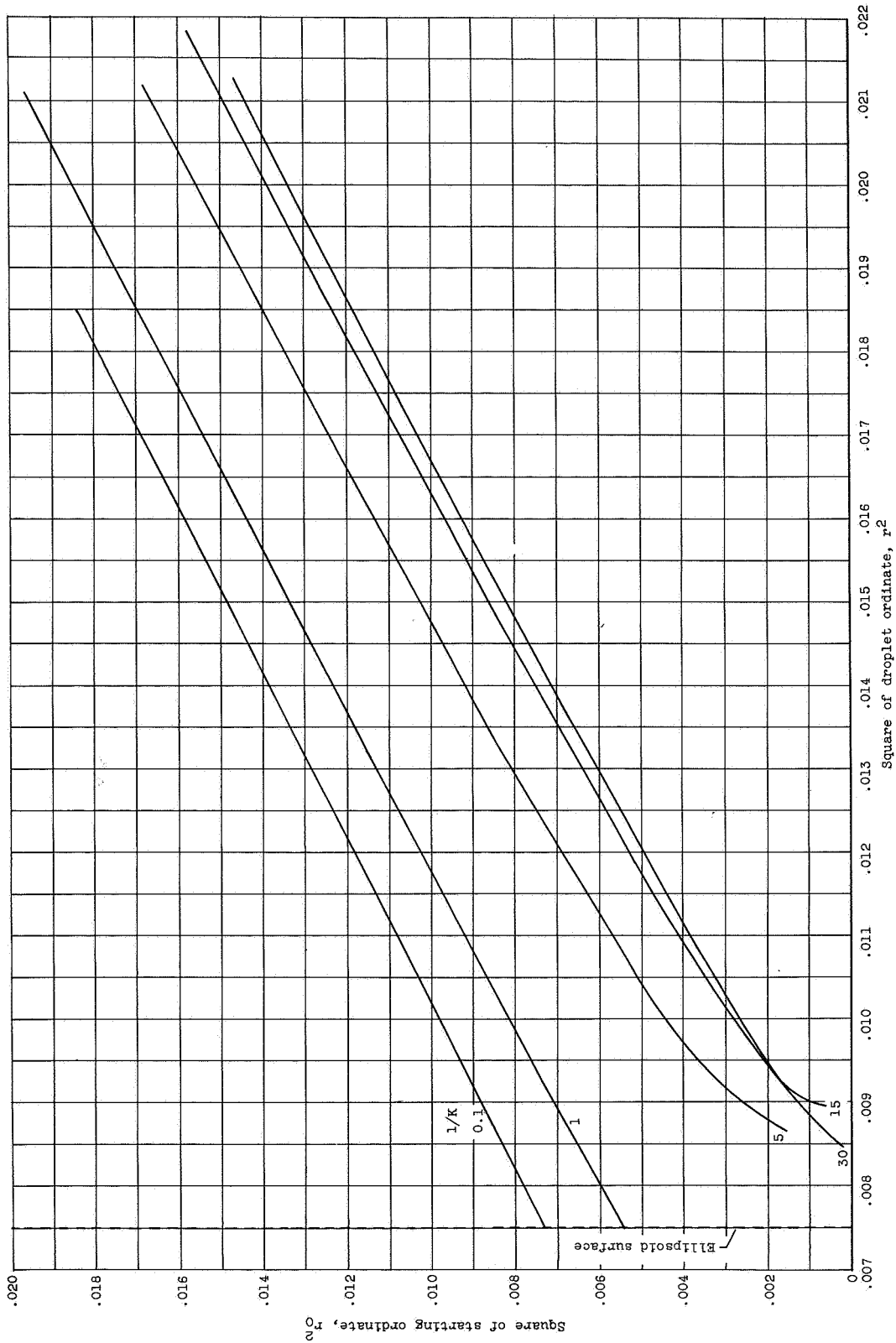


Figure 4. - Continued. Square of starting ordinate as function of square of droplet ordinate at constant z-position.  
(h)  $z = -0.25$ ;  $Re_0 = 128$ .

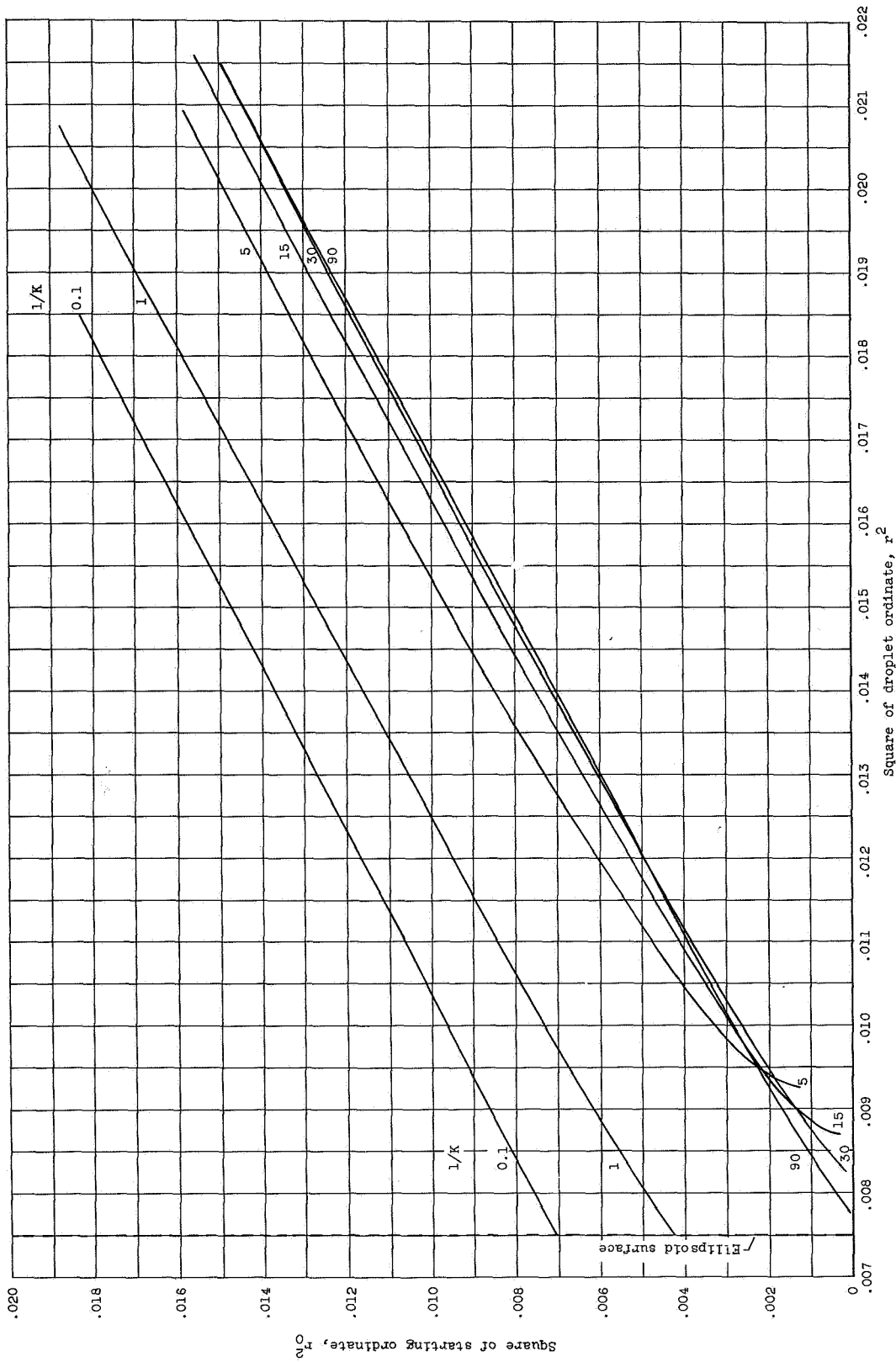


Figure 4. - Continued. Square of starting ordinate as function of square of droplet ordinate at constant z-position.  
(1)  $z = -0.25$ ;  $Re_0 = 512$ .

CE-5 3106

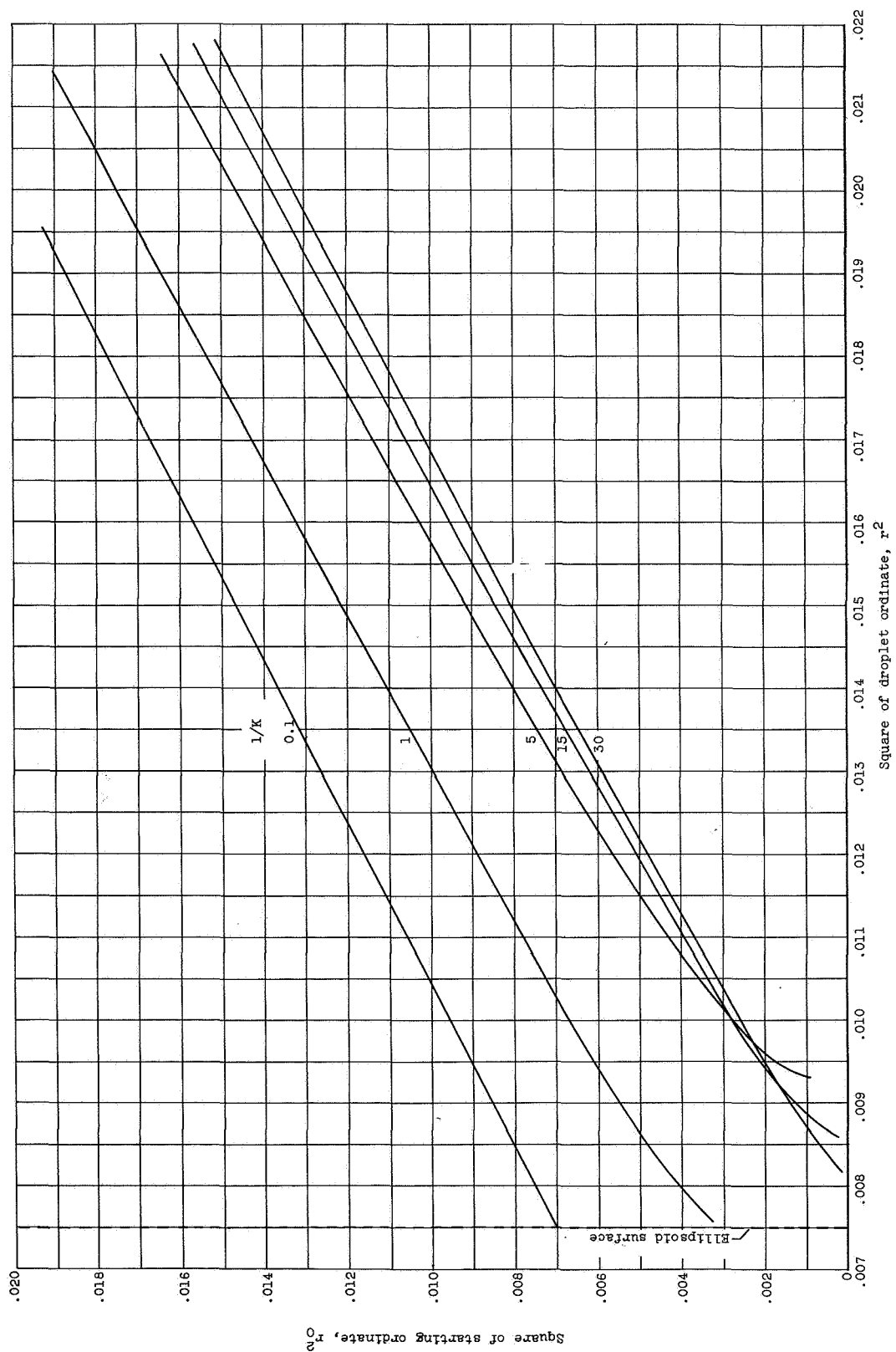


Figure 4. - Continued. Square of starting ordinate as function of square of droplet ordinate at constant z-position. (j)  $z = -0.25$ ;  $Re_0 = 1024$ .

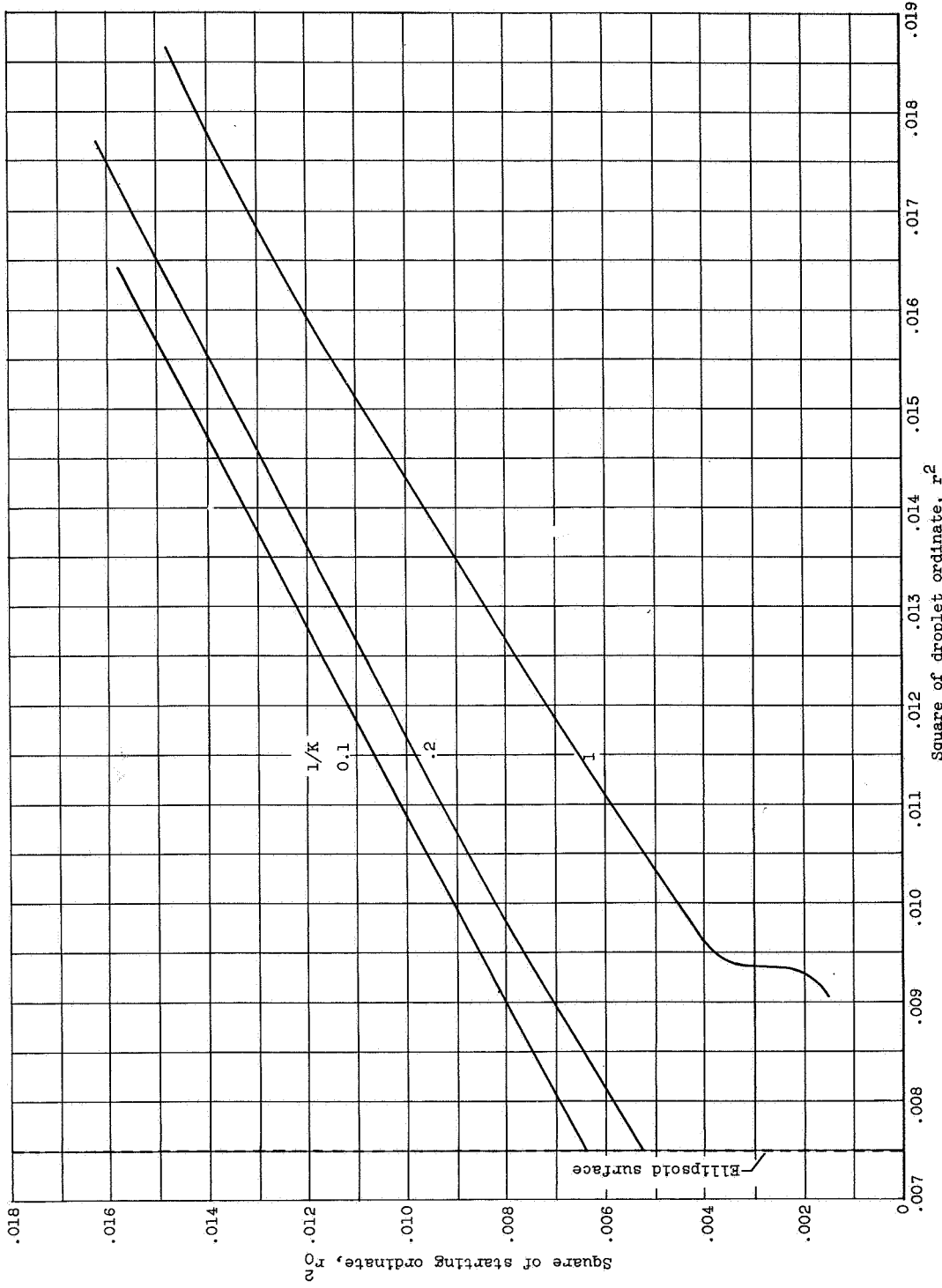
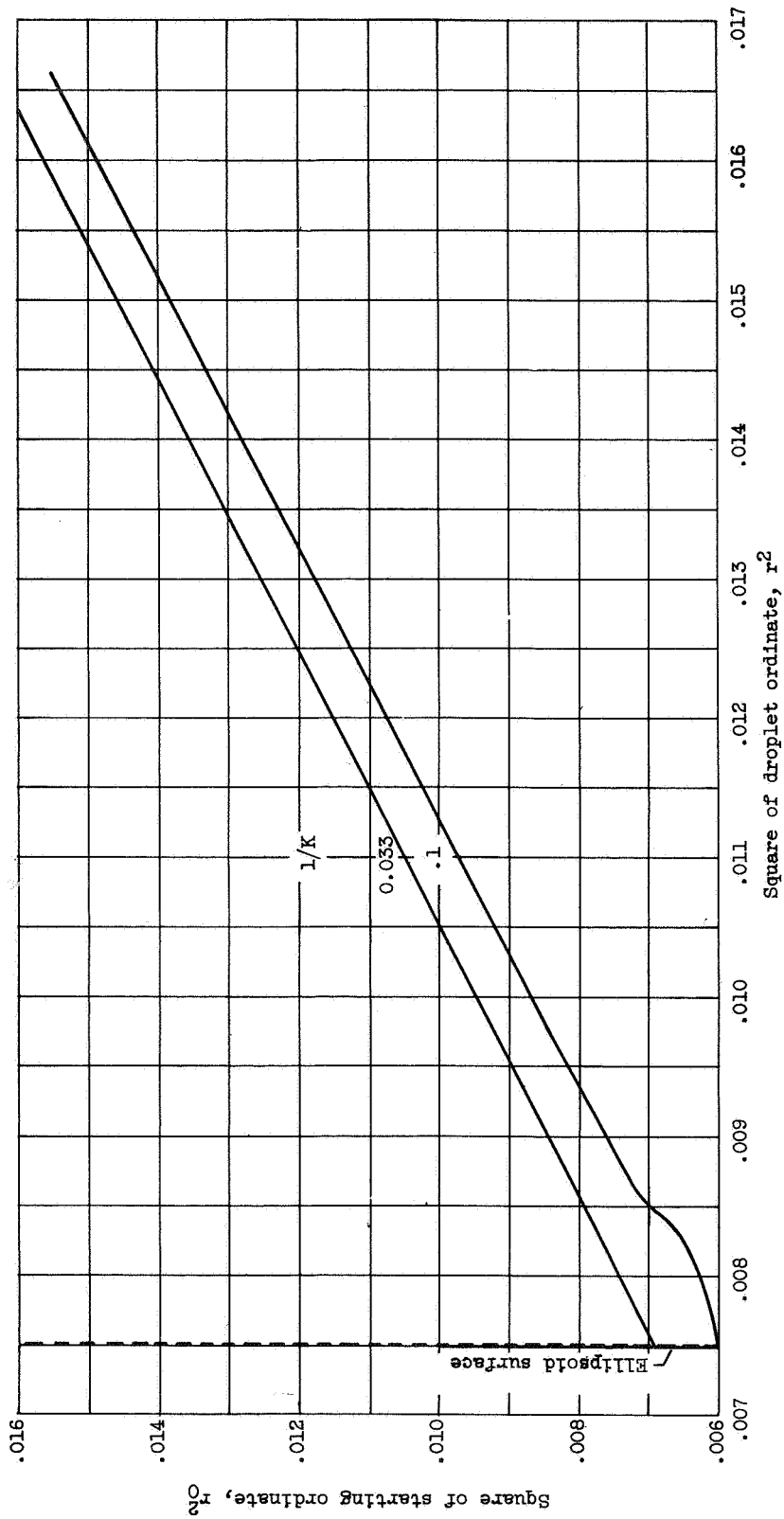


Figure 4. - Continued. Square of starting ordinate as function of square of droplet ordinate at constant z-position.  
(k) z = -0.25; Re<sub>0</sub> = 4096.

3106

CE-5 back



(1)  $z = -0.25$ ;  $Re_0 = 8192$ .

Figure 4. - Continued. Square of starting ordinate as function of square of droplet ordinate at constant z-position.



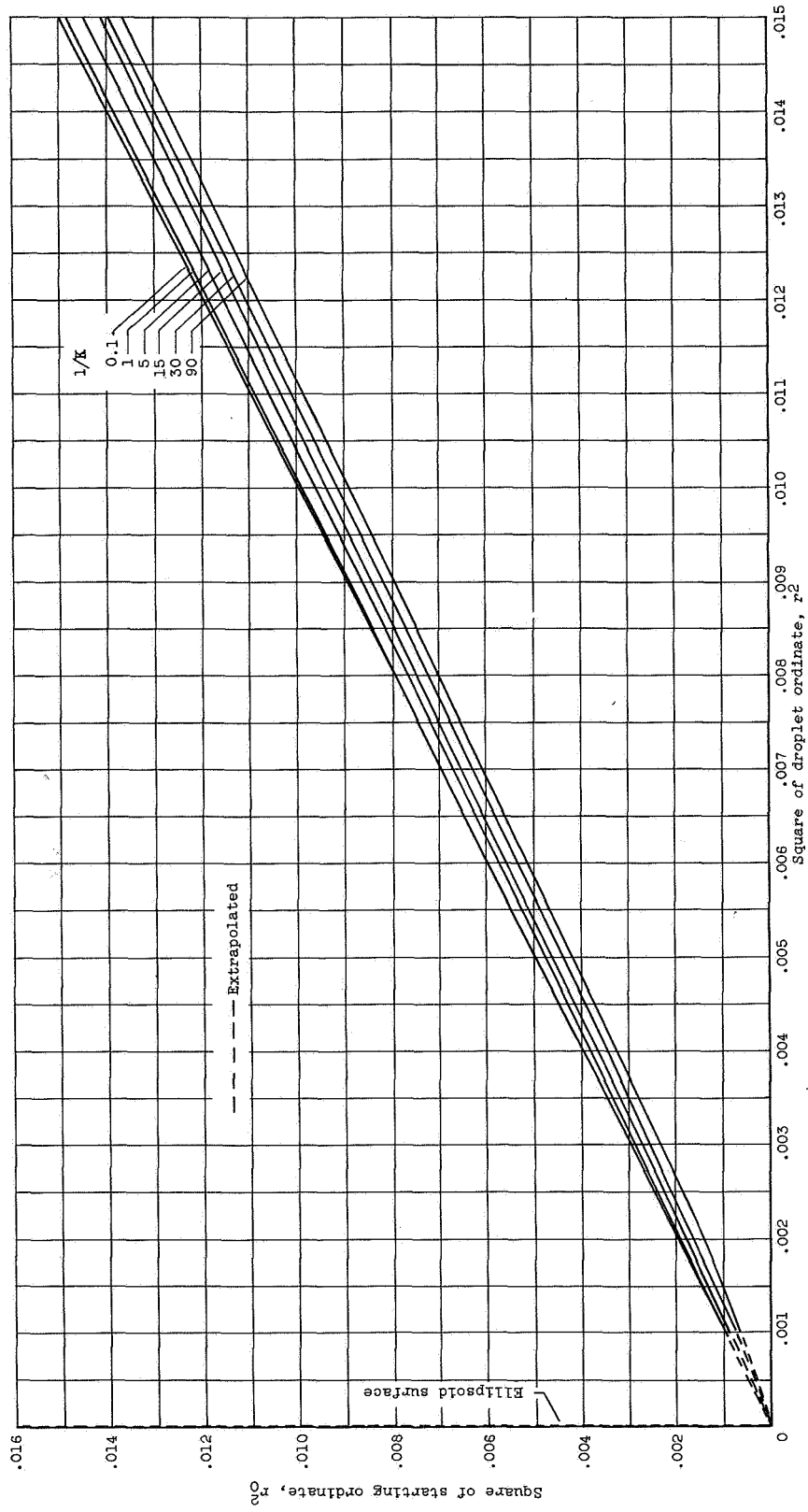


Figure 4. - Continued. Square of starting ordinate as function of square of droplet ordinate at constant z-position. ( $m$ )  $z = -0.5$ ;  $Re_0 = 0$ .

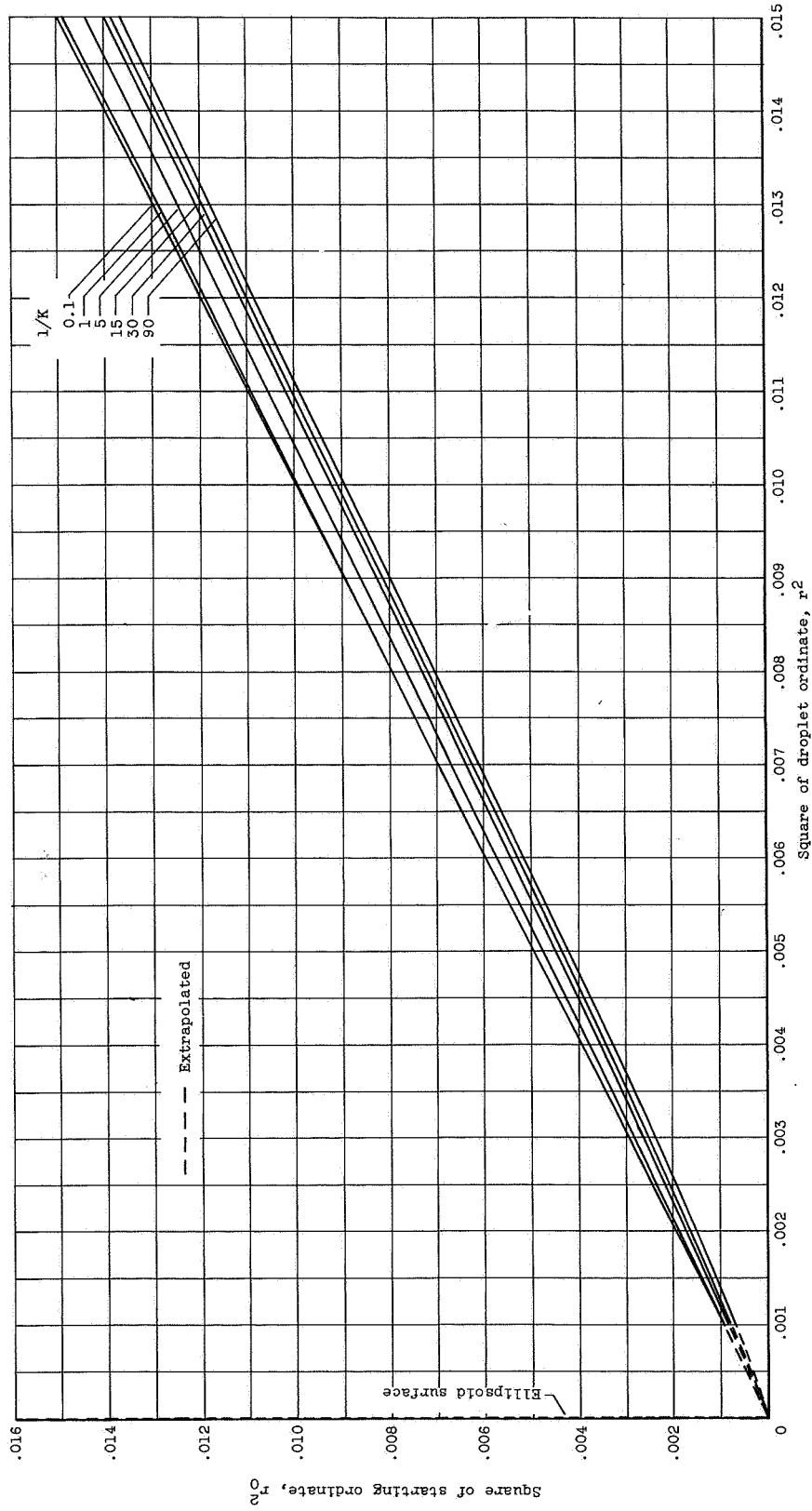


Figure 4. - Continued. Square of starting ordinate as function of square of droplet ordinate at constant z-position. (n)  $z = -0.5$ ;  $Re_0 = 128$ .

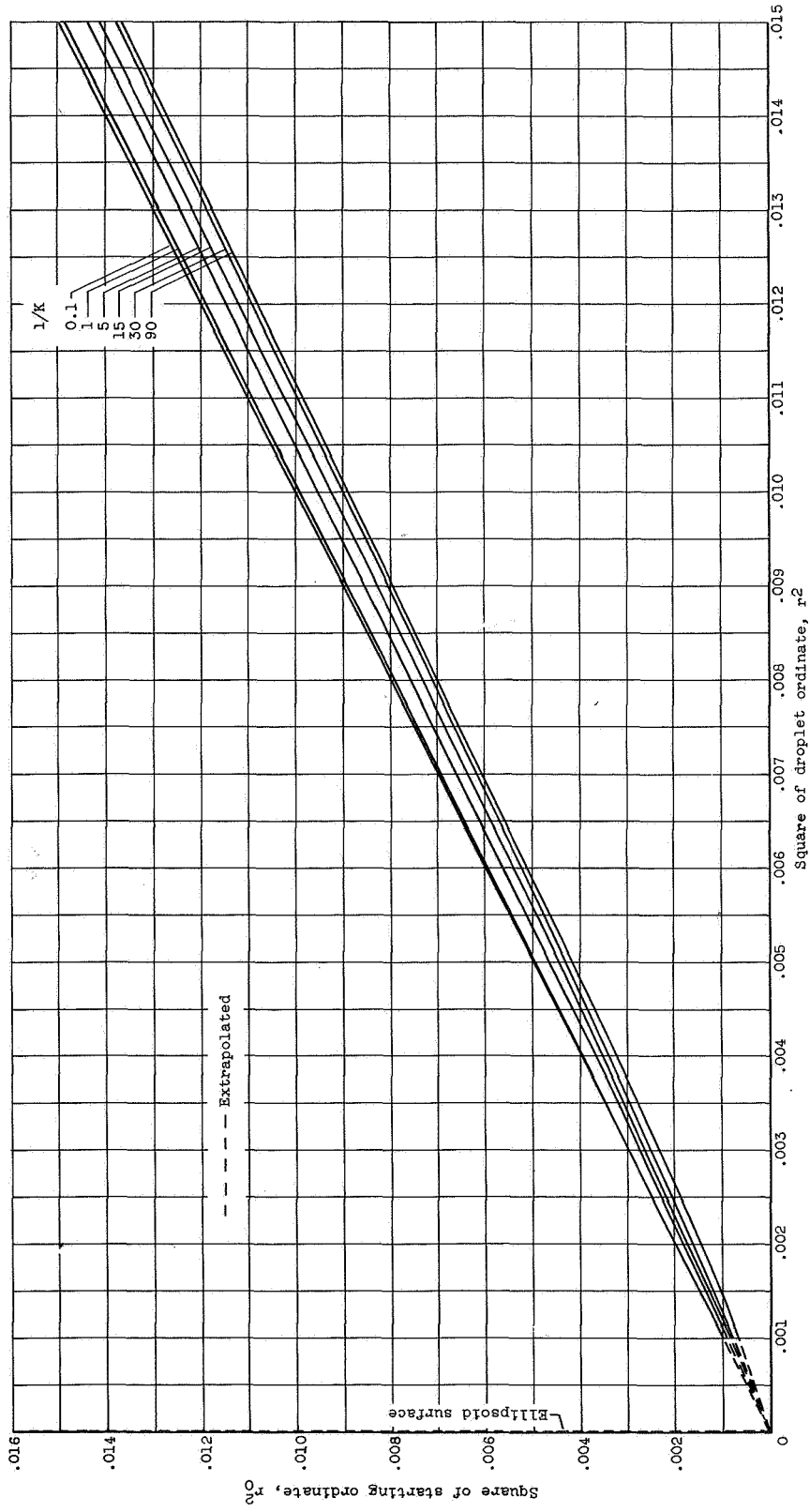


Figure 4. - Continued. Square of starting ordinate as function of square of droplet ordinate at constant  $z$ -position.  
(o)  $z = -0.5$ ;  $Re_0 = 512$ .

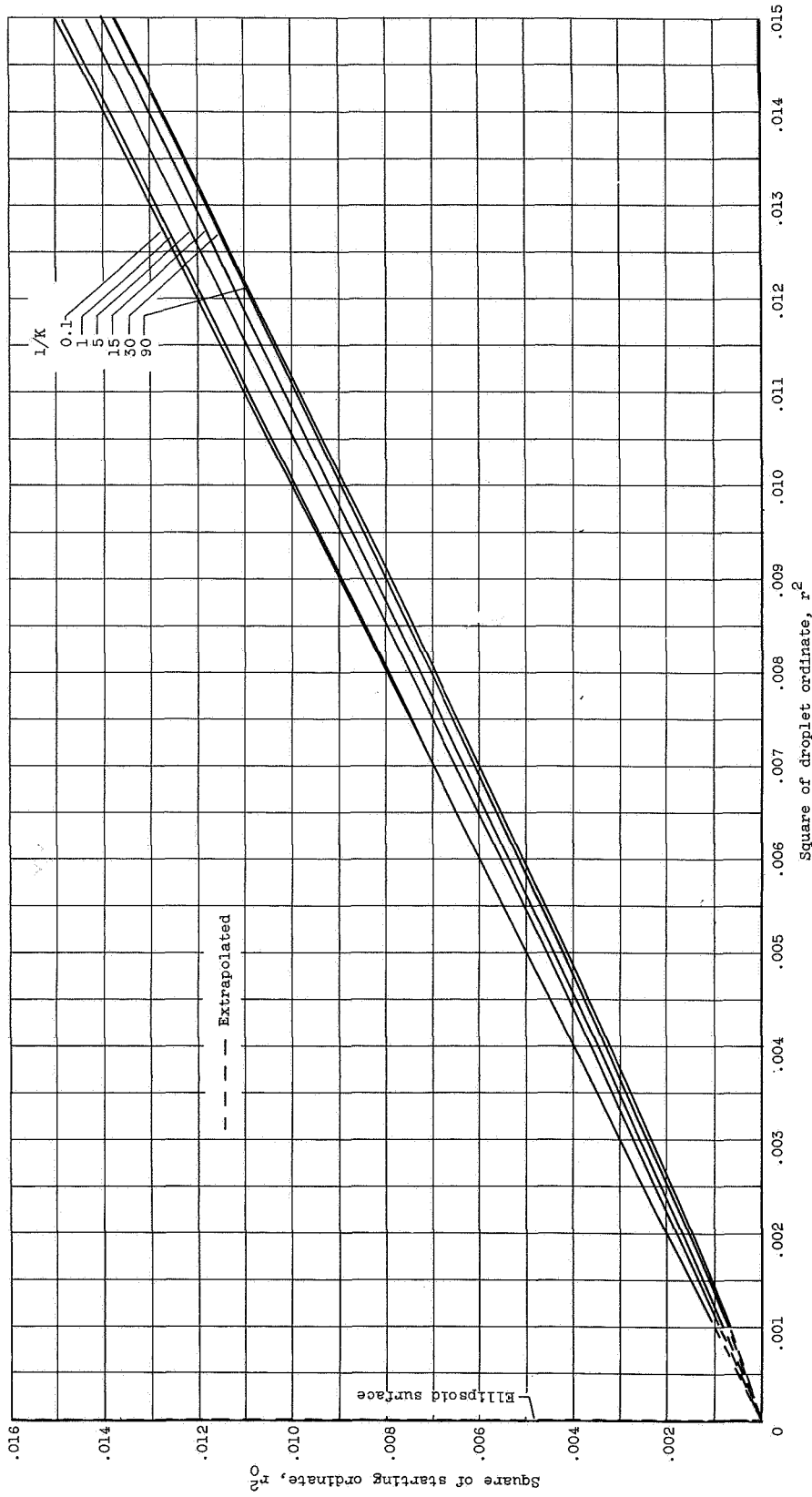


Figure 4. - Continued. Square of starting ordinate as function of square of droplet ordinate at constant  $z$ -position.  
(p)  $z = -0.5$ ;  $Re_0 = 1024$ .

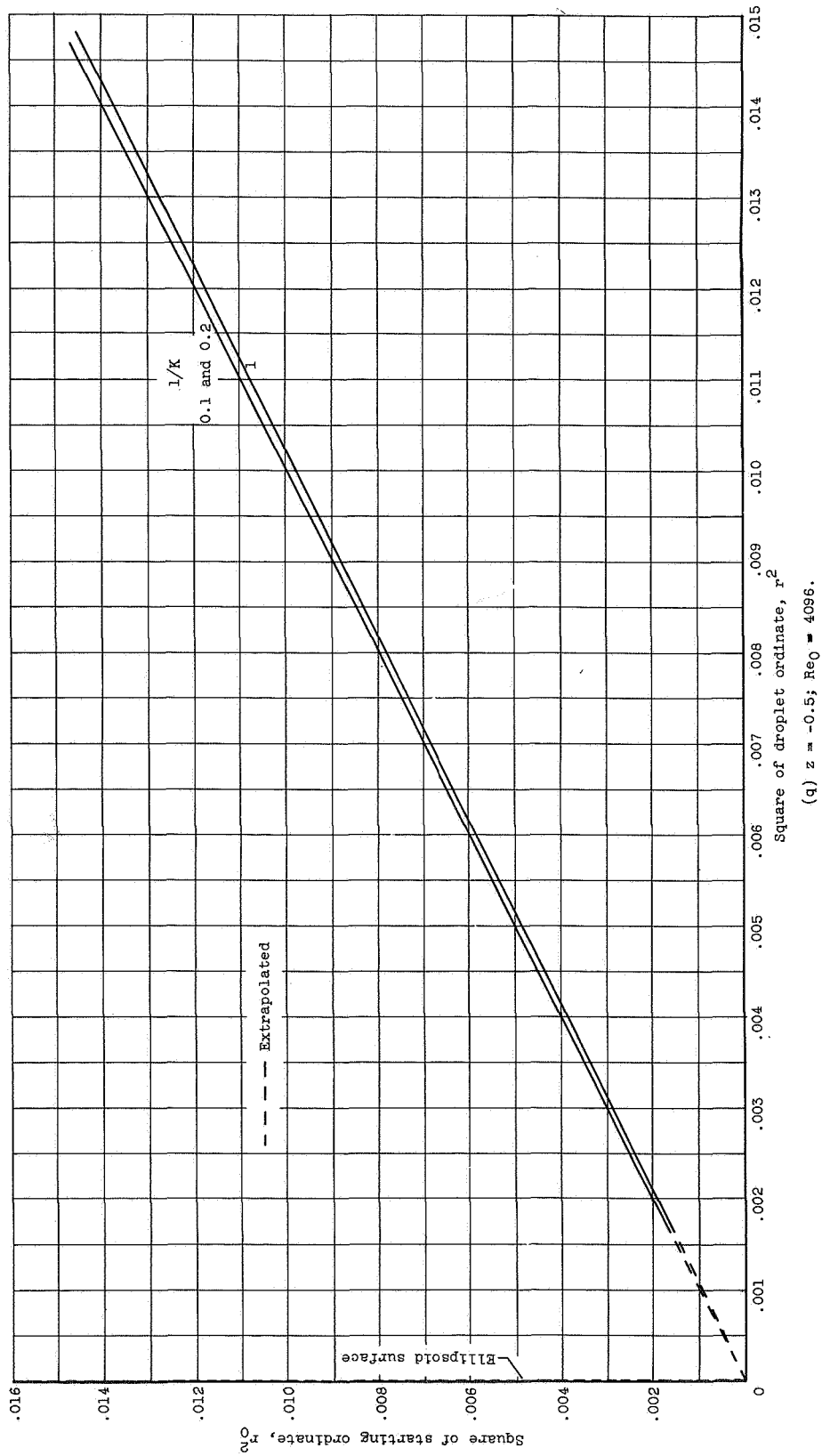


Figure 4. - Continued. Square of starting ordinate as function of square of droplet ordinate at constant z-position.  
(q)  $z = -0.5$ ;  $Re_0 = 4096$ .

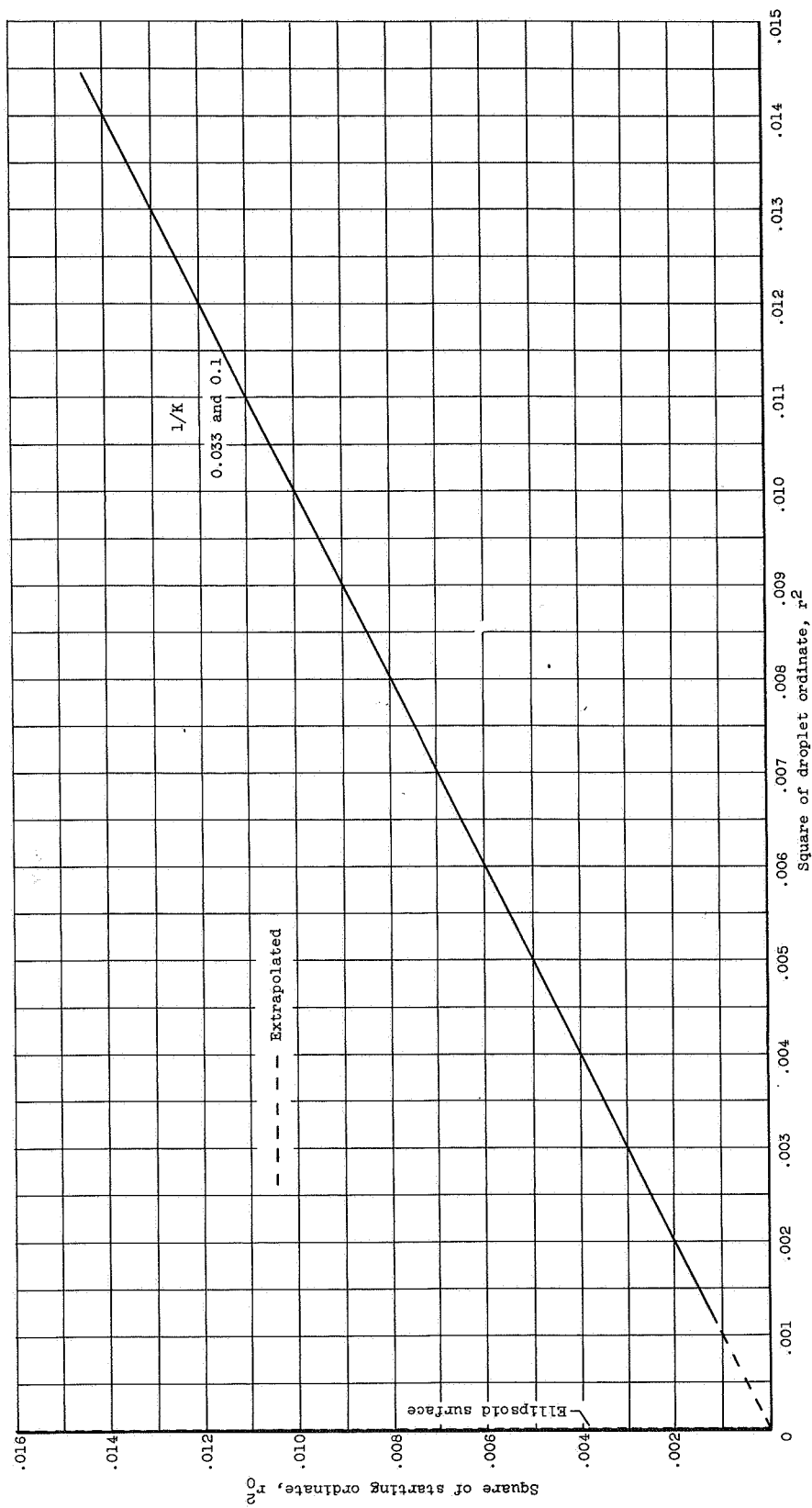


Figure 4. - Concluded. Square of starting ordinate as function of square of droplet ordinate at constant z-position.  
(r)  $z = -0.5$ ;  $Re_0 = 8192$ .

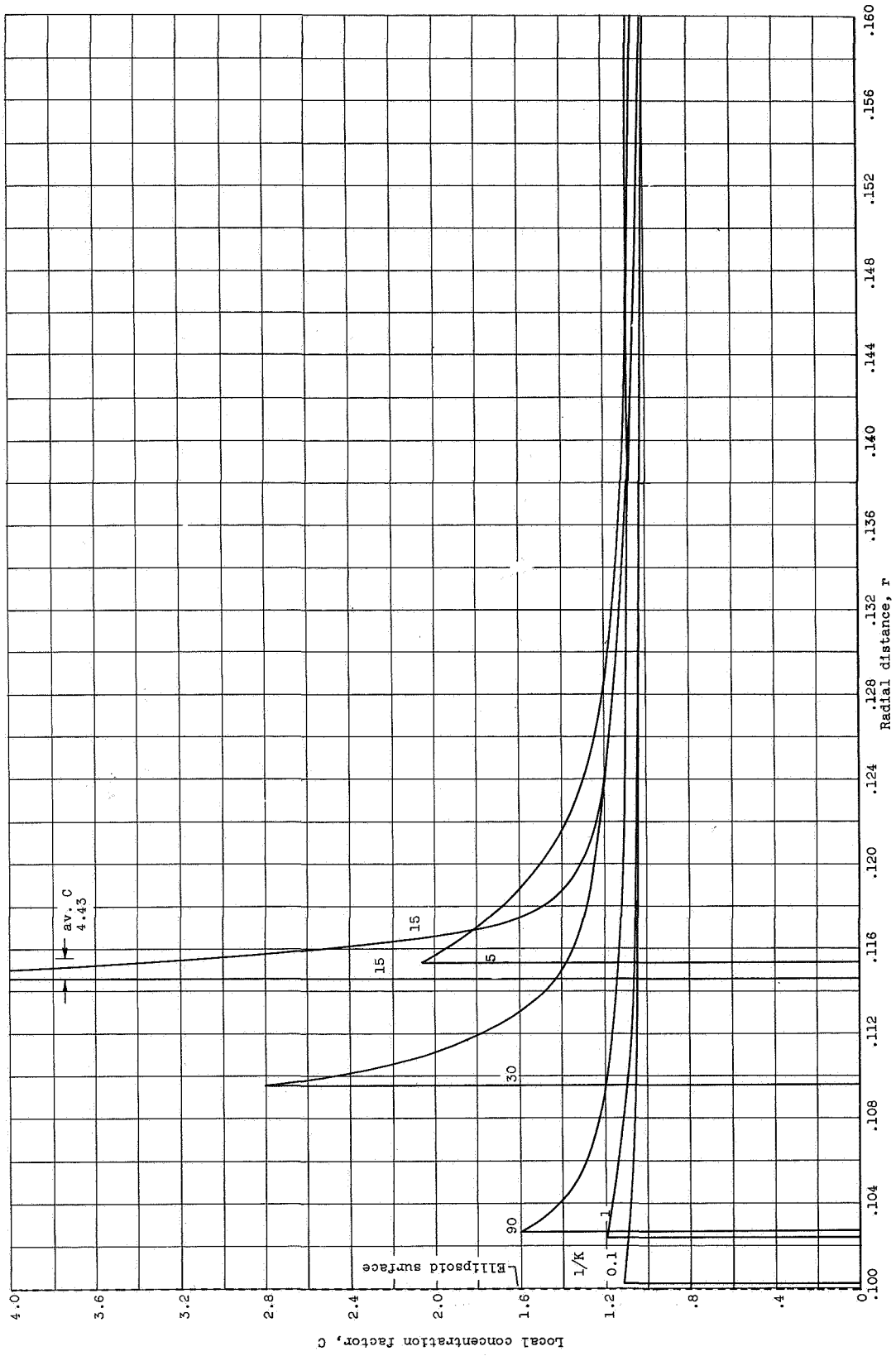


Figure 5. - Variation of local concentration factor with radial distance  $r$  at constant axial position  $z$ .  
 (a)  $z = 0$ ;  $Re_0 = 0$ .

CE-6 back 3106

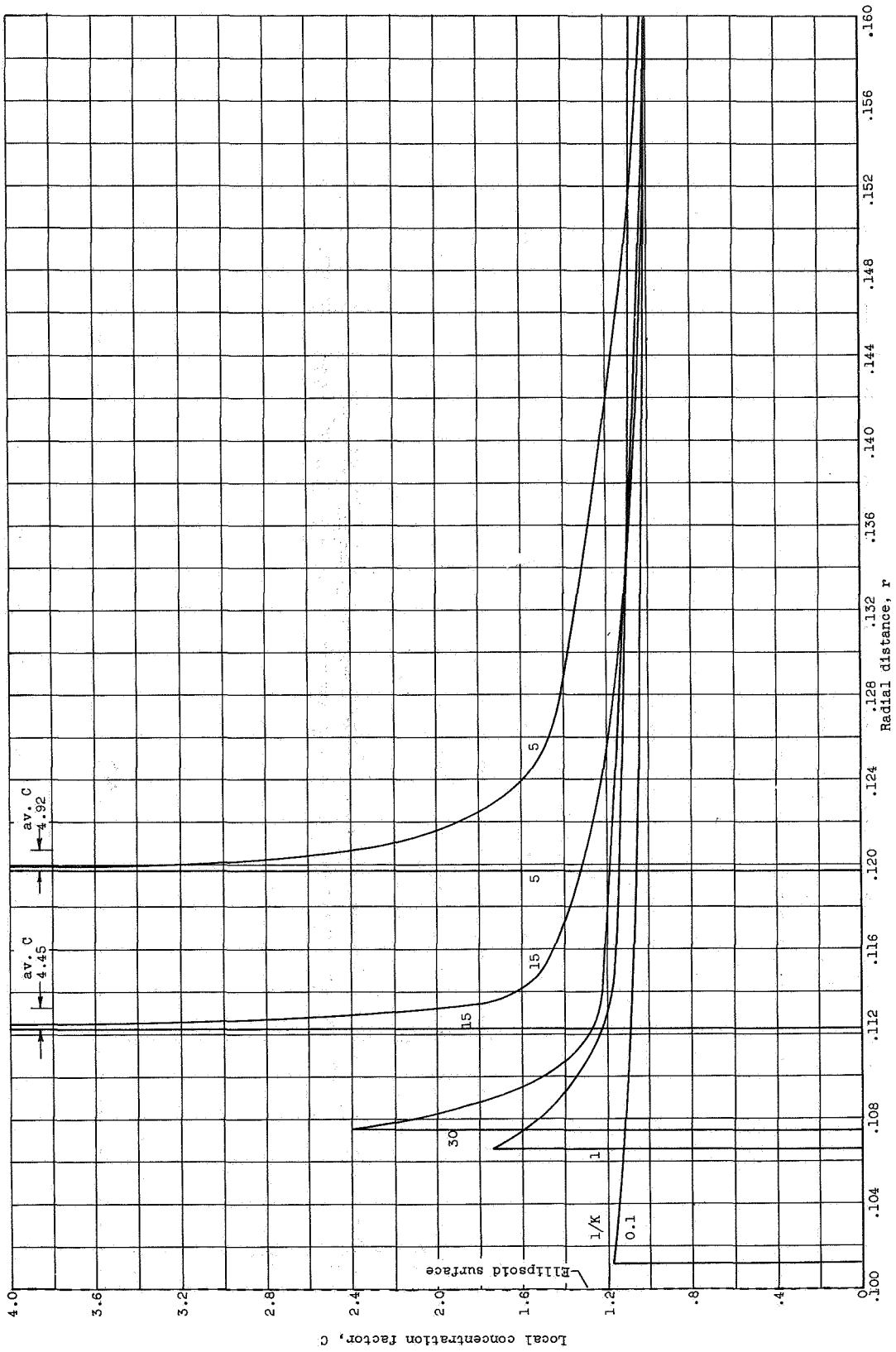


Figure 5. - Continued. Variation of local concentration factor with radial distance  $r$  at constant axial position  $z$ .  
(b)  $z = 0$ ;  $Re_0 = 128$ .



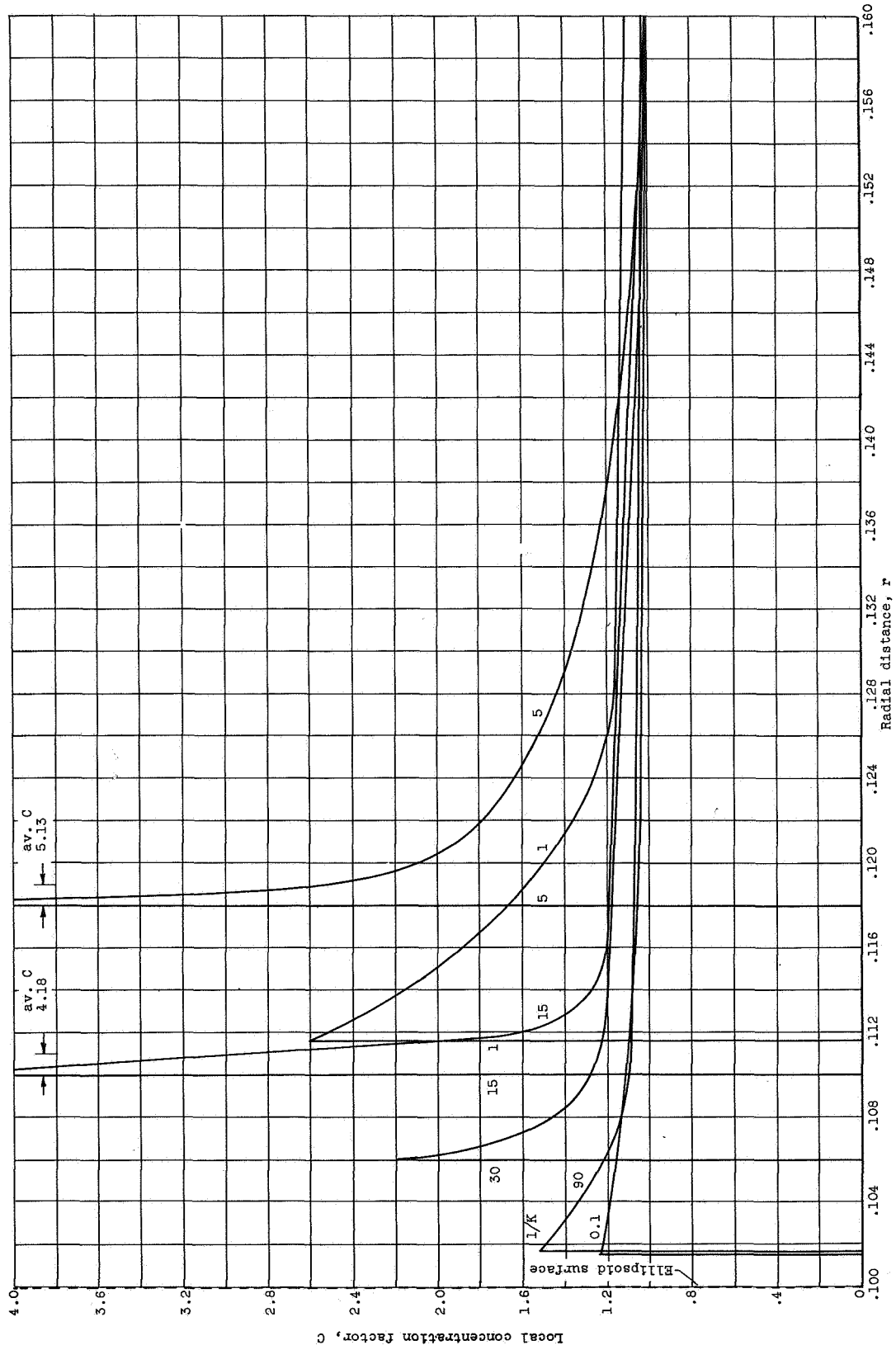


Figure 5. - Continued. Variation of local concentration factor with radial distance  $r$  at constant axial position  $z$ .  
(c)  $z = 0$ ;  $Re_0 = 512$ .

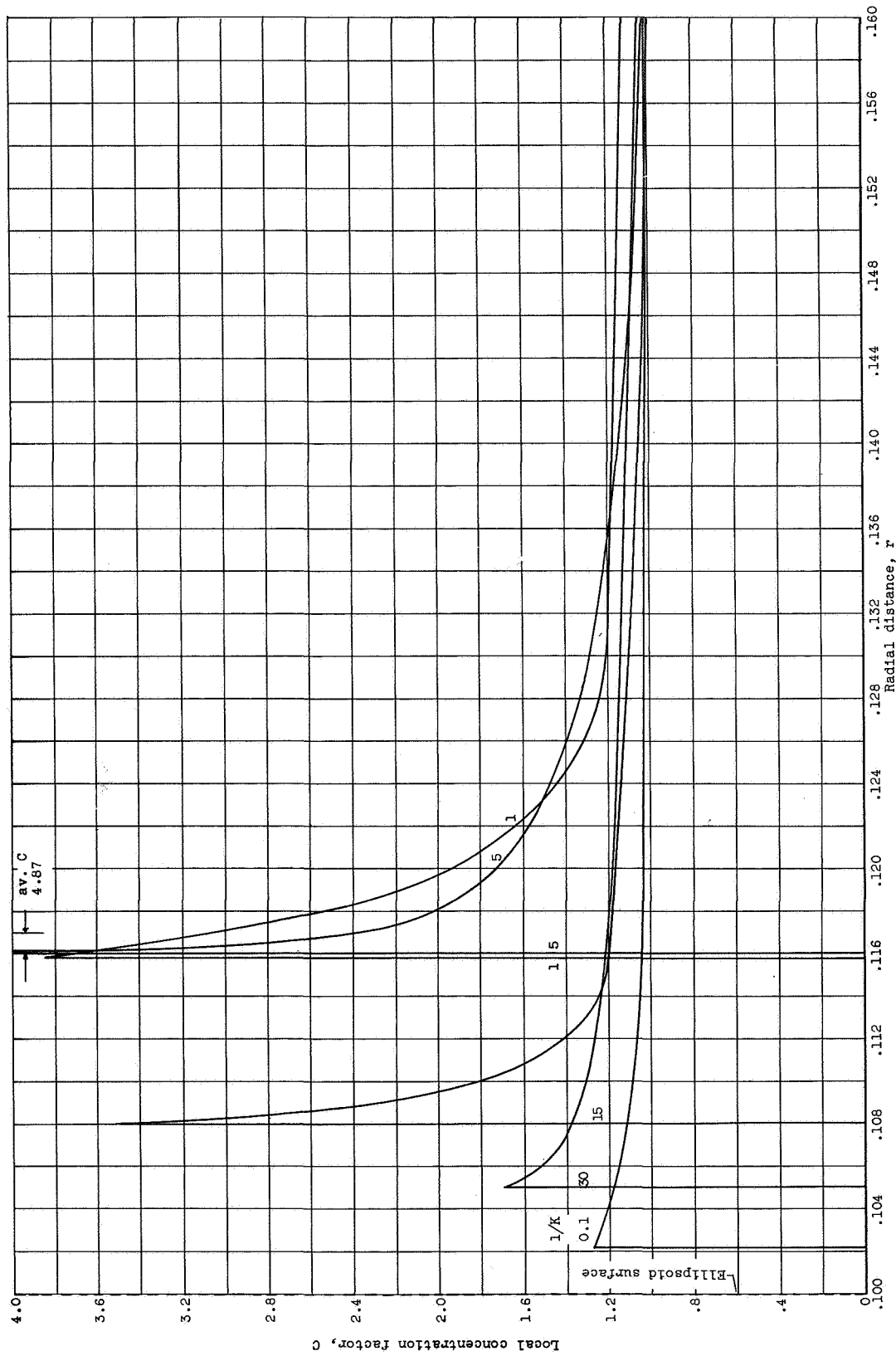


Figure 5. - Continued. Variation of local concentration factor with radial distance  $r$  at constant axial position  $z$ .  
(d)  $z = 0$ ,  $Re_0 = 1024$ .

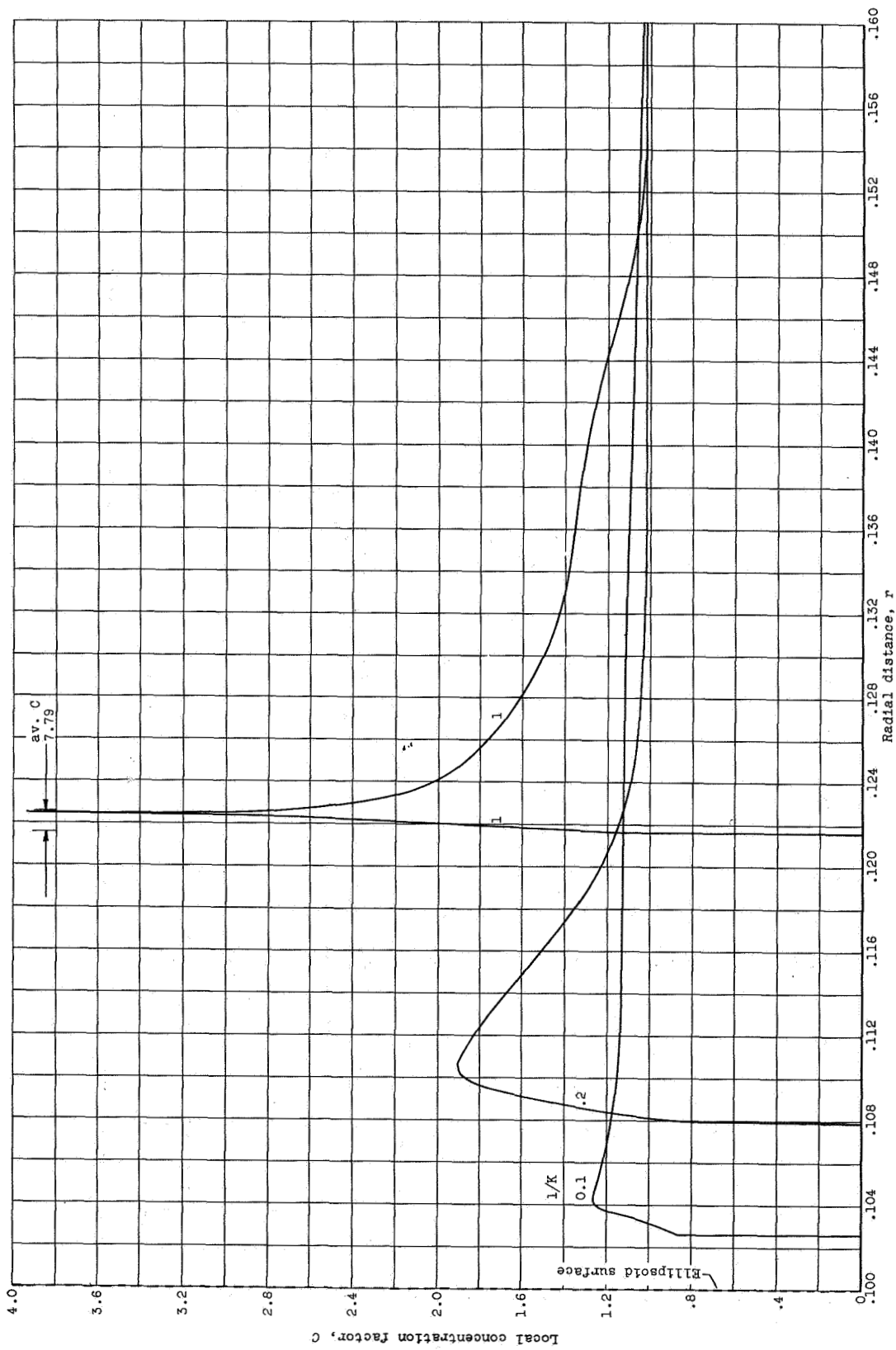


Figure 5. - Continued. Variation of local concentration factor with radial distance r at constant axial position z. (e) z = 0; Re<sub>0</sub> = 4096.

3106

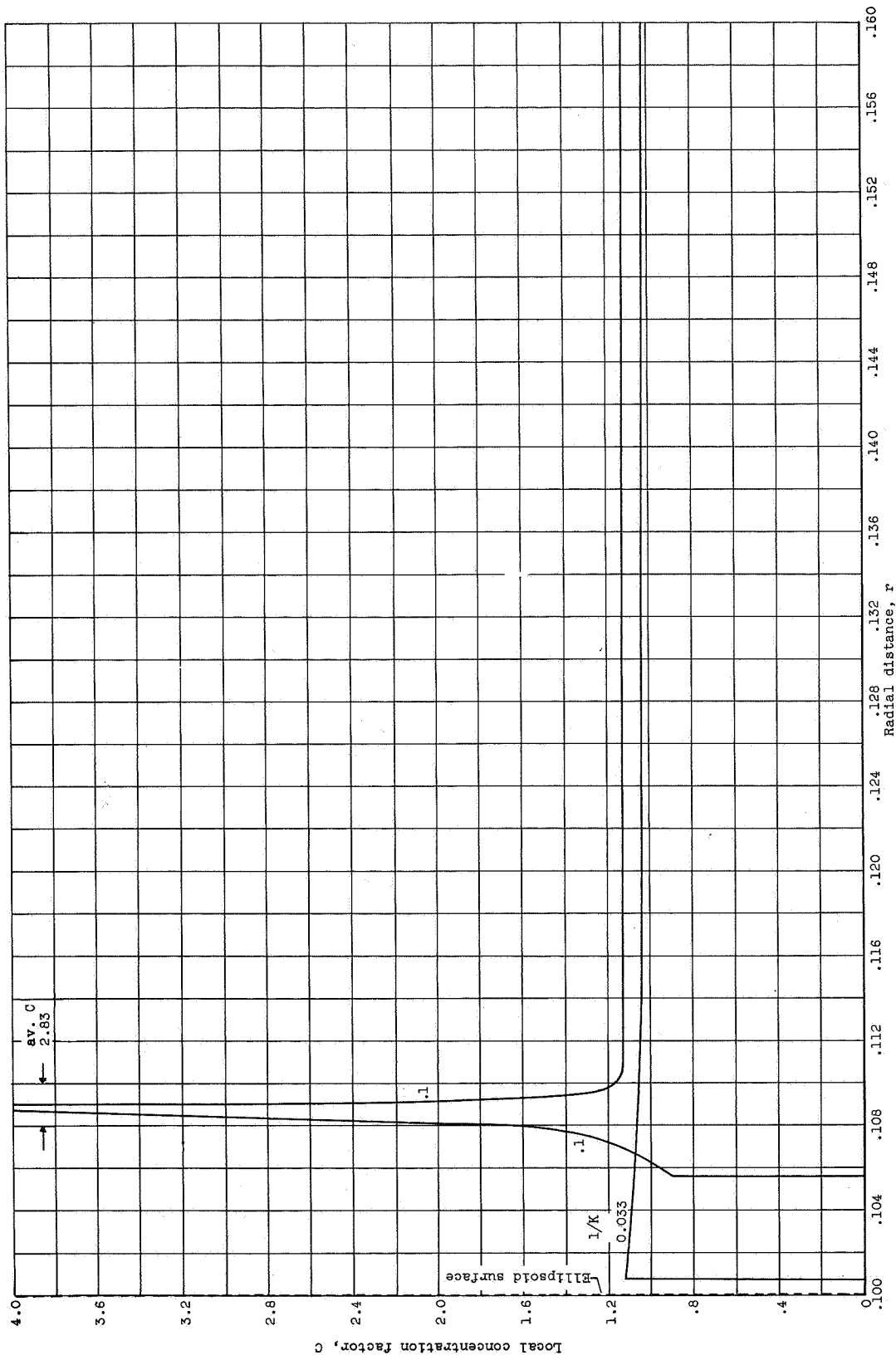


Figure 5. - Continued. Variation of local concentration factor with radial distance  $r$  at constant axial position  $z$ .  
(f)  $z = 0$ ;  $Re_0 = 8192$ .

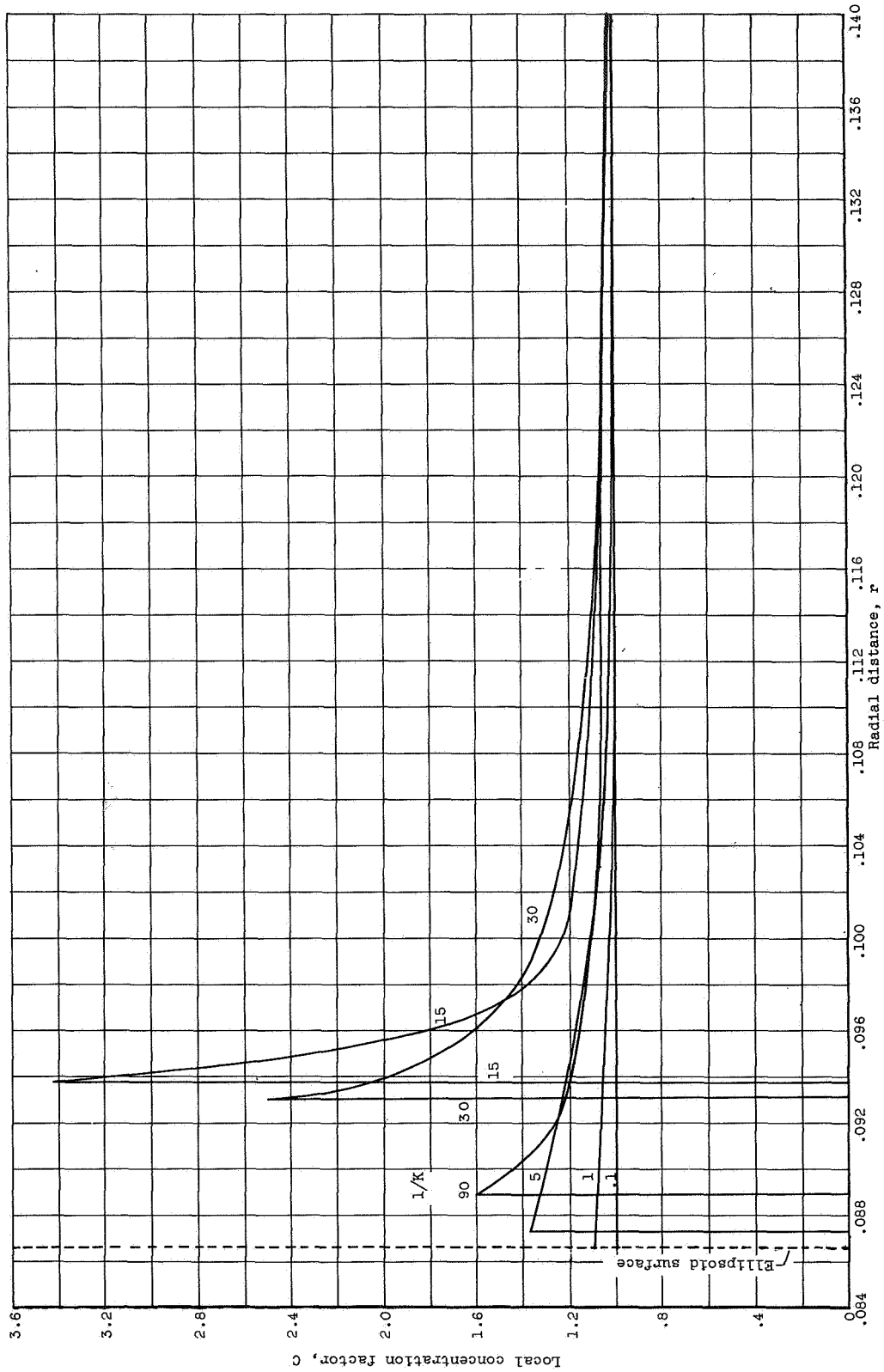


Figure 5. - Continued. Variation of local concentration factor with radial distance  $r$  at constant axial position  $z$ .  
(g)  $z = -0.25$ ;  $Re_0 = 0$ .

CE-7

2712

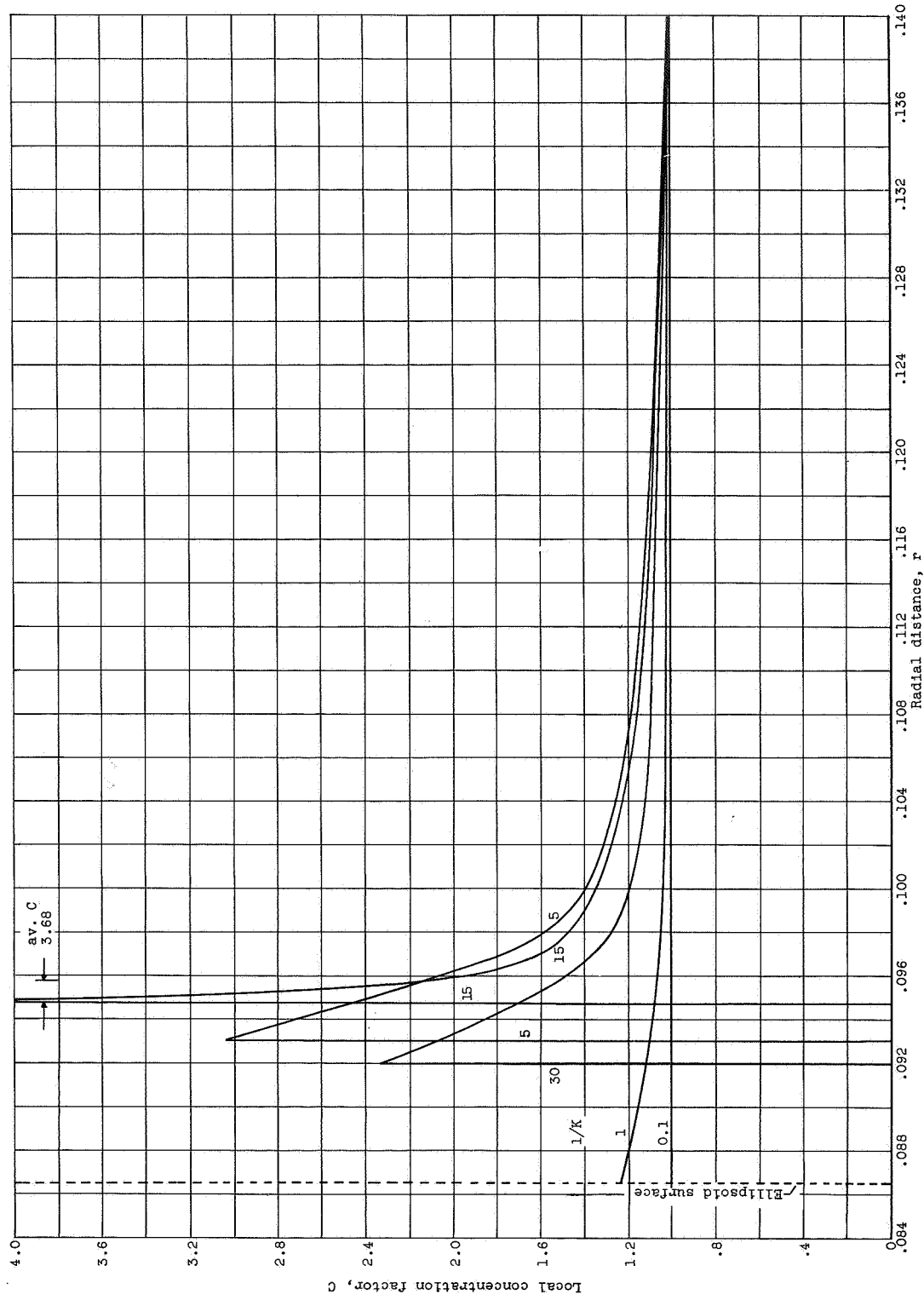


Figure 5. - Continued. Variation of local concentration factor with radial distance  $r$  at constant axial position  $z$ .  
 (h)  $z = -0.25$ ;  $Re_0 = 128$ .

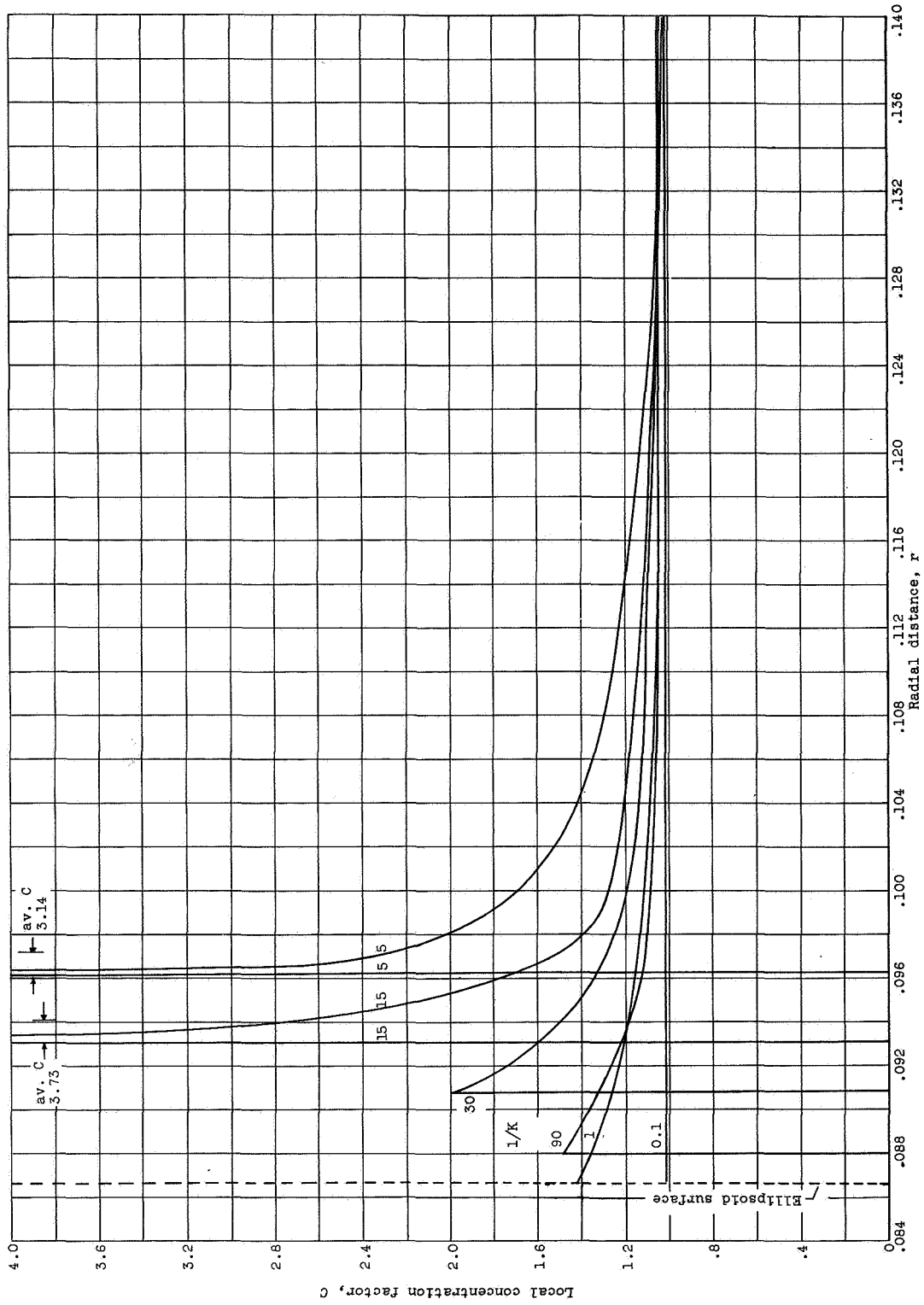


Figure 5.- Continued. Variation of local concentration factor with radial distance  $r$  at constant axial position  $z$ .  
 (1)  $z = -0.25$ ;  $Re_0 = 512$ .

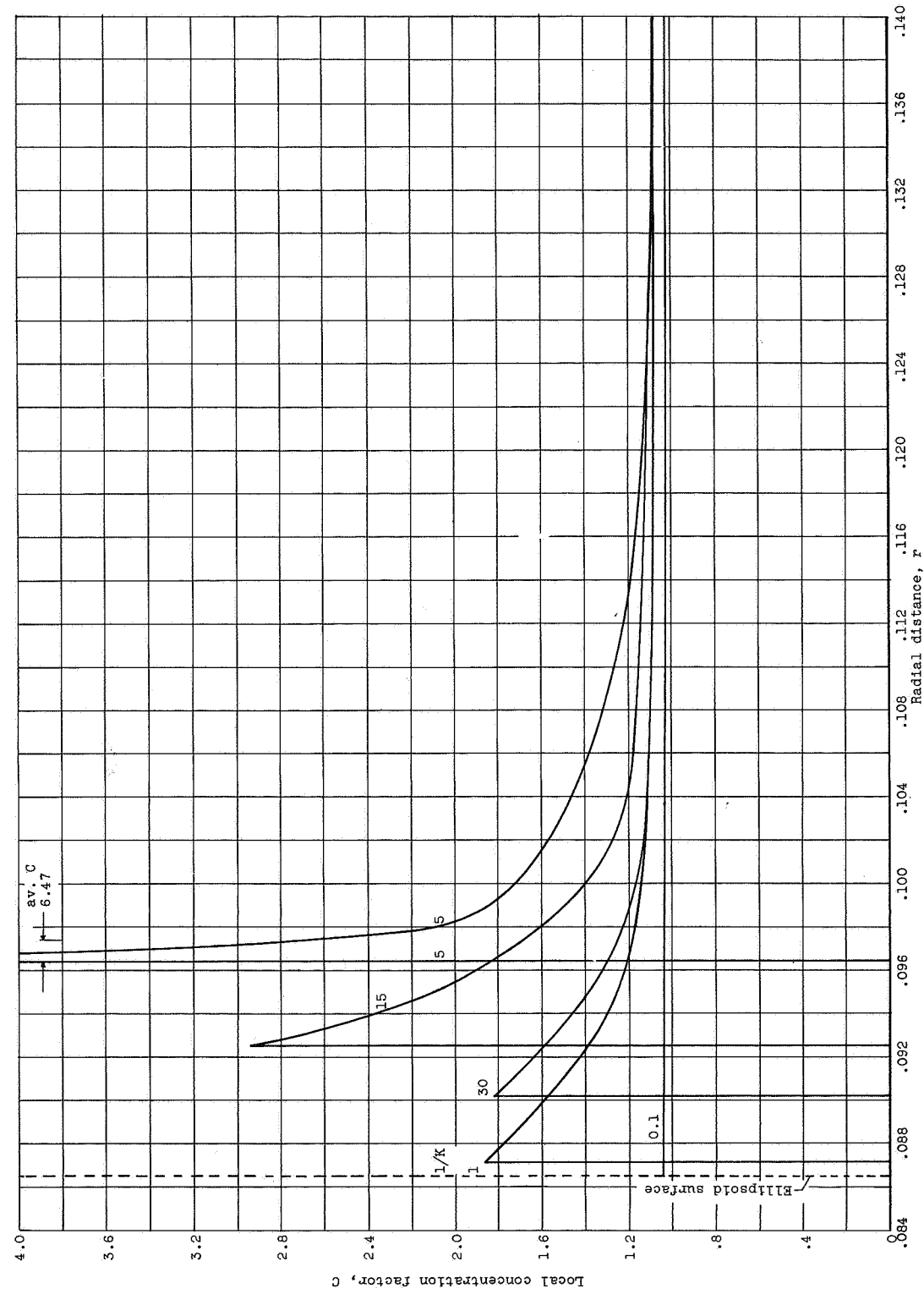


Figure 5. - Continued. Variation of local concentration factor with radial distance  $r$  at constant axial position  $z$ .  
(j)  $z = -0.25$ ;  $Re_0 = 1024$ .



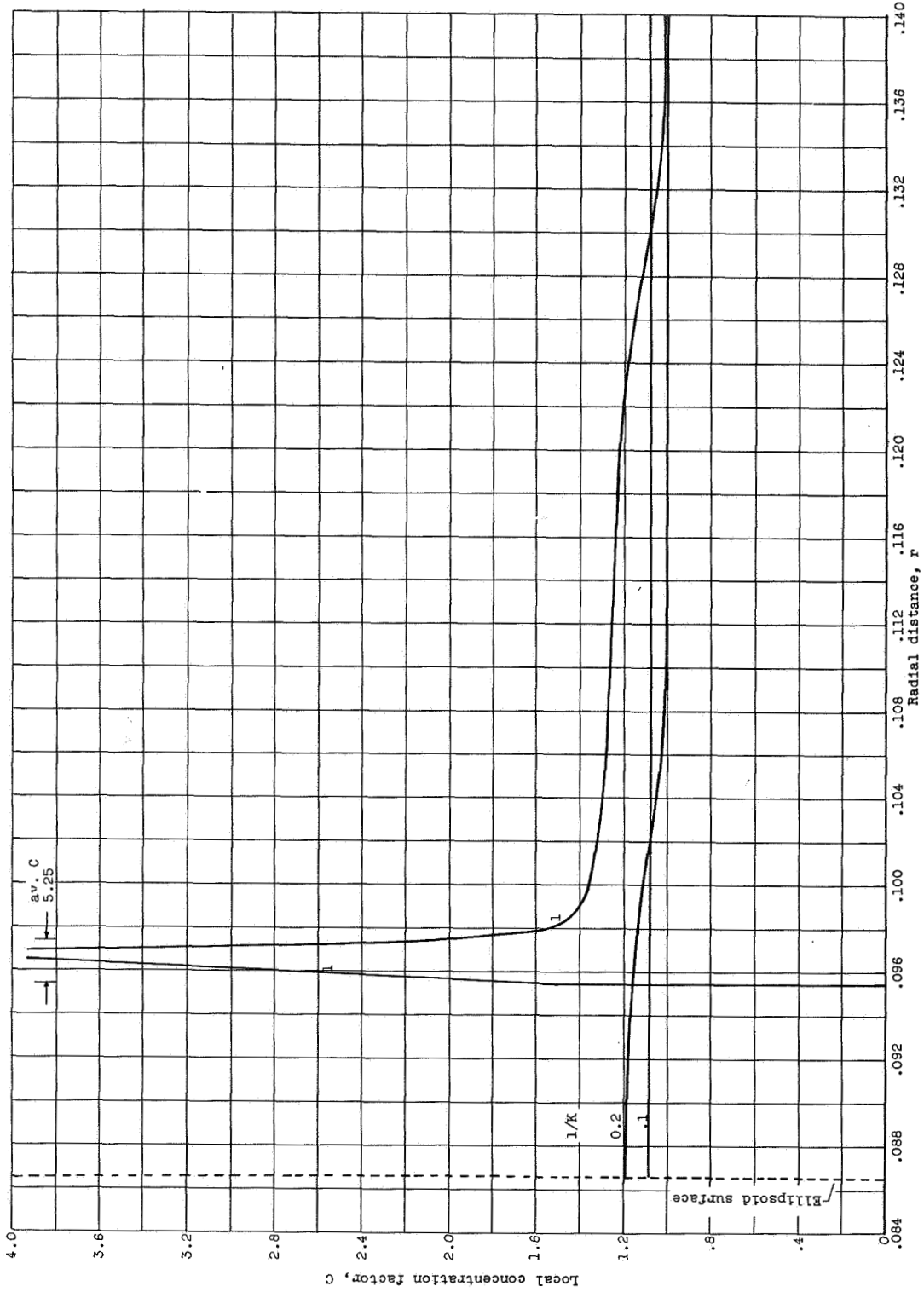


Figure 5. - Continued. Variation of local concentration factor with radial distance  $r$  at constant axial position  $z$ .  
( $k$ )  $z = -0.25$ ;  $Re_0 = 4096$ .

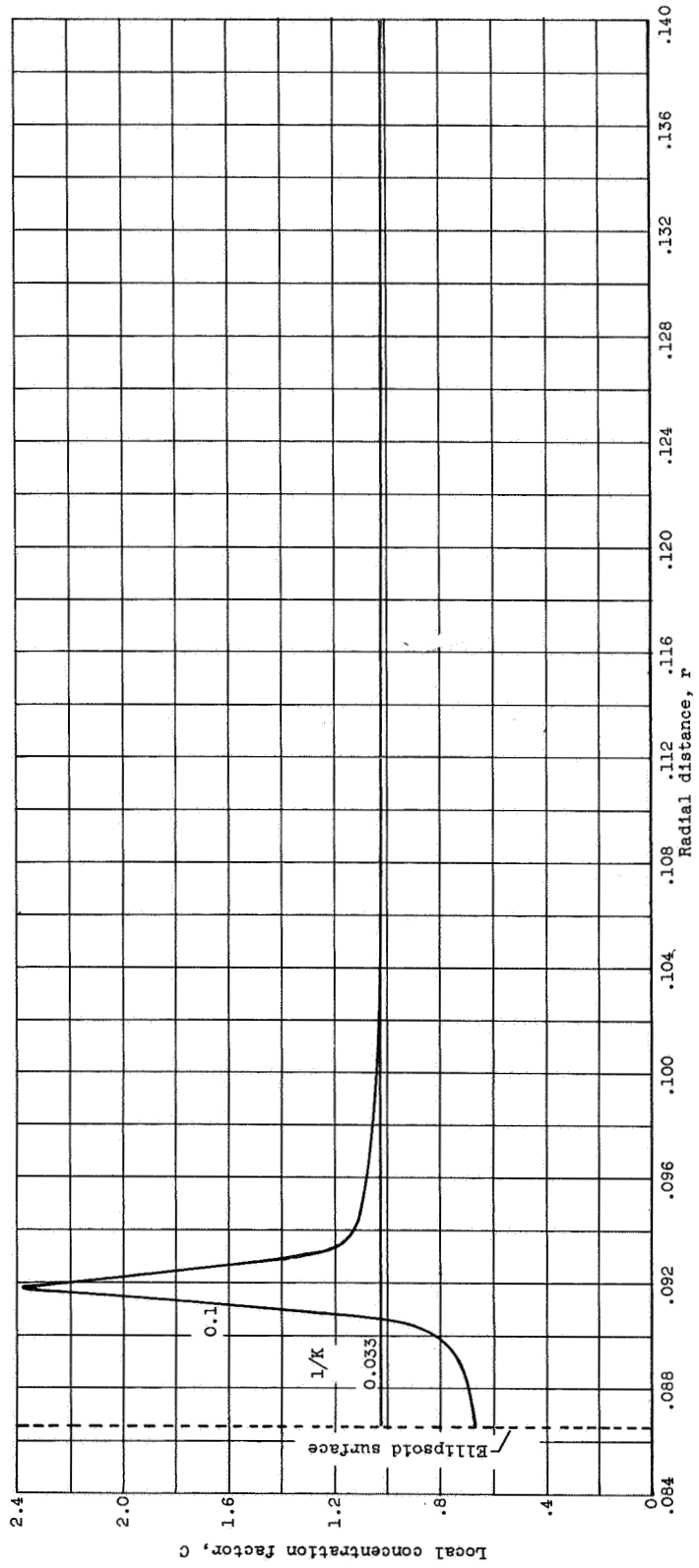


Figure 5. - Continued. Variation of local concentration factor with radial distance  $r$  at constant axial position  $z$ .  
 (†)  $z = -0.25$ ;  $Re_0 = 8192$ .

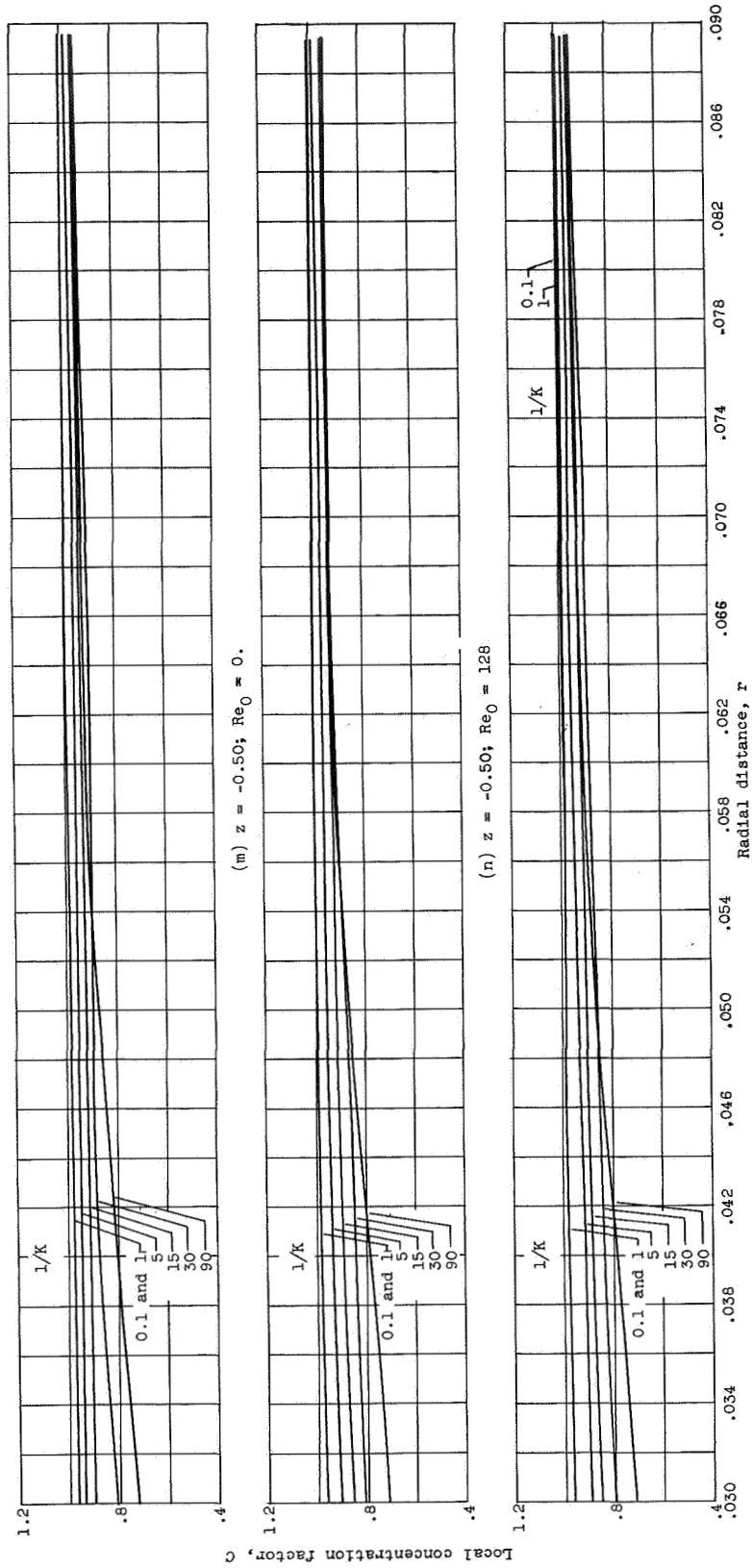


Figure 5. - Continued. Variation of local concentration factor with radial distance  $r$  at constant axial position  $z$ .

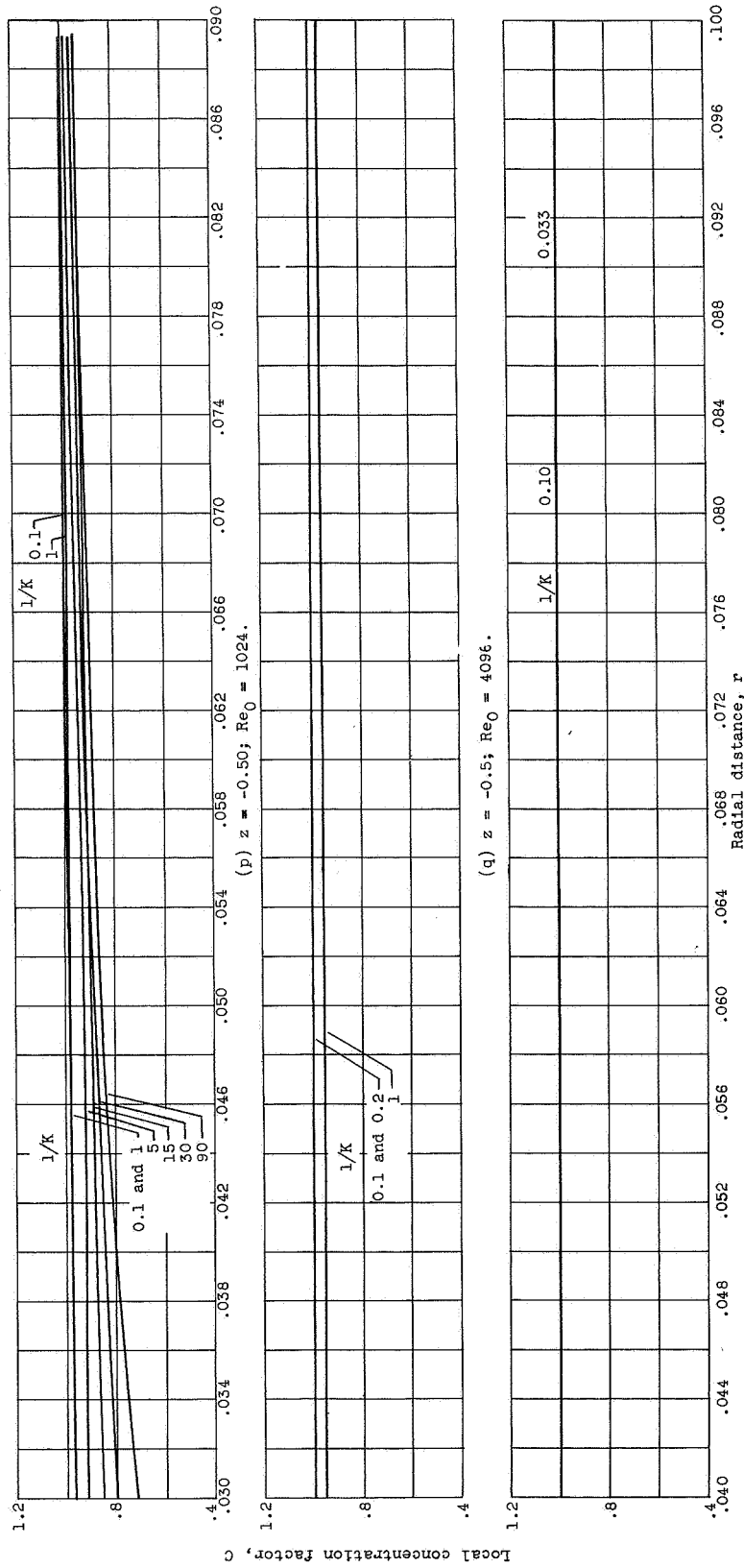
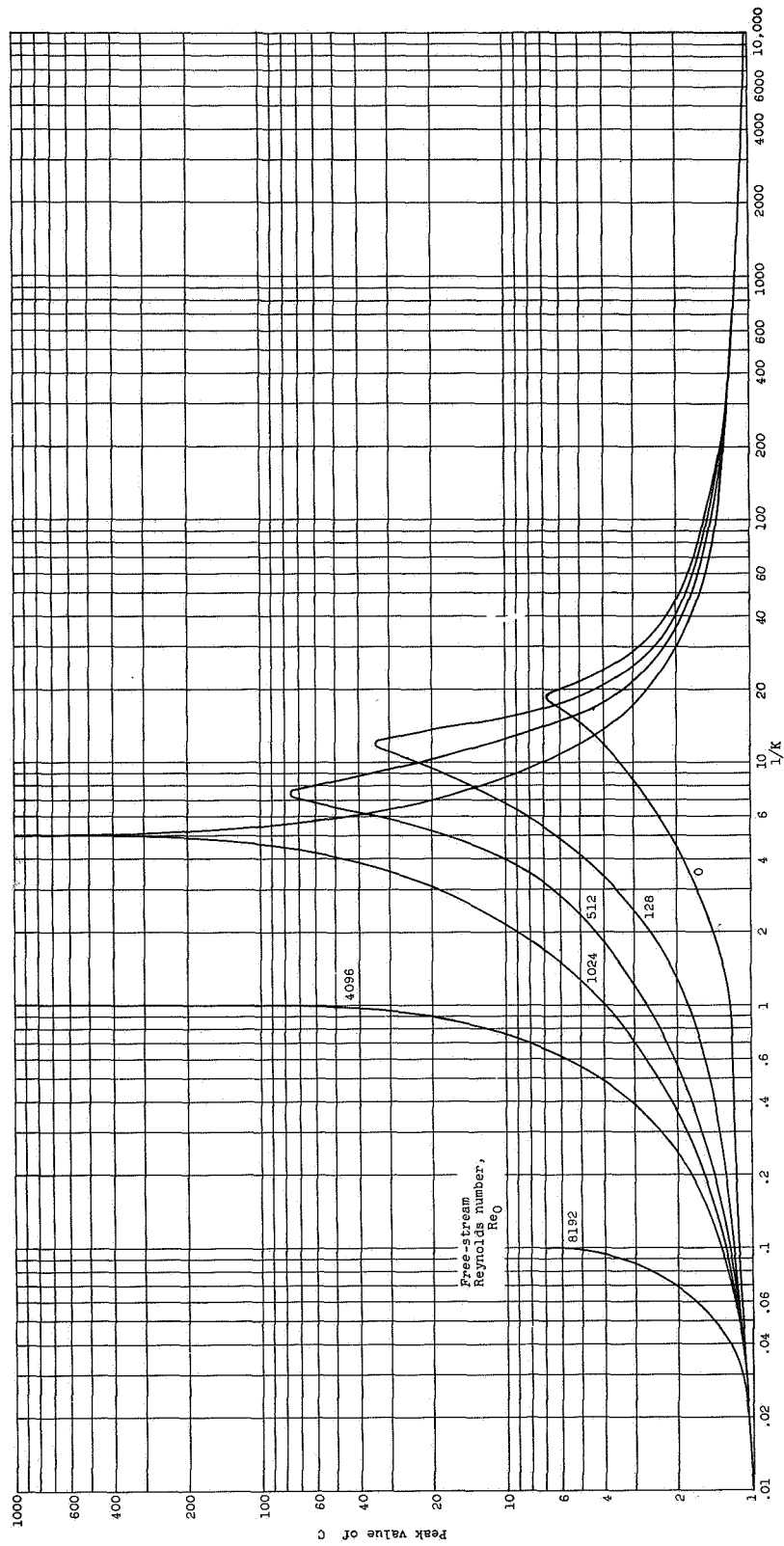


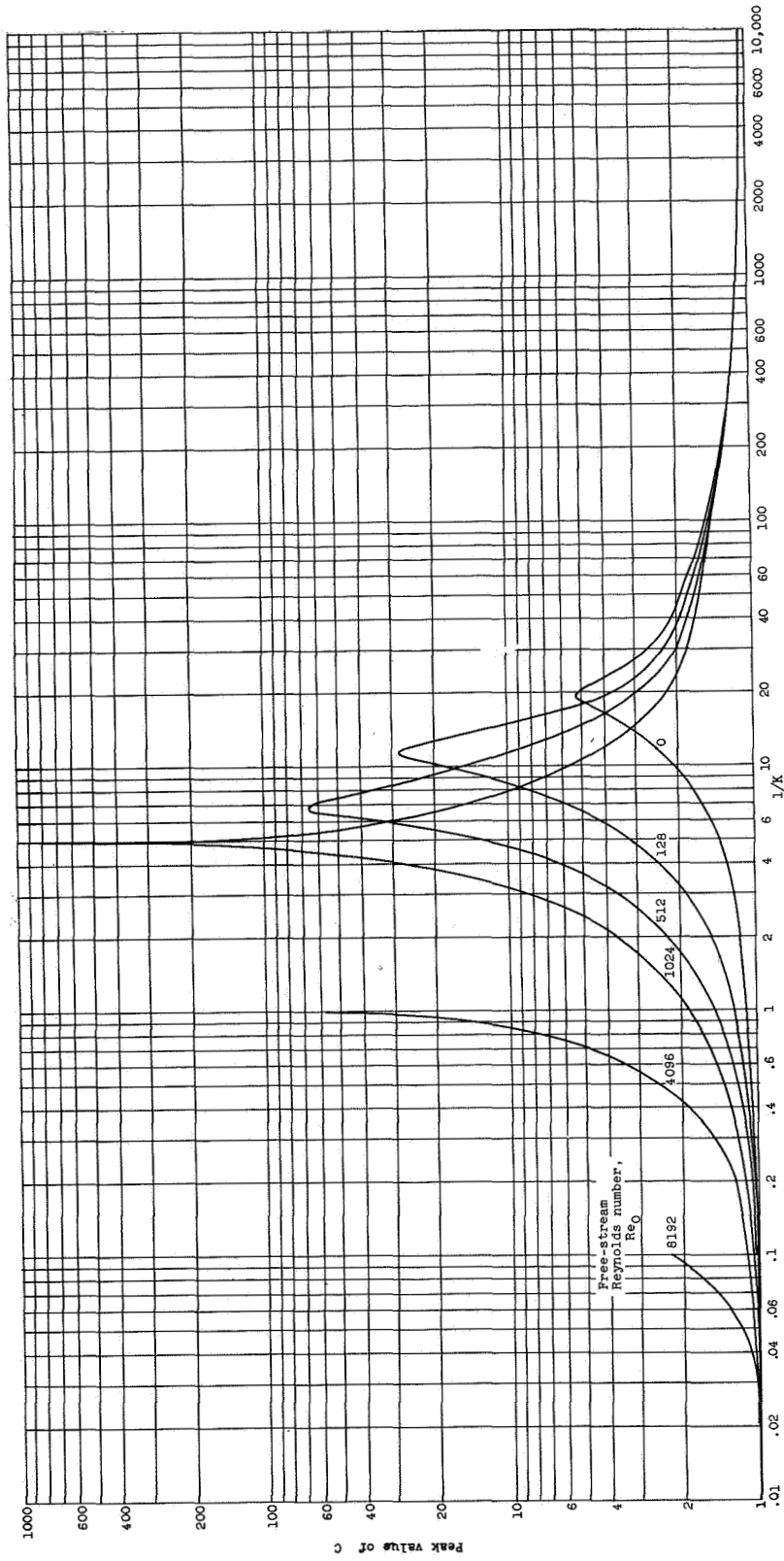
Figure 5. - Concluded. Variation of local concentration factor with radial distance r at constant axial position z.



(a)  $z = 0$ .

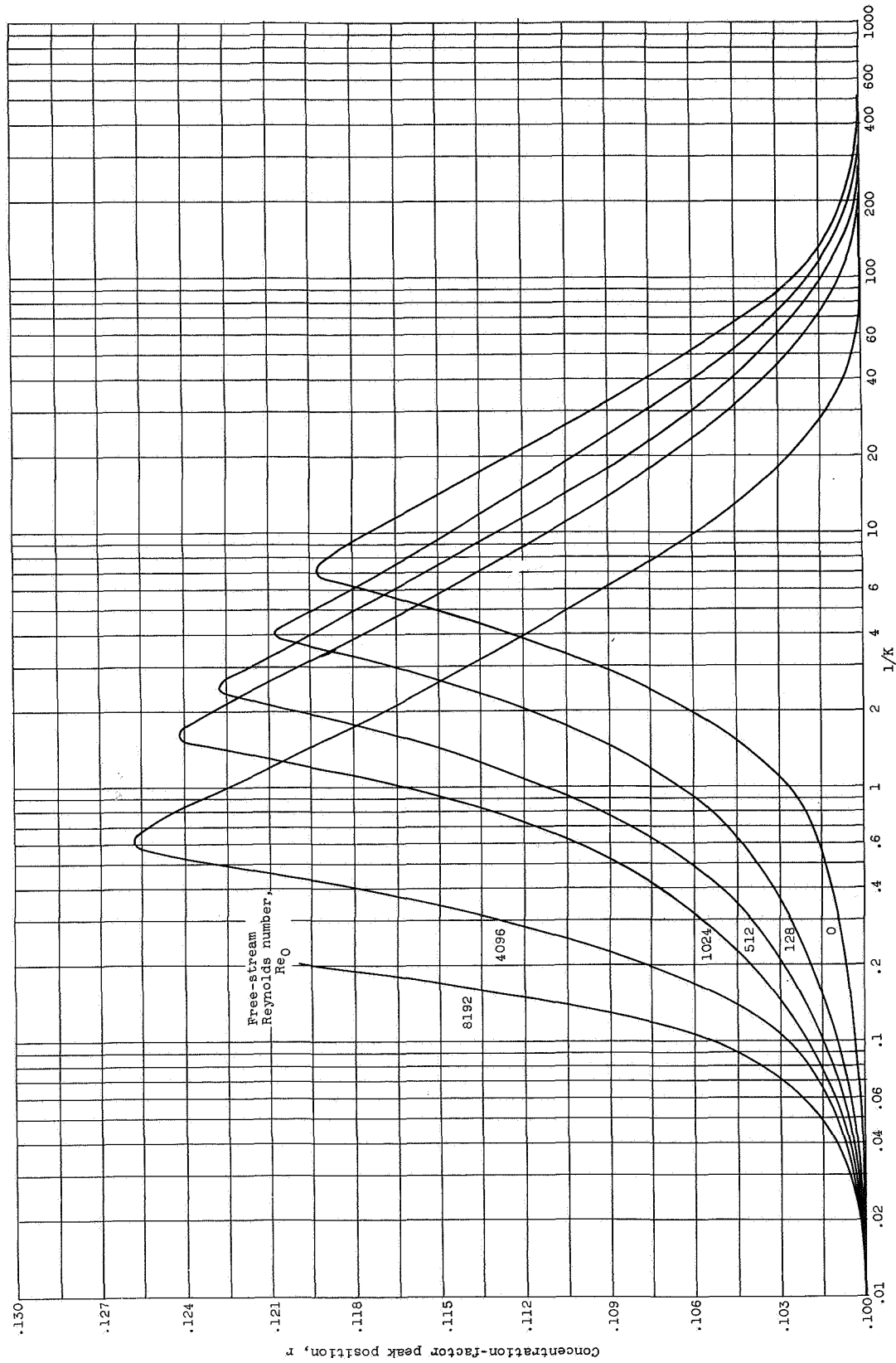
Figure 6. - Variation of peak value of concentration factor with  $1/K$  for constant free-stream Reynolds number.

CE-8



(b)  $z = -0.25$ .

Figure 6. - Concluded. Variation of peak value of concentration factor with  $1/K$  for constant free-stream Reynolds number.



(a)  $z = 0$ .  
 Figure 7. - Variation of peak position of concentration factor with  $1/K$  for constant free-stream Reynolds number.

CE-8 back

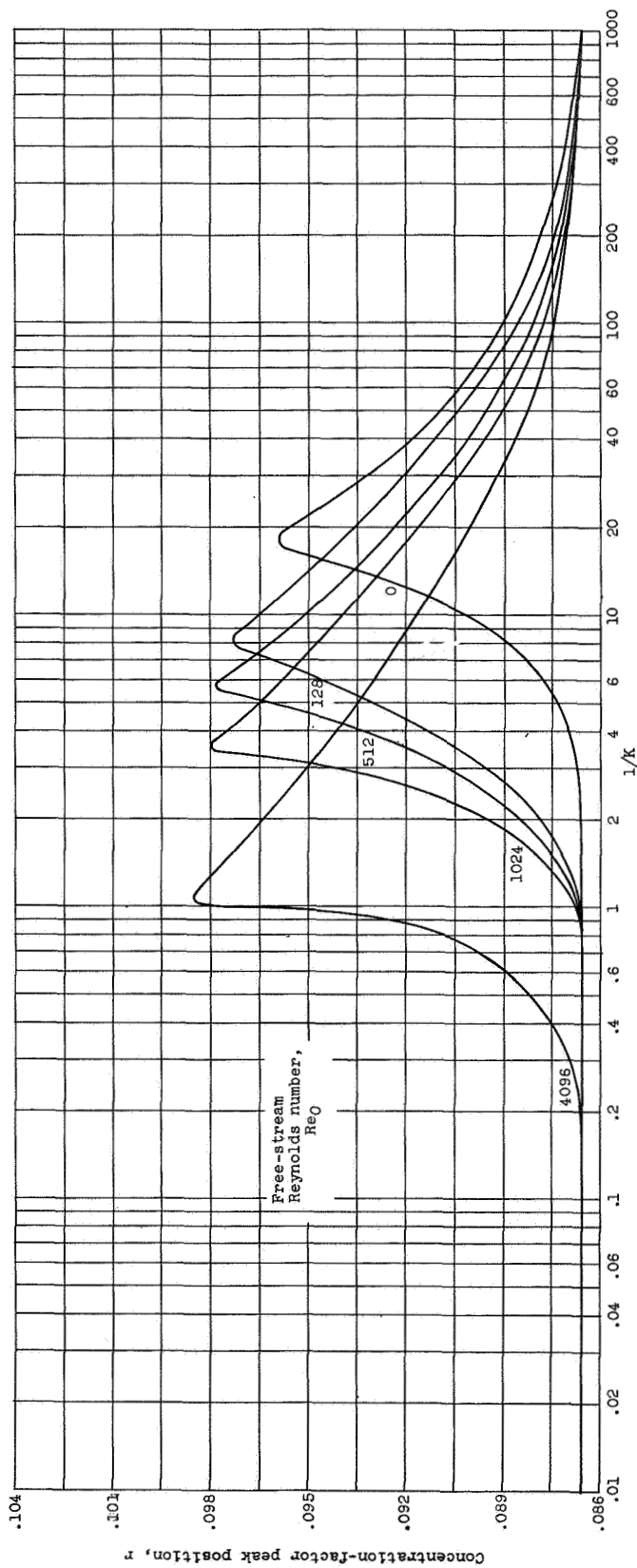
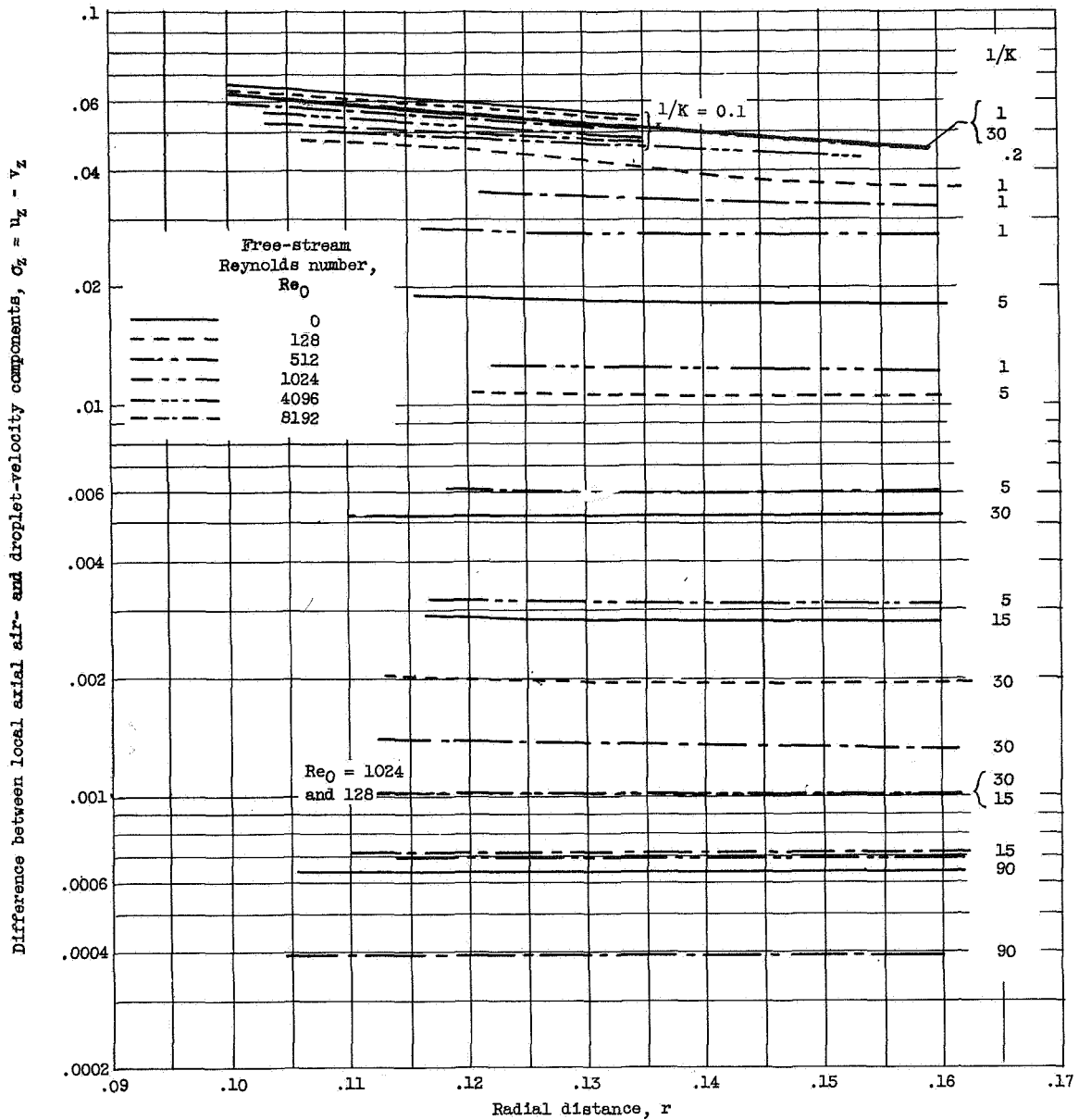


Figure 7. - Concluded. Variation of peak position of concentration factor with  $1/K$  for constant free-stream Reynolds number. (b)  $z = -0.25$ .



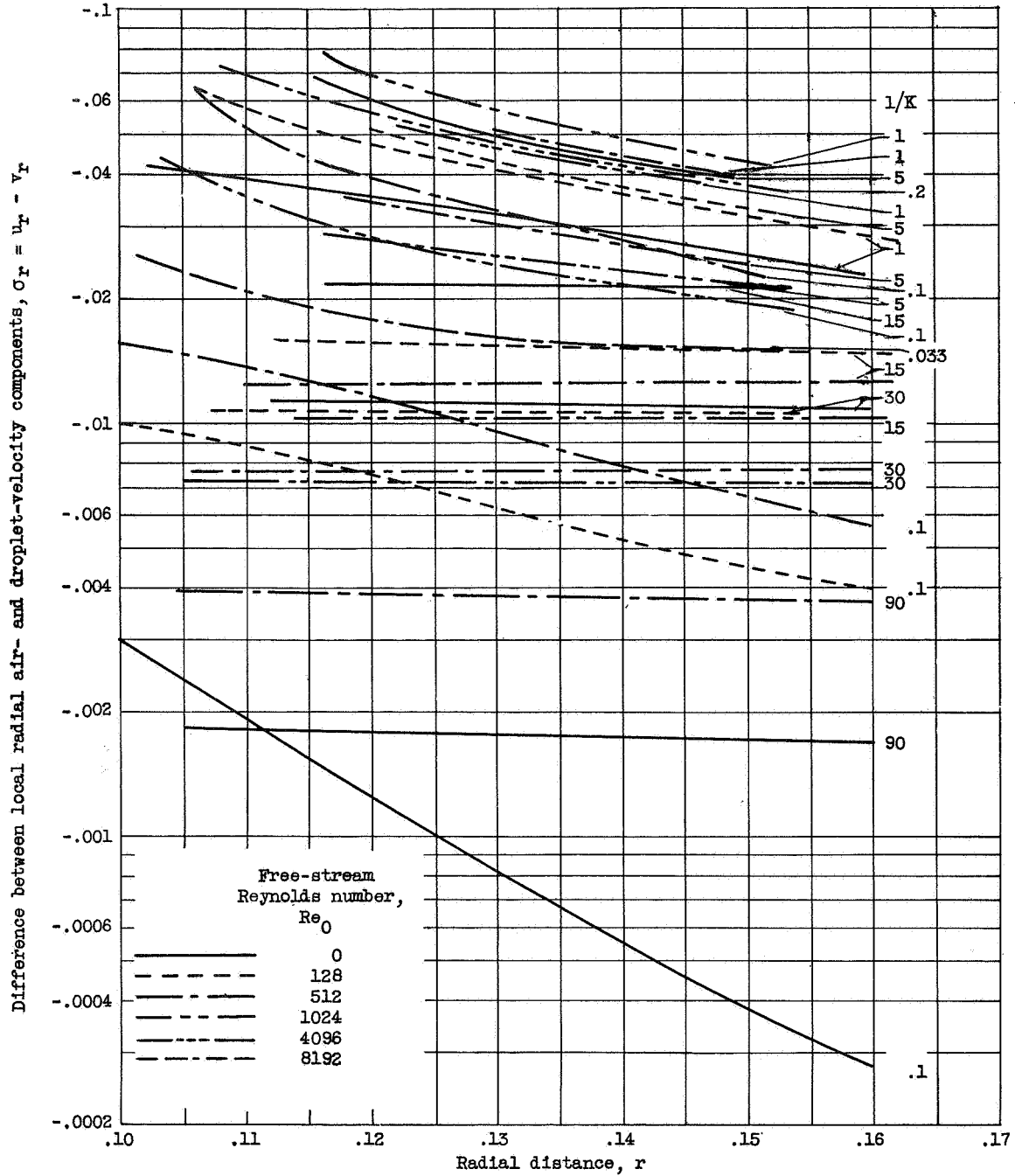


(a) Axial component.

Figure 8. - Difference between local air- and droplet-velocity components against radial distance  $r$  at  $z = 0$  position of ellipsoid of fineness ratio 5.

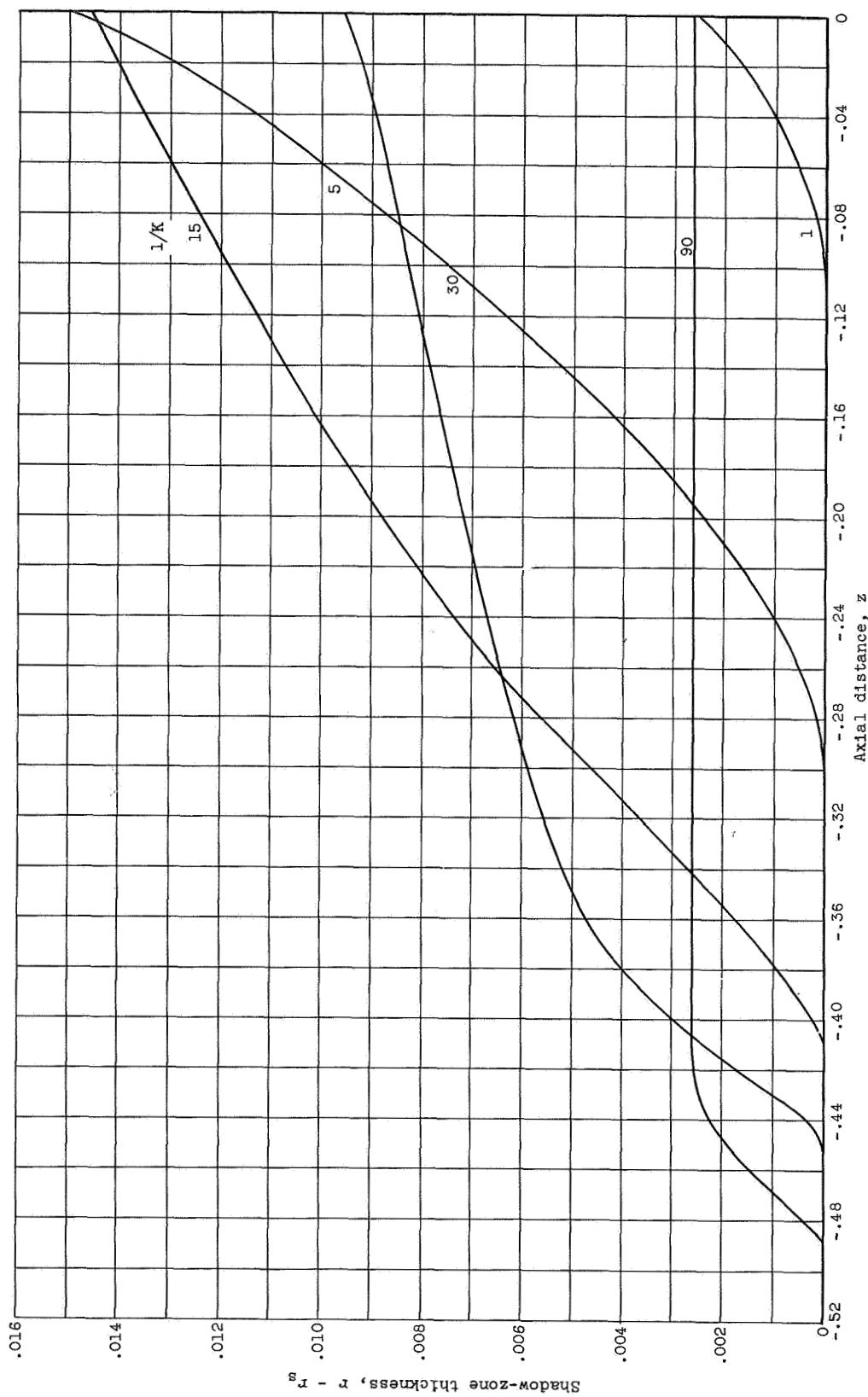
207C

5106



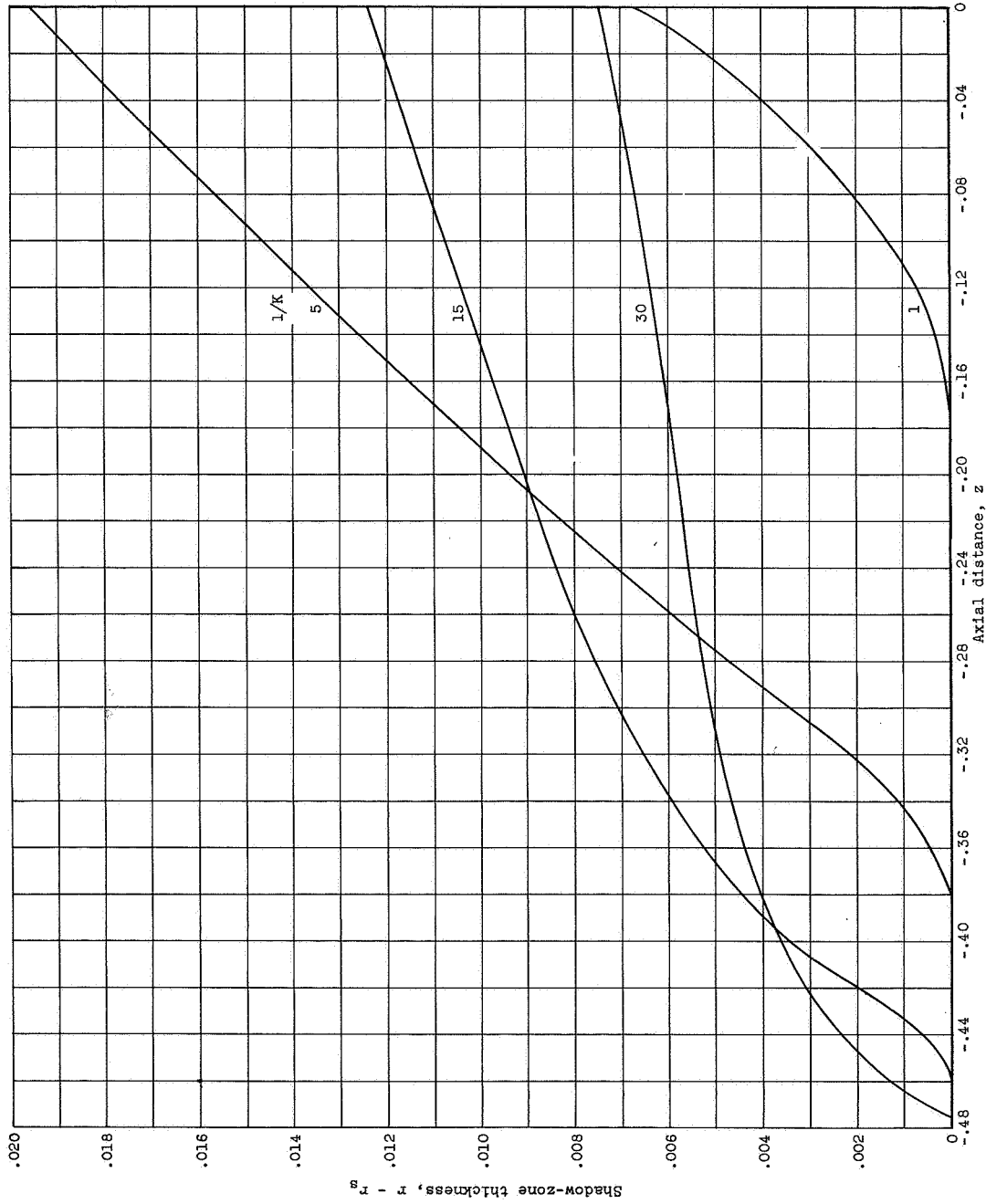
(b) Radial component.

Figure 8. - Concluded. Difference between local air- and droplet-velocity components against radial distance  $r$  at  $z = 0$  position of ellipsoid of finess ratio 5.

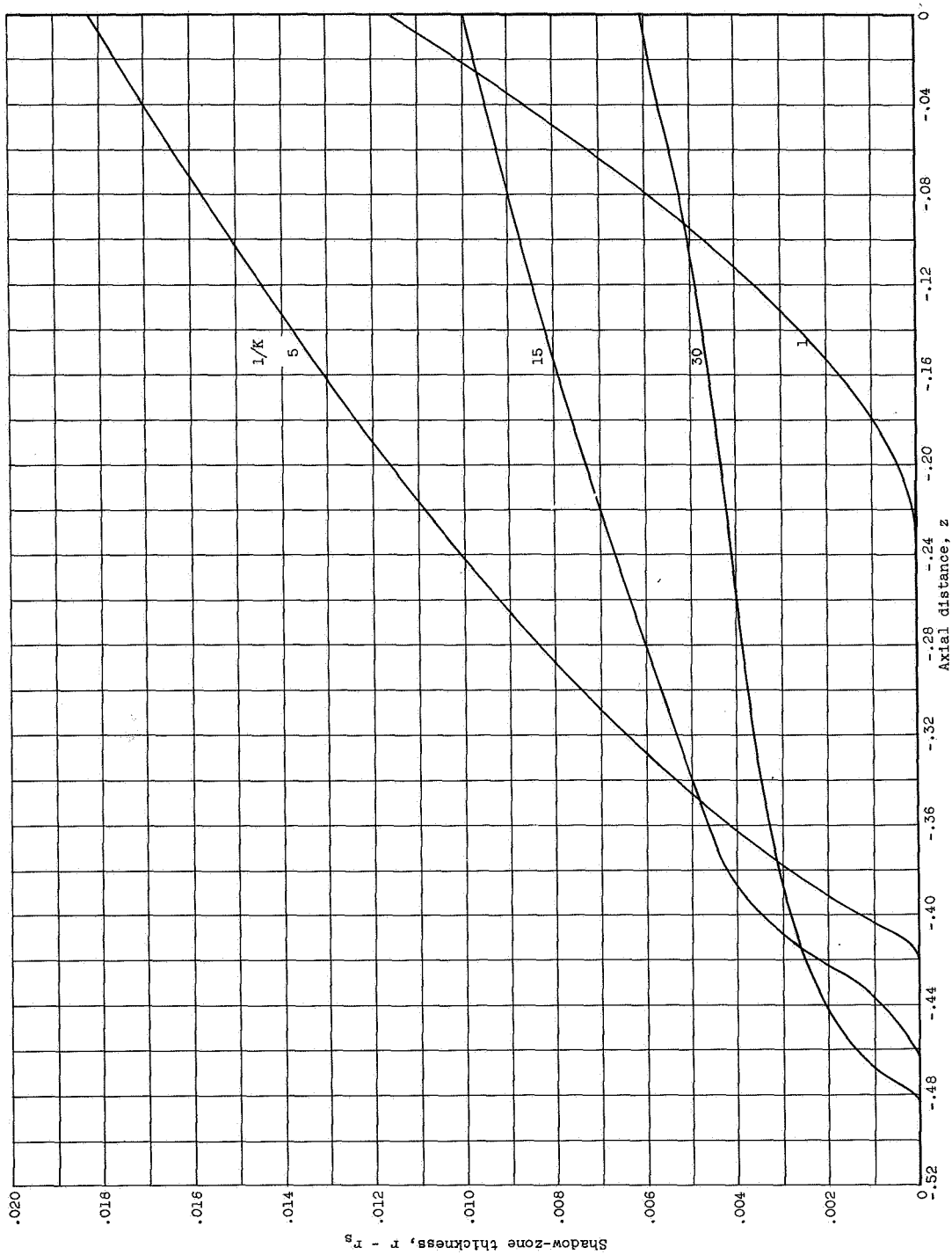


(a) Free-stream Reynolds number, 0.  
 Figure 9. - Thickness ( $r - r_s$ ) of shadow zone as function of  $z$ -position.

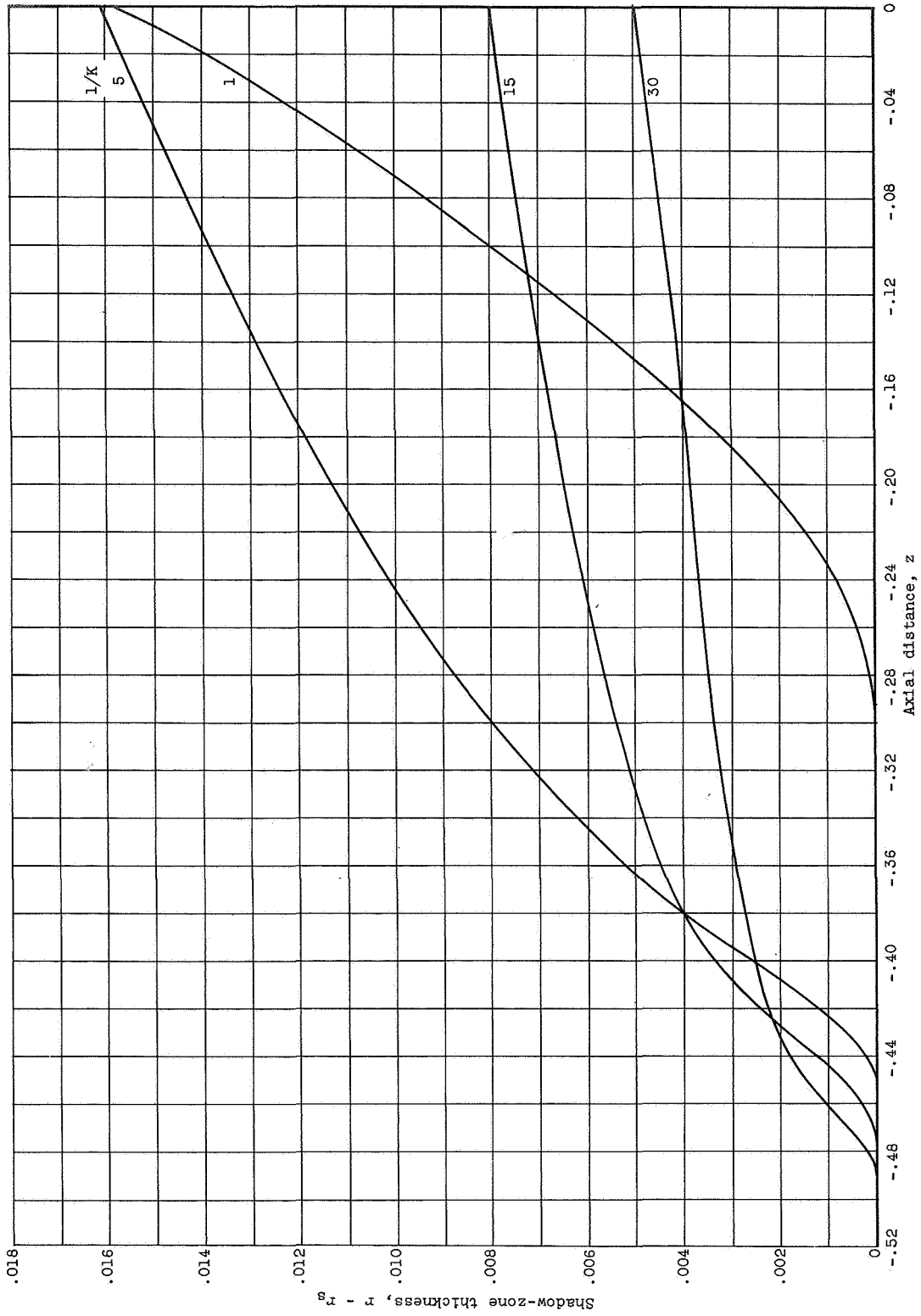
9012



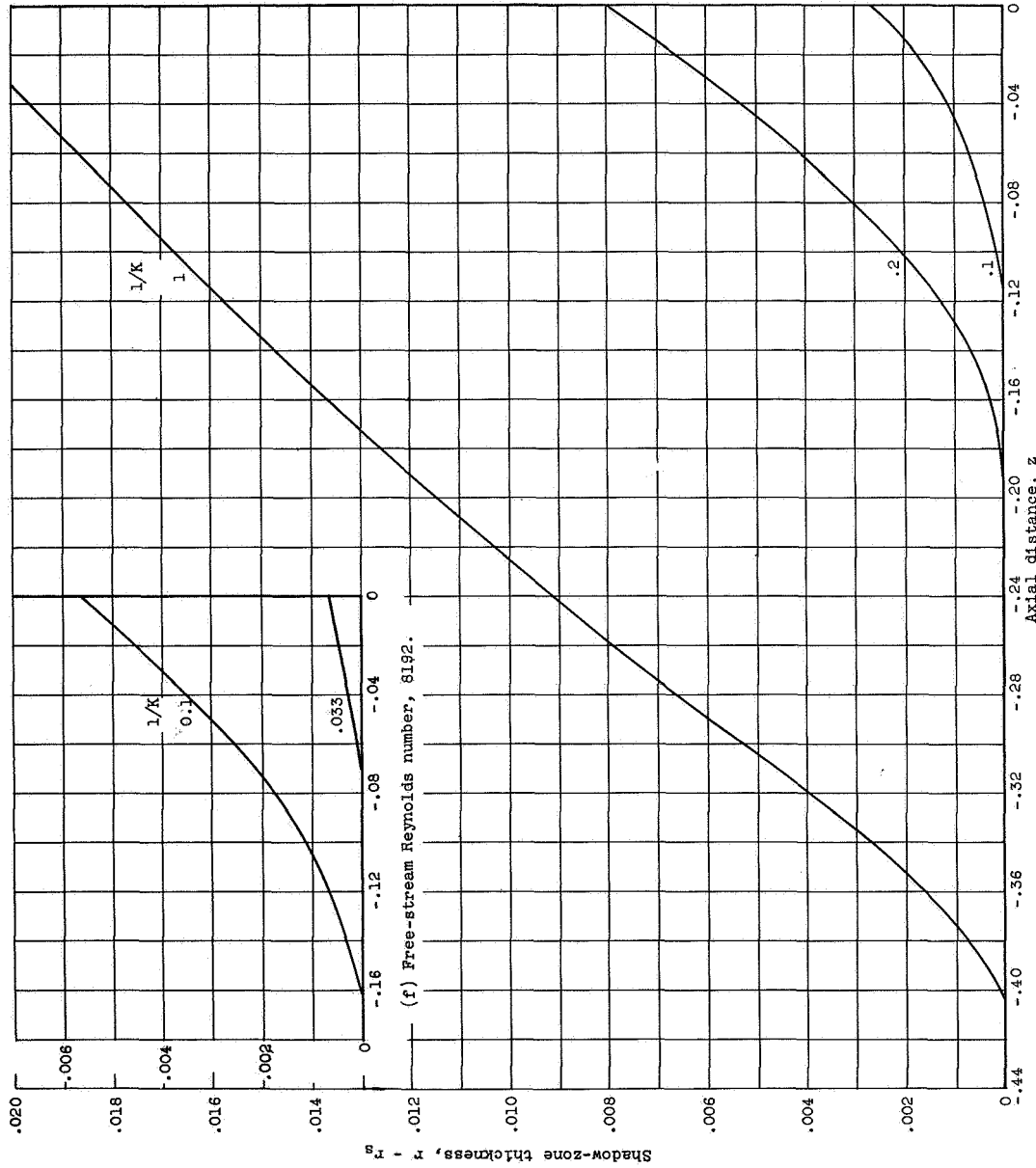
(b) Free-stream Reynolds number, 128.  
Figure 9. - Continued. Thickness ( $r - r_s$ ) of shadow zone as function of  $z$ -position.



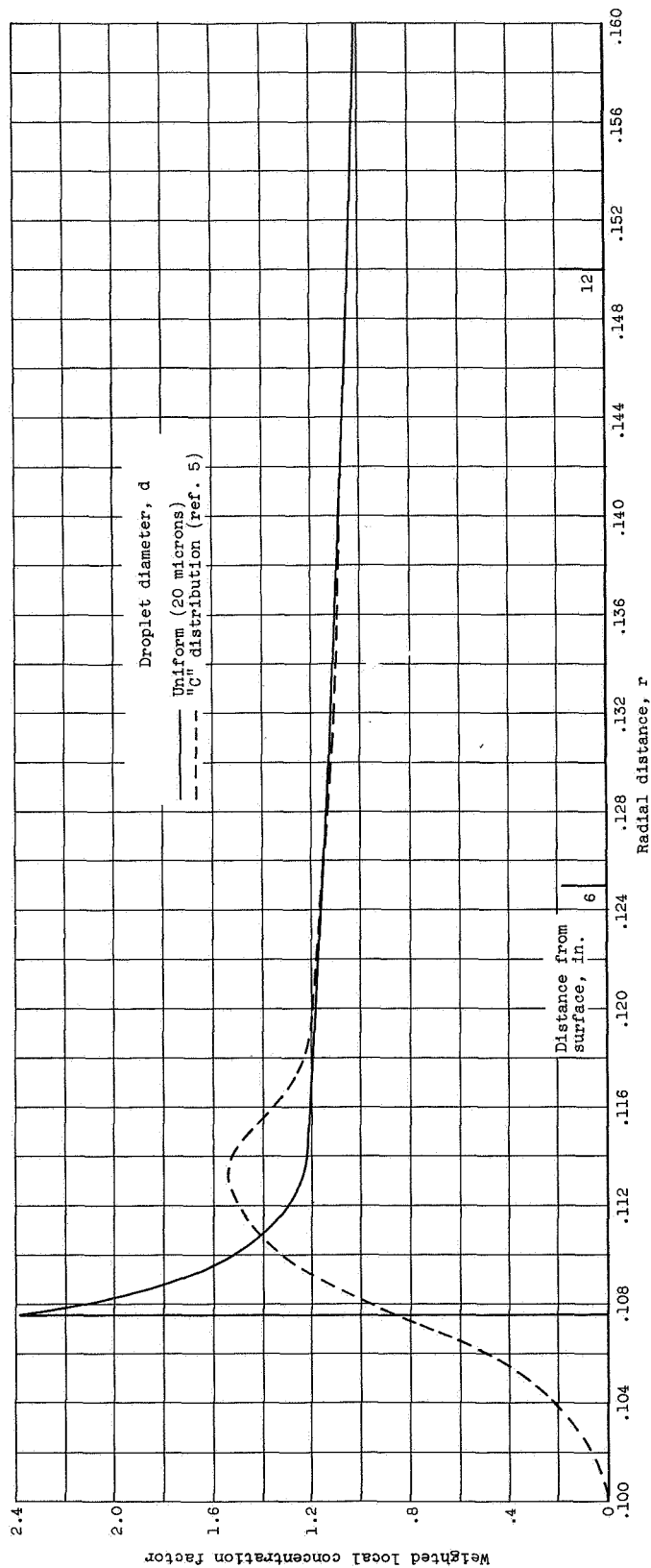
(c) Free-stream Reynolds number, 512. Thickness ( $r - r_s$ ) of shadow zone as function of  $z$ -position.



(d) Free-stream Reynolds number, 1024.  
Figure 9. - Continued. Thickness ( $r - r_s$ ) of shadow zone as function of  $z$ -position.

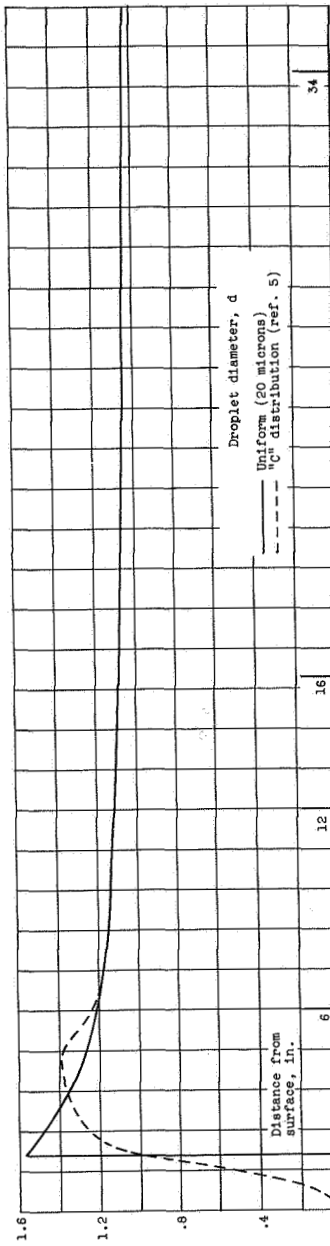


(e) Free-stream Reynolds number, 4096.  
 (f) Free-stream Reynolds number, 8192.  
 Figure 9. - Concluded. Thickness ( $r - r_s$ ) of shadow zone as function of  $z$ -position.

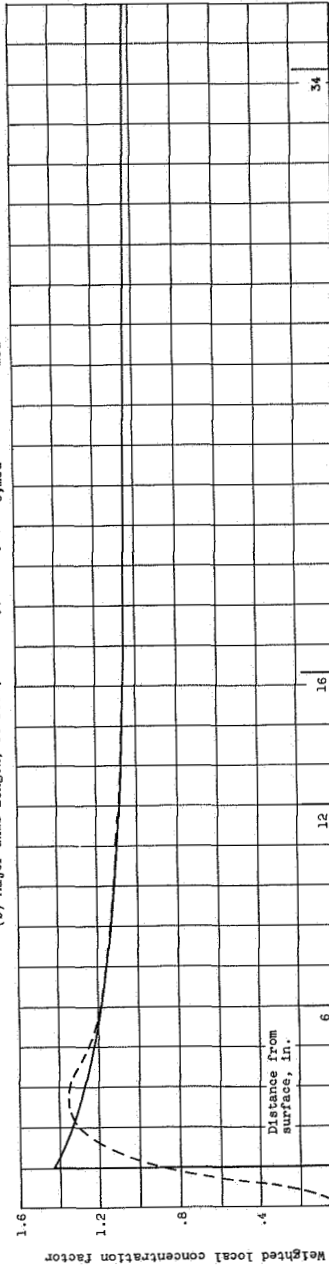


(a) Major axis length, 20 feet; velocity, 300 mph;  $Re_{0,med}$ , 128.7;  $1/K_{med}$ , 55.1.  
 Figure 10. - Effect of droplet-size distribution on concentration factor at  $z = 0$  for ellipsoid at altitude of 15,000 feet and air temperature of 1° F.  
 Volume-median droplet diameter, 20 microns.

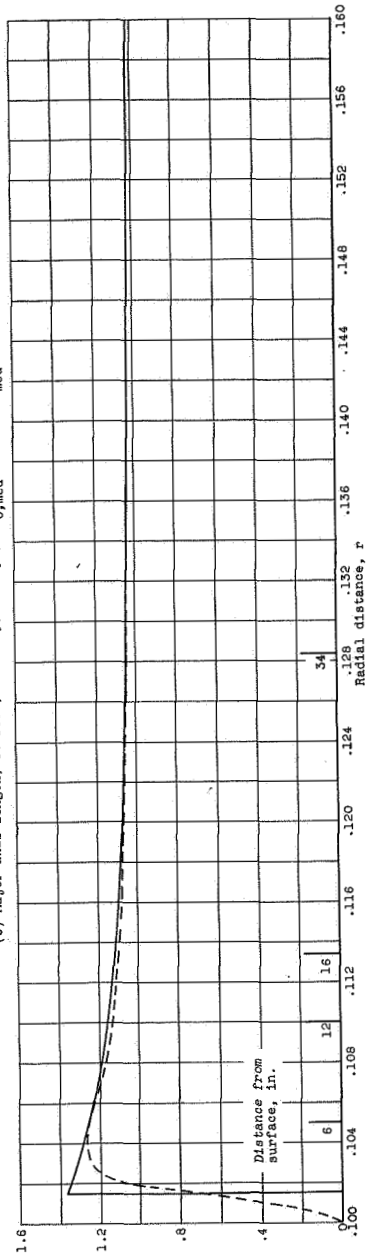




(a) Major axis length, 50 feet; velocity, 300 mph;  $Re_{0,med}$ , 128.7;  $1/K_{med}$ , 82.85.



(b) Major axis length, 100 feet; velocity, 200 mph;  $Re_{0,med}$ , 65.8;  $1/K_{med}$ , 124.3.



(c) Major axis length, 300 feet; velocity, 100 mph;  $Re_{0,med}$ , 128.7;  $1/K_{med}$ , 165.6.

(d) Major axis length, 15,000 feet and air temperature of 10 F. Volume-median droplet diameter, 20 microns.